Multiple dynamic interactions from basal ganglia direct and indirect pathways mediate action selection

Hao Li[1], and Xin Jin[1,2,3,4*]

[1] Molecular Neurobiology Laboratory, The Salk Institute for Biological Studies, 10010 North Torrey Pines Road, La Jolla, CA 92037, USA

[2] Center for Motor Control and Disease, Key Laboratory of Brain Functional Genomics, East China Normal University, 3663 North Zhongshan Road, Shanghai 200062, China

[3] NYU–ECNU Institute of Brain and Cognitive Science, New York University Shanghai, 3663 North Zhongshan Road, Shanghai 200062, China

[4] Lead Contact

*Correspondence to: xjin@bio.ecnu.edu.cn

Summary

The basal ganglia are known to be essential for action selection. However, the functional role of basal ganglia direct and indirect pathways in action selection remains unresolved. Here by employing cell-type-specific neuronal recording and manipulation in mice trained in a choice task, we demonstrate that multiple dynamic interactions from the direct and indirect pathways control the action selection. While the direct pathway regulates the behavioral choice in a linear manner, the indirect pathway exerts a nonlinear inverted-U-shaped control over action selection, depending on the inputs and the network state. We propose a new center (direct) - surround (indirect) - context (indirect) "Triple-control" functional model of basal ganglia, which can replicate the physiological and behavioral experimental observations that cannot be simply explained by either the traditional "Go/No-go" or more recent "Co-activation" model. These findings have important implications on understanding the basal ganglia circuitry and action selection in health and disease.

In Brief

Using behavior analysis, in vivo electrophysiology, optogenetics and computational modeling in mice, Li and Jin unveiled the neuronal dynamics of basal ganglia direct and indirect pathways underlying action selection, and proposed a new "Triple-control" functional model of basal ganglia.

Highlights

- Outputs of opponent SNr subpopulations determine the action selection
- Striatal direct/indirect pathways exhibit distinct physiology and function during action selection
- Cell ablation and optogenetic inhibition of indirect pathway exert opposite behavioral effects
- A new "Triple-control" functional model of basal ganglia pathways is proposed

Introduction

Selecting the proper actions is essential for organism's survival and reproduction in the ever-changing environment (Gallistel, 1980). Numerous studies have implicated that the basal ganglia, a series of interconnected subcortical nuclei including the striatum and substantia nigra, play a primary role in action selection (Graybiel, 1998; Hikosaka et al., 1998; Jin and Costa, 2015; Mink, 2003; Redgrave et al., 1999). Indeed, a wide range of neurological and psychiatric disorders associated with the dysfunctional basal ganglia circuitry, including Parkinson's disease (Benecke et al., 1987), Huntington's disease (Phillips et al., 1995), Obsessive-compulsive disorder (OCD) (Graybiel and Rauch, 2000), are characterized by major deficits in action selection and movement control. Anatomically, commands for motor control are processed by basal ganglia through two major pathways, termed direct and indirect pathway, originating from striatal D1- and D2-expressing spiny projection neurons (D1-/D2-SPNs), respectively (Albin et al., 1989; DeLong, 1990). These two pathways collectively modulate substantia nigra pars reticulata (SNr) activity and the basal ganglia output, thus influence behavioral decisions. There are currently two major types of thinking on how the basal ganglia pathways work. An early classic theory has suggested that the basal ganglia direct and indirect pathways oppose each other to facilitate and inhibit action, respectively (the "Go/No-go" model) (Albin et al., 1989; DeLong, 1990; Kravitz et al., 2010). In contrast, a recent theory has proposed that direct pathway selects the desired action, while the indirect pathway inhibits other competing actions in order to highlight the targeted choice (the "Co-activation" model) (Cui et al., 2013; Hikosaka et al., 2000; Mink, 1996).

The two theories have essentially agreed upon the function of direct pathway being the positive driving force for initiating or facilitating the desired actions. Yet, the ideas about the indirect pathway function are largely controversial as either impeding the desired action in the "Go/No-go" model or inhibiting the competing actions in the "Co-activation" model. While the precise neuroanatomy on how the D2-SPNs control SNr through indirect pathway has yet to be mapped out at single-cell level to differentiate the two hypotheses, either theory has found its supports from behavioral and physiological observations. For instance, it has been found that stimulation of striatal direct and indirect pathways can bidirectionally regulates locomotion (Durieux et al., 2012; Kravitz et al., 2010), consistent with the traditional 'Go/No-go' model. On the other hand, in vivo electrophysiological and imaging experiments revealed that the striatal direct and indirect pathways are both activated during action initiation (Barbera et al., 2016; Cui et al., 2013; Geddes et al., 2018; Isomura et al., 2013; Jin et al., 2014; Klaus and Plenz, 2016; Markowitz et al., 2018; Nonomura et al., 2018), as the 'Co-activation' model predicted. Furthermore, physiological and optogenetic studies concerning complex behavior such as learned action sequences have further complicated the issue, and unveiled various neuronal subpopulations in both pathways are activated during the initiation, termination and switching of actions (Geddes et al., 2018; Jin and Costa, 2015; Jin et al., 2014; Tecuapetla et al., 2016). So far, how exactly the basal ganglia direct and indirect pathways work together to control action selection has been controversial and inconclusive, and the underlying circuit mechanism remains largely unclear (Calabresi et al., 2014).

Here we trained mice to perform an operant action selection task where they were required to select one out of two actions to achieve reward, based on self-monitored time intervals (Howard et al., 2017). By employing in vivo neuronal recording, we found that the net

output of two opponent SNr neuron populations is predictive of the behavioral choices. Through identifying striatal pathway-specific neuronal activity with optogenetic tagging, we found that there are neuronal subpopulations in either direct or indirect pathway who are activated during selecting one action and suppressed during another. Optogenetic inhibition, as well as selective ablation of direct pathway impairs action selection, and optogenetic excitation of direct pathway enhances current choice, confirming a role of direct pathway in facilitating desired actions. Furthermore, optogenetic inhibition of indirect pathway improves action selection and excitation of indirect pathway impairs behavioral choices, as predicted by the 'Go/No-go' model. However, selective ablation of indirect pathway impairs action selection, opposite from the behavioral effect of optogenetic inhibition and at odds with the 'Go/No-go' model, but in consistent with the prediction from the 'Co-activation' model. To resolve these contradictions, we propose a new center (direct) - surround (indirect) - context (indirect) "Triple-control" functional model of basal ganglia pathways, in which there are two interacting indirect pathway subcircuits exerting opposite controls over the basal ganglia output. The new model can reproduce the neuronal and behavioral experimental results that cannot be simply explained by either the "Go/No-go" or the "Co-activation" model. Further systematic analyses from this new model suggested that the direct and indirect pathways modulate behavioral outputs in a linear and nonlinear manner, respectively. Notably, in the new 'Triple-control' model, the direct and indirect pathways can work together to dynamically control action selection and operate in a manner similar to 'Go/No-go' or 'Co-activation' model, depending on the activity level and the network state. These results revise our current understanding on how the basal ganglia control actions, and have important implications for a wide range of movement and psychiatric diseases where the dynamic balance

between the two pathways is compromised (Albin et al., 1989; Benecke et al., 1987; Calabresi et al., 2014; DeLong, 1990; Graybiel and Rauch, 2000; Mink, 1996; Phillips et al., 1995).

Results

Opponent SNr activities underlie action selection

To address the role of basal ganglia in action selection, we trained mice in a recently developed 2-8 s task in which they are required to choose the left versus right action based on self-monitored time intervals (Howard et al., 2017). Specifically, mice were put into an operant chamber with both left and right levers extended (Figure 1A, see Methods). For a given trial, both levers retract at trial initiation, and after either 2 s or 8 s (50% for each, randomly interleaved), both levers extend. The mouse has to judge the interval between lever retraction and extension as 2 s vs. 8 s and make a corresponding action choice by pressing the left vs. right lever, respectively (Figure 1A). The first lever press after lever extension was registered as the mouse's choice. The correct choice leads to sucrose delivery (10 µl) as reward, and any lever presses beyond the first press after lever extension yield no outcome. A new trial starts at lever retraction again after a random inter-trial-interval (ITI, 30 s on average; Figure 1A). Across 14 consecutive days of training, mice (n = 10) significantly increased the correct rate of choice from chance level to more than 90% (Figure 1B). In addition, the animals gradually shortened the choice latency and demonstrated a strong preference toward the left lever due to its association with the shorter waiting time (Figure S1A, B). As a result, during the longer-waiting 8 s trials the mouse initially moved toward the left lever, then crossing the midpoint between left and right levers at around 4 s, and stayed around the right lever afterwards (Howard et al., 2017) (Figure 1C; Supplemental Video 1). Note that, the mouse showed no stereotyped movement trajectories

during the incorrect trials (Figure 1C). This emerged stereotyped movement trajectory in the 8-s trials thus provided us a unique opportunity for investigating the neural mechanisms underlying the internally-driven, dynamic action selection process.

The substantia nigra pars reticulata (SNr) is one of the major output nuclei of basal ganglia (Albin et al., 1989; DeLong, 1990; Hikosaka et al., 2000; Mink, 1996). To investigate how the basal ganglia contribute to the dynamic process of action selection, we began by recording the SNr neuronal activity in mice trained in the 2-8 s task (Figure 1D, Figure S1C, see Methods). It was found that a large proportion (211/261, 80.8%; recorded from n = 9 mice) of SNr neurons changed firing rate significantly during the correct 8-s trials as mice dynamically shifted the internal action selection from the left to the right (Figure 1E). The Z-score of the task-related neuronal firing rate, reflecting the firing activity changes related to baseline, was defined as Firing Rate Index (FRI, see Methods). We focus on the data analyses in the 8-s trials since the first 2-s of 8-s trials consists of the identical behavioral and neuronal profiles of the 2-s trials due to the task design (Figure 1C, Figure S1D-F). The task-related SNr neurons were categorized into four subtypes based on the dynamics of FRI in the correct 8-s trials: Type 1 - monotonic decrease (Figure 1E, F, 102/211, 48.3%), Type 2 - monotonic increase (Figure 1E, G, 56/211, 26.5%), Type 3 - transient phasic increase (Figure 1E, H, 25/211, 11.9%) and Type 4 - transient phasic decrease (Figure 1E, I, 28/211, 13.3%). These types of neuronal dynamics in SNr only appeared in the correct but not the incorrect trials (Figure 1F-I), nor on the day 1 of task training (Figure S1G-K), suggesting a tight correlation between the SNr neuronal dynamics and the behavioral performance. Specifically, the Type 1 and Type 2, but not the Type 3 and Type 4 neurons, exhibit firing changes co-varying with the action selection and these two types together consist in around 80% of all task-related SNr neuron population (Figure 1J).

It has been suggested that SNr suppresses movements through the inhibition of downstream motor nuclei and releases action via disinhibition (Hikosaka et al., 2000; Mink, 1996). We thus ask whether the opponent neuronal dynamics in Type 1 and Type 2 SNr subpopulations mediate the dynamic shift of choice, by suppressing the competing selection of right vs. left action, respectively. Indeed, the SNr net output by subtracting Type 2 and Type 1 SNr neuronal dynamics (Figure 1K) is highly reminiscent of the animal's stereotyped movement trajectory during choice (Figure 1C). To further determine the relationship between the SNr net output and action selection, we tested the behavioral choice of the 2-8 s trained mice in a series of non-rewarded probe trials with novel intervals of 2.5, 3.2, 4, 5 and 6.3 s (see Methods). Consistent with what reported before (Howard et al., 2017), the probability of mice selecting the action associated with the long duration (8 s) gradually increases along with the time intervals of probe trials (Figure 1L). The resulting psychometric curve thus represents the animal's real-time action selection process during the 8-s trials. Further comparison between the psychometric curve and the SNr net output revealed a strong linear correlation (Figure 1M), indicating that the SNr net output faithfully predicts momentary behavioral choice. Together, these results suggest that mice can learn to dynamically shift their choice based on internally-monitored time, and the opponent neuronal activities in SNr correlate with the action selection.

SNr neuronal dynamics reflect action selection but not simply time or value

In the 2-8 s task, the passage of time and expectation of reward both change simultaneously with the animal's internal choice. One may argue that the Type 1 and Type 2 neuronal dynamics observed in SNr during the 8-s trials might reflect the passage of time or value of expected reward rather than action selection. To differentiate these possibilities and

175 specify the functional role of SNr activity, we presented mice previously trained in the 2-8 s task
176 with random probe trials of 16-s interval (Figure 2A). In these 16-s probe trials which they have
177 never experienced before during training, the animals sometimes wait on the right side and press
178 the right lever, or shift back to the left side and press the left lever when the levers are extended
179 at 16 s (Figure 2B, C). This arbitrary choice situation in the 16-s probe trials thus provides a
180 special window to determine the functional relationship between SNr activity and behavioral
181 choice. If the Type 1 and Type 2 SNr subpopulations encode information about time passage or
182 expectation value, their neuronal activities would continue changing monotonically between 8
183 and 16 s. In contrast, if the Type 1 and Type 2 SNr subpopulations encode action selection, their
184 neuronal activities would predict the behavioral choice and differentiate between the right vs. left
185 action selection. Indeed, it was found that when the firing activity of Type 1 SNr neurons
186 maintained below baseline from 8 to 16 s, the mice tended to select the right lever later (Figure
187 2D). However, when the firing activity reversed the decreasing tendency to increase, the mice
188 chose the left lever instead (Figure 2D). A similar relationship between the neuronal activity and
189 behavior choice was also evident in Type 2 SNr neurons, albeit with opposite dynamics (Figure
190 2E). This is especially evident in the subtraction of Type 2 and Type 1 SNr neuronal dynamics,
191 in which the SNr net output is strongly correlated with and predictive of behavioral choice
192 (Figure 2F). These results thus suggested that the neuronal activities in SNr likely encode the
193 ongoing action selection but not simply reflect time passage or reward value.
194 To further confirm this point, we recorded the firing activity from the same SNr neurons
195 during both the 2-8 s control task (Figure 2G, 2s-left and 8s-right) and a modified version of 2-8
196 s task in which the contingency between action and interval is reversed (Figure 2J, 2s-right and
197 8s-left) on the same day (see Methods). It was found that the mice performed at around 80%

correct in both tasks on the same day (Figure 2H, K, Figure S2A). Accordingly, the movement trajectories of the same mice in 8-s trials were reversed from left-then-right in the control task (Figure 2I) to right-then-left in the reversed task (Figure 2L). The left-lever preference during the ITI in the control task was also switched to right-lever preference in the reversed 2-8 s task (Figure S2B). Notably, the passage of time and expected value as well as other environmental factors are all identical in both versions of task, except that the animal's choice is now reversed from right to left for the 8-s trials (Figure 2H, I vs. Figure 2K, L). If Type 1 or Type 2 SNr neurons encode time or value, either neuronal population will exhibit the same neuronal dynamics in 8-s trials for both versions of task. On the other hand, if Type 1 and Type 2 SNr neurons encode action selection, their neuronal dynamics will reverse in the reversed version of 2-8 s task compared to the standard version. In fact, the Type 1 SNr neurons which showed monotonic decreasing dynamics in the control 2-8 s task (Figure 2M) reversed their neuronal dynamics to a monotonic increase in the reversed 2-8 s task (Figure 2P), consistent with the behavioral choice. The same reversal of neuronal dynamics was also observed in Type 2 SNr neurons in the reversed version of standard task (Figure 2N, Q). The SNr net output by subtracting Type 2 and Type 1 SNr neuronal dynamics, which was tightly correlated with the action selection in the standard 2-8 s task (Figure 2O), is reversed and now predictive of the new behavioral choice in the reversed 2-8 s task (Figure 2R). Notably, Type 3 and Type 4 SNr neurons exhibiting transient change when mice switching between choices maintained the same neuronal dynamics in both tasks (Figure S2C-F). Together, these results therefore demonstrate that the output of basal ganglia reflects the dynamic action selection rather than simply time or value.

221 **Distinct striatal direct vs. indirect pathway activity during action selection**

222 The basal ganglia output is largely controlled by two major neural pathways, called
223 'direct' and 'indirect' pathway, originating from D1- vs. D2-expressing spiny projection neurons
224 (D1- vs. D2-SPNs) in the striatum, respectively (Albin et al., 1989; DeLong, 1990; Hikosaka et
225 al., 2000; Mink, 1996). We then decided to determine the neuronal dynamics in the striatum,
226 specifically the neuronal activity in the direct and indirect pathways during action selection. We
227 employed in vivo extracellular electrophysiology to record the neuronal activity in the dorsal
228 striatum when mice perform the 2-8 s task, and classified putative SPNs based on the spike
229 waveforms and firing properties (Geddes et al., 2018; Jin and Costa, 2010; Jin et al., 2014).
230 Among all the SPNs recorded from the trained mice (n = 24), 341 out of 409 SPNs (83.4%) were
231 defined as task-related neurons for showing significant firing changes during the 2-s and 8-s
232 lever retraction period (Figure 3A, Figure S3A). Similar to the various types of neuronal
233 dynamics observed in SNr, task-related SPNs showed Type 1 (Figure 3B, monotonic decrease,
234 159/341, 46.6%), Type 2 (Figure 3C, monotonic increase, 103/341, 30.2%), Type 3 (Figure 3D,
235 transient phasic increase, 49/341, 14.4%) and Type 4 (Figure 3E, transient phasic decrease,
236 30/341, 8.8%) activity profiles during the correct 8-s trials (Figure 3A, Figure S3A). These
237 neural dynamics were largely absent in SPNs on day 1 of training (Figure S3B-F). These results
238 indicate that the striatum, as one of the major input nuclei of basal ganglia, demonstrates the four
239 types of neuronal dynamics similar with SNr during the dynamic process of action selection.

240 To further determine the neuronal activity in the direct and indirect pathways during
241 action selection, we utilized an optogenetics-aided photo-tagging method (Geddes et al., 2018;
242 Howard et al., 2017; Jin and Costa, 2010; Jin et al., 2014; Lima et al., 2009) to record and
243 identify striatal D1- vs. D2-SPNs in freely behaving mice. Channelrhodopsin-2 (ChR2) was

244 selectively expressed in D1- or D2-SPNs by injecting AAV-FLEX-ChR2 in the dorsal striatum
245 of D1- and A2a-Cre mice, respectively (Geddes et al., 2018; Jin et al., 2014). In the end of each
246 behavioral session with recording, optogenetic stimulation via an optic fiber attached to the
247 electrode array was delivered to identify D1- vs. D2-SPNs through photo-tagging (Figure 3F,
248 Figure S3G-J) (Geddes et al., 2018; Jin et al., 2014). Only those neurons exhibiting a very short
249 latency (≤ 6 ms) to light stimulation (Figure 3G-I) and showing identical spike waveforms (R ≥
250 0.95, Pearson correlation coefficient) between behavior and light-evoked response (Figure 3J, K)
251 were identified as Cre-positive thus D1- or D2-SPNs (Geddes et al., 2018; Jin et al., 2014).
252 Within all positively identified D1-SPNs (n = 92 from 6 mice) and D2-SPNs (n = 95 from 6
253 mice), 74 out of 92 (80.4%) D1-SPNs and 79 out of 95 (83.1%) D2-SPNs showed a significant
254 change in firing rate during the correct 8-s trials. In addition, all four types of neuronal dynamics
255 during action selection were found in both D1-SPNs (Figure 3L, M) and D2-SPNs (Figure 3N,
256 O), as observed in SNr. The Type 1 and Type 2 neuronal dynamics showing monotonic firing
257 change (Figure 3M, O) were the predominant task-related subpopulations within either D1-
258 (Figure 3L) or D2-SPNs (Figure 3N). Notably, the striatal D1-SPNs consist of significantly more
259 Type 1 than Type 2 neurons (Figure 3L), while D2-SPNs show a similar proportion between the
260 two Types (Figure 3N). These data thus suggest while neurons in both the striatal direct and
261 indirect pathways encode information related to behavioral choice, the two pathways might
262 reflect and contribute to distinct aspects of action selection.
263

264 **Ablation of striatal direct vs. indirect pathway differently impaired action selection**

265 Given the action-selection-related neuronal dynamics observed in striatum, we next asked
266 whether the neural activity in striatum is necessary for learning and execution of action selection,

267 and furthermore, what is the functional difference between the direct and indirect pathways. It
268 has been reported that the NMDA receptors on striatal SPNs are critical for sequence learning
269 (Geddes et al., 2018; Jin and Costa, 2010) and action selection (Howard et al., 2017). To further
270 identify the functional role of NMDA receptors on D1- vs. D2-SPNs for action selection, we
271 employed a genetic strategy to specifically delete NMDA receptors from D1- vs. D2-SPNs by
272 crossing mice carrying a floxed NMDAR1 (NR1) allele with a dorsal striatum-dominant D1-cre
273 line (Gong et al., 2007) and A2a-cre line (Geddes et al., 2018; Jin et al., 2014), respectively
274 (referred to as D1-NR1 KO and D2-NR1 KO mice, respectively; see Methods). Both the D1-
275 NR1 KO and D2-NR1 KO mice are significantly impaired in learning the 2-8 s task compared to
276 their littermate controls (Figure 4A, B), suggesting that NMDA receptors on either D1- or D2-
277 SPNs are critical for learning of proper action selection. In the end of two-week training, when
278 given the probe trials with various intervals across 2 to 8 s, it was found that D1-NR1 KO mice
279 showed a systematic bias toward the lever associated with short interval and made deficient
280 behavioral choice only in long interval trials (Figure 4C). In contrast, D2-NR1 KO mice showed
281 impaired action selection across various probe trials of both short and long intervals (Figure 4D).
282 These data suggest that while NMDA receptors on both D1- and D2-SPNs are required for action
283 learning, the deletion of NMDA receptors in direct and indirect pathways impairs action
284 selection in a different manner.

285 We then asked whether that neural activity in dorsal striatum is necessary for the proper
286 execution of action selection after learning. We first conduct striatal inactivation in trained
287 wildtype mice by bilateral intra-striatal infusion of muscimol (Figure 4E, see Methods). Striatal
288 muscimol infusion significantly reduced the animal's overall performance in comparison with
289 the pre- and post-saline injection controls (Figure 4F). When tested with probe trials, the

290 psychometric curve indicated that the inactivation of striatum impairs action selection for the
291 long trials (Figure 4G). These data thus suggested that the striatal neural activity is critical for
292 appropriate execution of learned action selection.

293 To further elucidate the functional role of specific striatal pathways in action selection,
294 we next employed a viral approach to bilaterally express diphtheria toxin receptors (AAV-
295 FLEX-DTR-eGFP) in the dorsal striatum of trained D1- and A2a-Cre mice, followed by
296 diphtheria toxin (DT) injections to selectively ablate D1- or D2-SPNs (Geddes et al., 2018)
297 (Figure 4H, I, N; see Methods). Ablation of either D1- or D2-SPNs significantly impaired action
298 selection and reduced the correct rate of choice (Figure 4J, O). Notably, the psychometric curve
299 revealed that D1-SPNs ablation mice showed a selective impairment of choice in long interval
300 trials (Figure 4K). In contrast, mice with D2-SPNs ablation exhibited choice deficits in both long
301 and short trials (Figure 4P). Consistent with the D1- and A2a-NR1 KO data, these results suggest
302 that the direct and indirect pathways are both needed yet play distinct roles in action selection.

303 The classic 'Go/No-go' model of basal ganglia suggests the direct and indirect pathways
304 work antagonistically to release and inhibit action, respectively (Albin et al., 1989; DeLong,
305 1990; Kravitz et al., 2010). On the other hand, more recent 'Co-activation' model of basal
306 ganglia proposes that direct pathway initiates the selected action and at the same time, the
307 indirect pathway inhibits the competing actions (Cui et al., 2013; Hikosaka et al., 2000; Mink,
308 1996). For visualization purpose, we diagram 'Go/No-go' and 'Co-activation' models as center-
309 surround receptive field with D1-SPNs as the center and D2-SPNs as the surround (Figure 4S;
310 Figure S4A, D). While the direct pathway plays the similar role in both models (Figure S4B, E),
311 the function of indirect pathway differs dramatically (Figure 4S). Lesion of the indirect pathway
312 thus leads to contrast predictions on action selection from the two models (Figure S4C, F).

313 Specifically, ablation of D2-SPNs would facilitate the action being selected through removing
314 inhibition according to the Go/No-go model (Figure S4C) (Albin et al., 1989; DeLong, 1990;
315 Kravitz et al., 2010), while blockage of indirect pathway would impair the action selection due to
316 disinhibition of competing actions according to the Co-activation model (Figure S4F) (Cui et al.,
317 2013; Hikosaka et al., 2000; Mink, 1996). Although our D1-SPNs ablation experiment indicates
318 that direct pathway is required for action selection as suggested in both models (Figure 4J, K),
319 the D2-SPNs ablation result favorably supports the Co-activation model over the Go/No-go
320 model (Figure 4O, P, Figure S4F). In fact, close inspection of the movement trajectories of D1-
321 SPNs lesioned mice in the 8-s trials showed that compared to control mice (Figure 4L), they tend
322 to stick on the left side more often with impaired right choice when lever extension at 8s (Figure
323 4M). In contrast, D2-SPNs lesioned mice demonstrated overall rather random movement
324 trajectories, and the stereotyped left-then-right movement sequences were largely disrupted in
325 comparison with the controls (Figure 4Q, R). These observations are mostly consistent with the
326 idea of indirect pathway inhibiting competing actions in the Co-activation model (Figure 4S) and
327 lesion of indirect pathway disrupts action selection for both the short and long trials (Figure 4P-
328 R). Together, these data suggest that ablation of direct and indirect pathways both impair choice
329 behavior but in a distinct manner due to their different roles in action selection.
330

331 **Optogenetic manipulation of D1- vs. D2-SPNs distinctly regulates action selection**

332 To further determine the specific function of direct vs. indirect pathway in action
333 selection, we employed optogenetics to alter the D1- and D2-SPNs activity in vivo with high
334 temporal precision and investigated its effects on the ongoing action selection process. Both the
335 classic 'Go/No-go' (Albin et al., 1989; DeLong, 1990; Kravitz et al., 2010) and more recent 'Co-

336 activation' (Cui et al., 2013; Hikosaka et al., 2000; Mink, 1996) models predict that activation of
337 the direct pathway enhances the action selection (Figure S5A, E, I, K, O, Q), while inhibition of
338 direct pathway reduces the correct choice (Figure S5B, F, L, R). To experimentally validate the
339 models' predictions, AAV-FLEX-ChR2 was injected into the dorsal striatum of D1- or A2a-Cre
340 mice and optic fibers were implanted bilaterally for in vivo optogenetic stimulation (Figure 5A,
341 Figure S3K, L; see Methods) (Geddes et al., 2018; Jin et al., 2014). After mice learned the 2-8s
342 task, 1-s pulse of constant light (wave length 473 nm) was delivered right before lever extension
343 in randomly chosen 50% of 2-s and 50% of 8-s trials (Figure 5B, C, see Methods). The correct
344 rate of optogenetic stimulation trials is compared with the non-stimulation trials of the same
345 animal as a within-subject design. We observed no significant change on the correct rate in 2-s
346 trials, whereas the correct rate was significant increased by optogenetic stimulation in 8-s trials
347 (Figure 5D), indicating a facilitation effect on action selection by stimulating the D1-SPNs. We
348 then sought to determine the effect of suppressing D1-SPN activity on action selection by viral
349 expression of Halorhodopsin (AAV5-EF1a-DIO-eNpHR3.0-eYFP) in the dorsal striatum of D1-
350 cre mice (Gradinaru et al., 2010). As expected, inhibiting D1-SPNs right before lever extension
351 in trained mice reduced the correct rates in 8-s but not 2-s trials (Figure 5C, E), opposite to D1-
352 SPN stimulation effects. These experimental data with bidirectional optogenetic manipulation
353 suggest that the D1-SPN activity is positively correlated with the choice performance, in
354 consistent with the hypothesis of direct pathway facilitating the action selected in both the
355 Go/No-go and Co-activation models (Figure S5K, L, Q, R).

356 Nevertheless, the two models have distinct views on the function of indirect pathway.
357 While the classic 'Go/No-go' model suggests that the indirect pathway inhibits the selected
358 action (Albin et al., 1989; DeLong, 1990; Kravitz et al., 2010), the 'Co-activation' model

359 hypothesizes that the indirect pathway inhibits the competing actions instead (Cui et al., 2013;
360 Hikosaka et al., 2000; Mink, 1996). These models thus provide contrast predictions about the
361 effect of activation of the indirect pathway on action selection, being decreased correct rate
362 based on the Go/No-go model (Figure S5M) and increased correct rate from the Co-activation
363 model (Figure S5S), respectively. We thus decided to test the distinct predictions from the two
364 models by optogenetic manipulation of indirect pathway during action selection in the 2-8s task.
365 ChR2 or Halorhodopsin (eNpHR3.0) was expressed in the dorsal striatum of A2a-cre mice for
366 bilaterally optogenetic activation or inhibition during behavior (Figure 5A, Figure S3L; see
367 Methods). Notably, optogenetic excitation of D2-SPNs for 1s right before lever extension
368 decreased the correct rate in both 2-s and 8-s trials (Figure 5F). In contrast, transient optogenetic
369 inhibition of D2-SPNs before behavioral choice increased correct rates for both 2-s and 8-s trials
370 (Figure 5G). These data suggest that opposite to the D1-SPN manipulation, optogenetic
371 stimulation of D2-SPNs impairs action selection, while inhibition of D2-SPNs facilitates
372 behavioral choice. These optogenetic results further unveil the distinct roles of direct vs. indirect
373 pathway in action selection, and are in line with the predictions from the Go/No-go (Figure 5H,
374 Figure S5M, N) but not the Co-activation model (Figure S5S, T).
375

376 **A 'Triple-control' model of basal ganglia circuit for action selection**

377 Our DT lesion experiments found that ablation of indirect pathway impairs action
378 selection (Figure 4O, P), as predicted from the Co-activation but not Go/No-go model (Figure
379 4S), while the optogenetic results suggested that inhibition of D2-SPNs enhances behavioral
380 choice (Figure 5G), a result in favor of the Go/No-go rather than Co-activation model (Figure
381 5H). We wonder whether these seemly discrepant effects are attributed to a more complex circuit

382 mechanism involving in the indirect pathway different from either the Go/No-go or Co-
383 activation model. To systematically investigate the cell type- and pathway-specific mechanisms
384 underlying action selection, we firstly add Go/No-go and Co-activation models together to
385 examine the whether the resulted combination model could explain the experimental
386 observations (Figure S4G). The lesion of D1-SPNs in the combination model indeed selectively
387 impaired choice in long interval trials (Figure S4H). However, the effect of D2-SPNs ablation in
388 the combination model was neutralized due to the opposing contributions from Go/No-go and
389 Co-activation models respectively (Figure S4I). Based on these simulation results, none of the
390 Go/No-go, Co-activation and combination models was able to fully capture the underlying
391 mechanism of basal ganglia in action selection. Inspired by the data in current experiments, we
392 decided to build a new computational model of the cortico-basal ganglia circuitry based on the
393 realistic neuroanatomy (Aoki et al., 2019; Mailly et al., 2003; Schmidt and Berke, 2017; Taverna
394 et al., 2008) and empirical neuronal physiology during action selection (Figures 1-3).
395 Different from the dual control of action by direct vs. indirect pathway in either the
396 Go/No-go or Co-activation model (Figure S4), our new model adds an additional layer of control
397 derived from the indirect pathway, thus called 'Triple-control' model for action selection.
398 Specifically, the new model consists of one direct pathway and two indirect pathways defined as
399 D2-SPN #1 and D2-SPN #2 two subpopulations, corresponding to the Co-activation and Go/No-
400 go functional modules, respectively (Figure 6A, B). In addition, the indirect pathway D2-SPNs
401 in the Co-activation module inhibits the indirect pathway D2-SPNs in the Go/No-go module
402 through the well-known D2-SPN collaterals with the properties of short-term depression in the
403 striatum (Gustafson et al., 2006; Schmidt and Berke, 2017; Taverna et al., 2008; Tecuapetla et al.,
404 2007) (Figure 6A; see Methods), providing asymmetric modulation to D2-SPN subgroups and

405 promoting Co-activation module as the dominant functional module at rest. In this 'Triple-
406 control' basal ganglia model, striatal D1- and D2-SPNs associated with left and right actions
407 receive excitatory inputs from corresponding cortical inputs (Figure 6A) to generate Type 1 and
408 Type 2 neuronal dynamics (Figure S6A-D) (Lo and Wang, 2006). The D1- and D2-SPNs then
409 regulate the SNr neuronal dynamics through the direct and indirect pathways, respectively
410 (Figure S6) (Albin et al., 1989; DeLong, 1990; Hikosaka et al., 2000; Mink, 1996). The net SNr
411 output (Figure S6F, I), which controls the downstream brainstem and thalamic circuits necessary
412 for action selection (Hikosaka, 2007; Lo and Wang, 2006; Redgrave et al., 1999), will determine
413 the final behavioral choice (Figure S6G, J). Our computational simulations showed that this
414 'Triple-control' network model could faithfully recapitulate the neuronal activity across the basal
415 ganglia circuitry and predict the behavioral choice (Figure S6).

416 To dissect the functional role of direct vs. indirect pathway in action selection, we
417 simulate the cell ablation experiments and examine the behavioral output in the 'Triple-control'
418 basal ganglia model. Ablation of D1-SPNs in the network model (Figure S6E) modulates both
419 Type 1 and Type 2 SNr dynamics but in different magnitude due to the biased striatal input to
420 SNr left output and mutual inhibition between SNr left vs. right outputs (Figure S6F; see
421 Methods). As a result, the lesion causes a downward shift in the net SNr output, especially
422 evident at the late section of 8 s (Figure S6G). This change in net SNr output predicts a
423 behavioral bias towards left choice as seen in the psychometric curve (Figure 6C), in consistent
424 with experimental results in mice with D1-SPNs ablation (Figure 4K). In contrast, ablation of
425 D2-SPNs in the network model (Figure S6H), by removing the indirect pathways of both the
426 Go/No-go and Co-activation modules, alters Type 1 and Type 2 SNr dynamics (Figure S6I) and
427 change the net SNr output dramatically around 2s as well as 8s (Figure S6J). The model thus

428 predicts behavioral choice deficits for both short and long trials during D2-SPNs ablation (Figure
429 6D), consistent with experimental observations (Figure 4P). Together, these data suggest that our
430 new 'Triple-control' basal ganglia model, based on realistic neuroanatomy and empirical
431 neuronal physiology, can perform action selection similar to the behavior of mice, and
432 successfully replicate the pathway-specific lesion effects on choice.

433 We further simulate the neuronal and behavioral effects of optogenetic manipulation of
434 D1- and D2-SPNs in the cortico-basal ganglia model. Consistent with the experimental results
435 (Figure 5D, F), optogenetic stimulation of D1-SPNs facilitates the ongoing choice (Figure 6E),
436 while optogenetic inhibition of D1-SPNs suppresses ongoing choice in the model (Figure 6G). In
437 addition, optogenetic stimulation of D2-SPNs impairs the ongoing choice and causes switching
438 (Figure 6F), while optogenetic inhibition of D2-SPNs facilitates ongoing choice, due to the now
439 dominant Go/No-go module mediated by the short-term depression of D2 collaterals in the
440 model (Figure 6H). Consistent with the experimental observations, the optogenetic inhibition
441 effect is opposite from the D2-SPNs cell ablation in the model (Figure 6D).

442 We next investigate how the striatum influence SNr outputs. Since the collateral
443 projection with STD in D2-SPNs is the key in our 'Triple-control' model to switch between
444 Go/No-go and Co-activation modules, we first built a motif of indirect pathway with two D2-
445 SPNs subgroups defined as D2-SPN #1 and D2-SPN #2 (Figure S7A). We tested this indirect
446 pathway motif with monotonic neural dynamics observed in experiments meanwhile simulating
447 the optogenetic activation at 1s and 7s (Figure S7D-I). The SNr therefore received more
448 activation at 1s than at 7s (Figure S7J, K), suggesting that the D2-SPNs with short-term
449 depression in collateral inhibition modulates SNr activities in a firing rate-dependent manner.

450 We next sought to test the model's predictions and experimentally investigate the
451 distinctions in modulating SNr activities between the direct and indirect pathways during action
452 selection. In order to manipulate D1- or D2-SPNs and monitor SNr responses at the same time,
453 we simultaneously implanted optogenetic fibers and recording array into striatum and SNr
454 respectively on a single mouse (Figure S7L). While the mice performing the 2-8s task,
455 optogenetic stimulation was delivered to activate either D1- or D2-SPNs. It was found that
456 optogenetic activation of D1- or D2-SPNs caused both inhibition and excitation in Type 1 and
457 Type 2 SNr neurons (Figure S7M-O). To further compare SNr activities responding to striatal
458 activation at different time points during the lever retraction period, for a given trial, we
459 activated D1-SPNs (or D2-SPNs) either at 1s or 7s after the lever retraction (Figure S7P-R). For
460 direct pathway, the change of FRI in SNr activities caused by activation of D1-SPNs showed no
461 significant difference between 1s and 7s (Figure S7P, S). For indirect pathway, activating D2-
462 SPNs at 1s caused smaller activation of FRI than at 7s in Type 1 SNr neurons (Figure S7Q),
463 whereas for Type 2 SNr neurons, activating D2-SPNs at 1s induced bigger FRI increase at 1s
464 than at 7s (Figure S7R). Overall, activating D2-SPNs tended to bias the firing rate downward at
465 1s but upward at 7s in Type 1 SNr neurons, which was counteractive to the decreasing tendency
466 of Type 1 SNr neuron (Figure S7T). In contrast, Type 2 SNr neurons showed higher FRI increase
467 and smaller decrease in response to activating D2-SPNs at 1s than at 7s, which was opposing to
468 the increasing dynamics of Type 2 SNr neurons (Figure S7T). This firing rate-dependent
469 modulation on SNr activities through indirect pathway is consistent with the computational
470 simulation (Figure S7J, K; Figure S8). Therefore, the underlying D2-SPNs collaterals might
471 indeed be a key mechanism contributing to the modulation of SNr activity and action selection in
472 vivo, as simulated in the 'Triple-control' model.

473 Taken together, our new 'Triple-control' basal ganglia model, based on realistic
474 neuroanatomy and empirical neurophysiology, successfully reproduces both the lesion and
475 optogenetic data we collected during the animal experiments. It could thus potentially provide
476 essential insights into the circuit mechanism of basal ganglia underlying action selection.
477

478 **Linear and nonlinear control of action selection by direct vs. indirect pathway**

479 To gain an overall picture of how basal ganglia control action selection, we run through
480 the model with a wide continuous range of manipulation to mimic the effects from lesion to
481 optogenetic inhibition and optogenetic activation (Figure 7A, B, E, F). The simulations of cell
482 ablation and bidirectional optogenetic manipulations of D1-SPNs activity in the model reveal no
483 significant effects at 2-s trials (Figure 7C), but a linear relationship between the neuronal activity
484 in direct pathway and the behavioral performance of choice in 8 s trials (Figure 7D), as observed
485 in animal experiments. It thus further confirms that direct pathway selects action and facilitates
486 ongoing choice, consistent with the predictions from both the classic Go/No-go and recent Co-
487 activation models (Figure 7I, Figure S9A-D) (Albin et al., 1989; DeLong, 1990; Hikosaka et al.,
488 2000; Mink, 1996).

489 In contrast, manipulations of D2-SPNs activity from cell ablation to optogenetic
490 inhibition and then optogenetic stimulation in the model demonstrate an inverted-U-shaped
491 nonlinear relationship between the neuronal activity in indirect pathway and action selection, for
492 both 2-s and 8-s trials (Figure 7G, H). Detailed analyses reveal that D2-SPNs ablation removes
493 both the Co-activation and Go/No-go module in the indirect pathway and leaves SNr activity
494 dictated by D1-SPN inputs. However, due to the inhibition from Co-activation to Go/No-go
495 module in the indirect pathway via D2-SPN collaterals and short-term plasticity of these

synapses (Figure S7A-C; see Methods), optogenetic manipulation of D2-SPNs differentially affects the D2-SPN subpopulations groups and promotes Go/No-go module to dominate the basal ganglia network (Figure S7C-S). This dynamic switch of dominance between Co-activation and Go/No-go modules on the basal ganglia network gives rise to a nonlinear relationship between D2-SPNs manipulation and the behavioral outcome (Figure 7J).

Note that when the same inputs were applied to the Go/No-go or Co-activation model alone, the behavioral performance in either model exhibits linear negative (Figure S9E) or positive correlation (Figure S9F) with D2-SPNs activity, respectively. Both our experimental and modeling results thus indicate that different from either the Go/No-go or Co-activation model, the indirect pathway regulates action selection in a nonlinear manner, depending on the state of the network and D2-SPNs activity level. Besides collaterals within D2-SPNs, other collateral connections, for example connections between D1-SPNs or connections between D1- and D2-SPNs, could also contribute to the regulation of action selection (Taverna et al., 2008). We tested our 'Triple-control' model with adding additional collateral connections as D1→D1 (Figure S10A-C), D1→D2 (Figure S10D-F) and D2→D1 (Figure S10G-I), respectively. It was found while these additional collaterals further quantitatively regulate action selection, the general principle of linear vs. nonlinear modulation of action selection by direct and indirect pathways still qualitatively hold (Figure S10). Interestingly, our current 'Triple-control' model can also replicate the behavioral effects of optogenetic manipulation of nigrostriatal dopamine on behavioral choice (Howard et al., 2017), and further unveils an inverted-U-shaped relationship between striatal dopamine concentration change and action selection (Figure S11). Together, these results suggest that there are multiple levels of interactions from D1- and D2-SPNs to

518 dynamically control SNr output, and the basal ganglia direct and indirect pathways distinctly
519 control action selection in a linear and nonlinear manner, respectively.
520
521 **Discussion**
522 Here, by using an internally-driven 2-8s action selection task in mice, we investigated the
523 function of basal ganglia direct and indirect pathways in mediating dynamic action selection. We
524 found that the neuronal activities in SNr, the major output of basal ganglia, directly reflect animals'
525 internal action selection process, other than simply time or value. It was also observed that the
526 striatum, the main input of basal ganglia, shares the similar action selection-related neuronal
527 dynamics with SNr and is needed for both learning and execution of proper action selection.
528 Furthermore, the striatal direct and indirect pathways exhibit distinct neuronal activity and during
529 manipulation, they have different functional effects on controlling action selection. Notably, the
530 experimental observations on the physiology and function of direct and indirect pathways cannot be
531 simply explained by either the traditional 'Go/No-go' model or the more recent 'Co-activation'
532 model. We proposed a new 'Triple-control' functional model of basal ganglia, suggesting a critical
533 role of dynamic interactions between different neuronal subpopulations within the indirect pathway
534 for controlling basal ganglia output and behavior. In the model, a 'center (direct pathway) – surround
535 (indirect pathway) – context (indirect pathway)' three layers of structure exerts dynamic control of
536 action selection, depending on the input level and network state. This new model respects the realistic
537 neuroanatomy, and can recapitulate and explain the essential in vivo electrophysiological and
538 behavioral findings. It also provides a new perspective on understanding many behavioral phenomena
539 involving in dopamine and basal ganglia circuitry in health and disease.

Our current 2-8s action selection task offers a unique opportunity to observe the animal's internal switch from one choice to another and monitor the underlying neuronal dynamics correspondingly. We observed two major types of monotonically-changing SNr neuronal dynamics during the internal choice switching, presumably one type associated with selecting one action and another with selecting the competing action, respectively. The classic view on SNr activity is that it tonically inhibits the downstream motor nuclei and releases action via disinhibition (Albin et al., 1989; DeLong, 1990; Hikosaka and Wurtz, 1983; Wurtz and Hikosaka, 1986). The increased response in SNr, however, could potentially inhibit the competing actions or the movements toward the opposing direction through projections to the contralateral brain regions like superior colliculus (Jiang et al., 2003). Here, we found that two subpopulations in SNr showed opposite monotonic firing change during the left-then-right choice, and notably, their neuronal dynamics switched when the animals performed the reversed version of task which requires a right-then-left choice. It thus suggests that these SNr neurons are indeed associated with different action options during choice behavior, and actively adjust their firing rates to facilitate respective action selection. Given the opposite neuronal dynamics and functionally antagonistic nature of these two groups of SNr neurons, we defined the net output of basal ganglia by the subtracting the neuronal activity between the two SNr subpopulations and correlated it with the behavioral choice. We found that the basal ganglia net output exhibited a tight correlation with the psychometric curve of behavioral choice, and faithfully represented a neural basis for the dynamic action selection process.

As one of the major input nuclei of basal ganglia, striatum influences SNr activity through direct/indirect pathways and undisputedly, plays an essential role in action selection (Ding and Gold, 2012; Geddes et al., 2018; Jin et al., 2014; Lauwereyns et al., 2002; Tai et al., 2012). By genetic manipulation and pharmacological inactivation, we showed that striatum is

563 indispensable for both learning action selection and the proper performance of learned behavioral
564 choice. The recording of striatal neuronal activity during action selection further revealed that
565 striatal spiny projection neurons share the similar types of neuronal dynamics as SNr. Through
566 optogenetic-tagging in freely behaving mice, we further found that striatal SPNs in the direct and
567 indirect pathways show distinct activity profile, with D1-SPNs representing a strong bias
568 towards the preferred choice, while D2-SPNs encoding two choices equally.

569 Two prevailing models have been proposed to explain the functional distinction between
570 D1- and D2-SPNs. The canonical model of the basal ganglia suggests that the D1- and D2-SPNs
571 play antagonistic roles in controlling action as mediating "Go" and "No-go" signals, respectively
572 (Albin et al., 1989; DeLong, 1990; Kravitz et al., 2010). A more recent model, however, implies
573 that as D1-SPNs initiate an action, D2-SPNs co-activate with D1-SPNs to inhibit other
574 competing actions (Cui et al., 2013; Hikosaka et al., 2000; Isomura et al., 2013; Jin et al., 2014;
575 Mink, 1996). Essentially, these two models agree upon the functional role of D1-SPNs in
576 releasing or facilitating the desired action, but contradict on the function of D2-SPNs on which
577 targeted action of inhibiting. Here, our in vivo recording data indicate that both D1- and D2-
578 SPNs share similar neuronal dynamics during action selection, and the neural activity alone is
579 not sufficient to separate and determine whether "Go/No-go" or "Co-activation" model is
580 supported (Cui et al., 2013; Isomura et al., 2013; Jin et al., 2014). To resolve the functional
581 distinction of the direct vs. indirect pathway, we applied a series of cell-type-specific
582 manipulations on striatal D1- and D2-SPNs during action selection behavior. First, we generated
583 mutant mice in which NMDA receptors are deleted from either striatal D1- or D2-SPNs (Geddes
584 et al., 2018; Jin et al., 2014). Both the D1-NR1 KO and D2-NR1 KO mice showed learning
585 deficits and behavioral choice impairments when tested with probe trials, suggesting that both

586 D1- and D2-SPNs are necessary for learning and performing action selection. Notably, while the
587 D1-NR1 KO mice are mostly impaired in the choice associated with 8s, a less-preferred option
588 compared to 2s, the D2-NR1 KO mice are compromised in both 2s and 8s choice. Additional
589 experiments with cell-type specific ablation further confirmed these results, consistent the
590 distinct neuronal activity profile in these two pathways revealed during in vivo neuronal
591 recording. While both the "Go/No-go" and "Co-activation" models predict the suppression of
592 D1-SPNs activity leads to impaired action selection, supported by current KO and cell-ablation
593 data, the manipulation experiments on D2-SPNs favor the "Co-activation" but not the "Go/No-
594 go" model which the latter suggests D2-SPNs ablation would improve rather than impair action
595 selection.

596 Next, we directly introduced transient bidirectional manipulations to D1- and D2-SPNs
597 activity by optogenetics while mice performing the task. Our findings revealed that activation or
598 inhibition of D1-SPNs increased and decreased the correct rate of choice respectively, suggesting
599 a facilitating role of direct pathway in action selection, which again fits well with the "Go/No-go"
600 as well as the "Co-activation" model. In contrast, optogenetic activation of D2-SPNs decreased
601 the correct rate of choice, while inhibition of D2-SPNs promoted the correct choice. These
602 results were supportive to the "Go/No-go" model but contradicted to the prediction of "Co-
603 activation" theory, which the latter predicts that activation of D2-SPNs inhibits competing
604 actions to facilitate desired choice, whereas inhibition of D2-SPNs releases competing actions
605 and compromises the ongoing choice.

606 In summary, neither "Go/No-go" nor "Co-activation" models could fully explain the
607 experimental results we found, particularly for experiments on D2-SPNs in the indirect pathway.
608 Through computer simulation, we further demonstrated that a simple additive combination of

609 “Go/No-go” nor “Co-activation” models by linear addition cannot reproduce all the experimental
610 observations. To resolve these theoretical difficulties, we proposed a new center-surround-
611 context “Triple-control” model of basal ganglia pathways for action selection. Specifically, two
612 subpopulations of D2-SPNs in the indirect pathway function as “Co-activation” and “Go/No-go”
613 modules respectively, and an activity-dependent inhibition from “Co-activation” to “Go/No-go”
614 module mediates the dynamic switch between the dominant module depending on the inputs and
615 network state. Due to the dominant “Co-activation” module in the default state, excessive
616 inhibition of D2-SPNs or ablating the entire indirect pathway eliminates the promotive
617 contribution and impairs action selection in the “Triple-control” model, consistent with the
618 experimental observations. In contrast, transient increase of D2-SPNs firing activity during
619 optogenetic stimulation introduces shift toward the “Go/No-go” dominance from the “Co-
620 activation” module via firing-rate-dependent short-term depression of the inhibitory synapses
621 between them, which amplifies the “No-go” signal and compromises action selection as
622 experimentally found. In contrast, transient decrease of D2-SPNs firing activity during
623 optogenetic inhibition results in disinhibition of “Go/No-go” module from inhibitory control of
624 “Co-activation” module, with an attenuated “No-go” signal which leads to better performance in
625 choice. These results from our new “Triple-control” model thus suggest that the basal ganglia
626 circuitry could be much more dynamic than previously thought, and it could employ a complex
627 mechanism of functional module reconfiguration for context- or state-dependent flexible control.
628 In the “Triple-control” model, we posited the collateral connections among striatal D2-
629 SPNs and its short-term plasticity could serve as an operational mechanism for the dominant
630 module switching. However, besides these well-known striatal local connections as one of the
631 simplest possible mechanisms, other anatomical circuits within basal ganglia circuitry could

632 potentially fulfill this functional role alone or additionally as well. For example, striatal D2-SPNs
633 project to external global pallidus (GPe) through striatopallidal pathway, and meanwhile they
634 receive arkypallidal projections from GPe to both the striatal SPNs and interneurons (Abdi et al.,
635 2015; Fujiyama et al., 2016; Mallet et al., 2016). It is thus also possible that the dynamic
636 interaction between "Co-activation" and "Go/No-go" modules is mediated through di-synaptic or
637 tri-synaptic modulation with GPe and/or striatal interneurons involved. Furthermore, in theory
638 this dynamic interaction between "Co-activation" and "Go/No-go" modules can also occur
639 outside striatum in the downstream nuclei including GPe and SNr, given their specific neuronal
640 subpopulations receiving inputs from corresponding striatal D2-SPNs subgroups and proper
641 collateral connections within the nuclei (Atherton et al., 2013; Cazorla et al., 2014; Fujiyama et
642 al., 2011; Lee et al., 2020; Wu et al., 2000). Considering the crucial role of dopamine in basal
643 ganglia circuitry, the new "Triple-control" model can also reproduce our previous experiments
644 results on the effect of nigrostriatal dopamine on action selection (Howard et al., 2017).
645 Importantly, it unveils that there is an inverted-U-shaped relationship between dopamine
646 concentration change and action selection (Cools and D'Esposito, 2011). The model simulation
647 suggests while moderate dopamine increase improves decision making, too much dopamine
648 changes, either increase or decrease, dramatically impairs the choice behavior. These results
649 might be able to explain some of behavioral observations involving in obscure decision making
650 under the influence of addictive substances.

651 Our findings also have important implications in many neurological and psychiatric
652 diseases. It was known that the loss of dopamine leads to hyperactivity of D2-SPNs and
653 disruption of local D2-SPNs collaterals in Parkinson's disease (Taverna et al., 2008; Wei and
654 Wang, 2016). These alterations will not only break the balance of direct vs. indirect pathway, but

655 also disrupt the multiple dynamic controls from the indirect pathway. The action selection will
656 thus be largely problematic, even with L-DOPA treatment, which might restore the dopamine
657 partially but not necessarily the altered basal ganglia circuitry and its circuit dynamics (Bastide et
658 al., 2015). The current "Triple-control" model also provides some mechanistic insights into the
659 inhibitory control deficits observed Schizophrenia (Taverna et al., 2008; Wei and Wang, 2016).
660 For instance, an increase in the density and occupancy of the striatal D2 receptors (D2R) has
661 been frequently reported in schizophrenia patients (Abi-Dargham et al., 2000; Howes and Kapur,
662 2009; Laruelle et al., 1997; Wong et al., 1986). Many antipsychotic medications primarily aim to
663 block the D2R (la Fougere et al., 2005; Lally and MacCabe, 2015; Yokoi et al., 2002), but the
664 drug dose is the key to the treatment and severer adverse effects are associated with overdose of
665 D2R antagonism (Levine and Ruha, 2012). In addition, prolonged exposure to antipsychotics
666 often causes extrapyramidal symptoms, including Parkinsonian symptoms and tardive dyskinesia
667 (Jarskog et al., 2007; Seeman, 2002). The dose-dependent effects when modulating D2R were
668 also found in cognitive functions such as serial discrimination, in which relatively low and high
669 dose of D2R agonist in striatum impair the performance in the discrimination task, while the
670 intermediate dose of D2R agonist produces significant improvement (Cools and D'Esposito,
671 2011; Goldman-Rakic et al., 2000; Horst et al., 2019; Mattay et al., 2003). These observations
672 thus further underscore the dynamic interplays and complexity of basal ganglia pathways in
673 action control, as demonstrated in current study and the new triple-control functional model.
674

675 **Acknowledgments:** The authors would like to thank Tom Jessell and members of Jin lab for
676 discussion and comments on the manuscript. This research was supported by grants from the
677 NIH (R01NS083815), the Dystonia Medical Research Foundation and the McKnight Memory
678 and Cognitive Disorders Award to X.J.

679

680 **Author Contributions:** X.J. conceived the project. X.J. and H.L. designed the experiments. H.L.
681 performed the experiments and analyzed the data. X.J. supervises all aspects of the work. H.L.
682 and X.J. wrote the manuscript.

683

684 **Conflicts of Interest:** None of the authors declare any conflict of interest, financial or otherwise.

685

686 **Figure Legends:**

687

688 **Figure 1. The neuronal dynamics in SNr during the 2-8 s action selection task.** (A)
689 Schematic diagram for the design of 2-8 s task. (B) Correct rate for wild type mice across 14
690 days training (n = 10 mice, one-way repeated-measures ANOVA, significant effect of training
691 days, $F_{13,117} = 32.54$, $p < 0.0001$). (C) Movement trajectory of an example mouse in correct
692 (left panel) and incorrect (right panel) 8-s trials (gray line: trajectory of each trials; red/black line:
693 the average trajectory). (D) Diagram of electrode array implanted into substantia nigra pars
694 reticulata (SNr). (E) Firing Rate Index (FRI) of neuronal activity for all task-related SNr neurons
695 in correct 8-s trials. The magnitude of FRI is color coded and the SNr neurons are classified as
696 four different types based on the activity dynamics. (F-I) Averaged FRI for Type 1 (F), Type 2
697 (G), Type 3 (H), Type 4 (I) of SNr neurons in correct (red) and incorrect 8-s trials (gray). (J) The
698 proportion of four types of SNr neurons. Type 1 and Type 2 are major types and significantly
699 more than Type 3 and Type 4 (Z-test, $p < 0.05$). (K) Integrated SNr output defined as the
700 subtraction of averaged FRI between Type 1 and Type 2 SNr neurons. (L) Averaged
701 psychometric curve (n = 10 mice) of choice behavior. (M) The correlation between the Type 1
702 and Type 2 FRI subtraction and the behavioral choice ($R = 0.98$, $p < 0.0005$). Error bars denote
703 s.e.m., same for below unless stated otherwise.

704

705 **Figure 2. SNr neuronal dynamics reflect action selection but not interval time or reward**
706 **value.** (A) Task diagram of 2-8 s control task with 10% 16-s probe trials. (B) Percentage of
707 behavioral choice in 2-s, 8-s and 16-s trials (blue: left choice; red: right choice) (n = 9 mice,
708 paired t-test, $p < 0.05$). (C) Movement trajectory of an example mouse in 16-s trials (blue: left
709 choice; red: right choice). (D) Averaged SNr Type 1 FRI in 16-s trials (red: left choice; black:

710 right choice). Firing rates from 8s to 16s (highlighted area) are compared between left and right
711 choice (n = 26 neurons, two-way repeated-measures ANOVA, significant difference between left
712 and right choices, $F_{1,25} = 6.646$, $p = 0.016$). (E) Averaged SNr Type 2 FRI in 16-s trials (red:
713 left choice; black: right choice). Firing rates from 8s to 16s are compared between left and right
714 choice (n = 16 neurons, two-way repeated-measures ANOVA, significant difference between left
715 and right choices, $F_{1,15} = 5.785$, $p = 0.029$). (F) Subtraction of FRI for SNr Type 1 and Type 2
716 neurons in 16-s probe trials (red: left choice; black: right choice). (G) Task design of 2-8 s
717 standard task. (H) Percentage of behavioral choice in 2-s and 8-s trials (blue: left choice; red:
718 right choice) (n = 6 mice, paired t-test, $p < 0.05$). (I) Movement trajectory of an example mouse
719 in 8-s trials (blue: left choice; red: right choice). (J) Task design of reversed 2-8 s task. (K)
720 Percentage of behavioral choice in 2-s and 8-s trials in the reversed 2-8 s task (blue: left choice;
721 red: right choice) (n = 6 mice, paired t-test, $p < 0.05$). (L) Movement trajectory of the same
722 mouse as (I) in 8-s trials in the reversed 2-8 s task (blue: left choice; red: right choice). (M)
723 Averaged FRI of the SNr Type 1 neurons in correct 8-s trials (n = 14 neurons). (N) Averaged
724 FRI of the SNr Type 2 neurons in correct 8-s trials (n = 11 neurons). (O) Integrated SNr output
725 as the subtraction of FRI for SNr Type 1 (M) and Type 2 neurons (N) in the standard 2-8 s task.
726 (P) Averaged FRI of the same neurons as (M) in correct 8-s trials of the reversed 2-8 s task. (Q)
727 Averaged FRI of the same neurons as (N) in correct 8-s trials of the reversed 2-8 s task. (R)
728 Integrated SNr output as the subtraction of FRI for SNr Type 1 (P) and Type 2 neurons (Q) in the
729 reversed 2-8 s task.
730
731 **Figure 3. Neuronal activity of striatal D1- and D2-SPNs during action selection.** (A) FRI of
732 neuronal activity for all task-related SPNs in correct 8-s trials. SPNs were classified as Type 1 - 4.

733 (B-E) Averaged FRI for Type 1 (B), Type 2 (C), Type 3 (D), Type 4 (E) of SPNs in correct (red)
734 and incorrect 8-s trials (gray). (F) Diagram of simultaneous neuronal recording and optogenetic
735 identification of D1- vs. D2-SPNs in dorsal striatum. (G) Top panel: Raster plot for a
736 representative D1-SPN response to 100 ms optogenetic stimulation. Each row represents one
737 trial and each black dot represents a spike. Bottom panel: Peristimulus time histogram (PETH)
738 aligned to light onset at time zero. (H) PETH for the same neuron as shown in (G) with a finer
739 time scale. (I) Distribution of light response latencies for D1- and D2-SPNs. (J) Action potential
740 waveforms of the same neuron in (G) for spontaneous (black) and light-evoked (orange) spikes
741 ($R = 0.998$, $P < 0.0001$, Pearson's correlation). (K) Principal component analysis (PCA) of
742 action potential waveforms showing the overlapped clusters of spontaneous (black) and light-
743 evoked (orange) spikes. (L) Proportion of D1-SPN subtypes. Type 1 neurons are significantly
744 more than other three types of neurons in D1-SPNs (Z-test, $p < 0.05$). (M) Averaged FRI for
745 Type 1 (blue) and Type 2 (red) D1-SPNs in correct 8-s trials. (N) Proportion of D2-SPN
746 subtypes. (O) Averaged FRI for Type 1 (blue) and Type 2 (red) D2-SPNs in correct 8-s trials.
747

748 **Figure 4. Selective genetic knockout and ablation of D1- or D2-SPNs distinctly alters action**
749 **selection.** (A) Correct rate of control (n = 11 mice) and D1-NR1 KO mice (n = 16) in 2-8 s task
750 during 14 days training (two-way repeated-measures ANOVA, significant difference between
751 control and KO mice, $F_{1,25} = 10.8$, $p = 0.003$). (B) Correct rate of control (n = 17) and D2-NR1
752 KO mice (n = 10) in 2-8 s task during 14 days training (two-way repeated-measures ANOVA,
753 significant difference between control and KO mice, $F_{1,25} = 8.728$, $p = 0.007$). (C) The
754 psychometric curve for control (n = 11) and D1-NR1 KO mice (n = 16) (two-way repeated-
755 measures ANOVA, significant difference between control and KO mice, $F_{1,25} = 12.27$, p =

0.002). (D) The psychometric curve for control (n = 17) and D2-NR1 KO mice (n = 10) (two-way repeated-measures ANOVA, significant difference between control and KO mice, $F_{1,25} = 9.64$, $p = 0.005$). (E) Schematic of muscimol infusion into the dorsal striatum in trained mice. (F) Correct rate for control (black: pre-muscimol, gray: post-muscimol) and mice with muscimol infusion (magenta) in dorsal striatum (n = 9 mice, paired t-test, $p < 0.01$). (G) The psychometric curve for control (n = 9 mice, black: pre-muscimol, gray: post-muscimol control) and mice with muscimol infusion (n = 9 mice, magenta) in dorsal striatum (two-way repeated-measures ANOVA, significant difference between control and muscimol infusion, $F_{2,16} = 11.74$, $p = 0.0007$). (H) Timeline for selective diphtheria toxin (DT) ablation experiments. (I) Schematic of diphtheria toxin receptor (DTR) virus (AAV-FLEX-DTR-GFP) injection in dorsal striatum of D1-Cre mice. (J) Correct rate for control (n = 9 mice) and mice with dorsal striatum D1-SPNs ablation (D1-DTR, n = 8 mice) (two-sample t-test, $p = 0.0016$). (K) The psychometric curve for control (n = 9 mice) and D1-SPNs ablation mice (n = 8 mice) (two-way repeated-measures ANOVA, main effect of ablation, $F_{1,15} = 1.84$, $p = 0.195$; interaction between trial intervals and ablation, $F_{6,90} = 4.14$, $p = 0.001$). (L) Movement trajectory of a control mouse in 8-s trials. (M) Movement trajectory of a D1-DTR mouse in 8-s trials. (N) Schematic of diphtheria toxin receptor (DTR) virus (AAV-FLEX-DTR-GFP) injection in dorsal striatum of A2a-Cre mice. (O) Correct rate for control (n = 8 mice) and mice with dorsal striatum D2-SPNs ablation (D2-DTR, n = 8 mice) (two-sample t-test, $p = 0.005$). (P) The psychometric curve for control (n = 9 mice) and D2-SPNs ablation mice (n = 8 mice) (two-way repeated-measures ANOVA, main effect of ablation, $F_{1,15} = 0.477$, $p = 0.5$; interaction between trial intervals and ablation, $F_{6,90} = 12.6$, $p < 0.001$). (Q) Movement trajectory of a control mouse in 8-s trials. (R) Movement trajectory of a D2-DTR mouse in 8-s trials. (S) Schematic of center-surround receptive field diagram for

779 Go/No-Go (left) and Co-activation (right) models. '+' indicates facilitating effect to selection. '-'
780 indicates inhibitory effect to selection.
781
782 **Figure 5. Optogenetic manipulation of D1- vs. D2-SPNs differently regulates action**
783 **selection.** (A) Schematic of optic fiber implantation for experimentally optogenetic excitation or
784 inhibition of D1- or D2-SPNs in the dorsal striatum. (B, C) Schematic for optogenetic excitation
785 (B) and inhibition (C) of D1-/D2-SPNs for 1 s right before lever extension in 2-8 s task. (D)
786 Change of correct rate for optogenetic excitation of D1-SPNs in 2-s and 8-s trials ($n = 11$ mice,
787 one-sample t-test, 2-s trials: $p = 0.248$; 8-s trials: $p < 0.05$). (E) Change of correct rate for
788 optogenetic inhibition of D1-SPNs in 2-s and 8-s trials ($n = 6$ mice, one-sample t-test, 2-s trials:
789 $p = 0.557$; 8-s trials: $p < 0.05$). (F) Change of correct rate for optogenetic excitation of D2-SPNs
790 in 2-s and 8-s trials ($n = 8$ mice, one-sample t-test, 2-s trials: $p < 0.05$; 8-s trials: $p < 0.05$). (G)
791 Change of correct rate for optogenetic inhibition of D2-SPNs in 2-s and 8-s trials ($n = 5$ mice,
792 one-sample t-test, 2-s trials: $p < 0.05$; 8-s trials: $p < 0.05$). (H) Schematic of center-surround
793 receptive field diagram for Go/No-Go (left) and Co-activation (right) models. '+' indicates
794 facilitating effect to selection. '-' indicates inhibitory effect to selection.
795
796 **Figure 6. A triple-control computational model of basal ganglia direct and indirect**
797 **pathways for action selection.** (A) Network structure of the cortico-basal ganglia model based
798 on realistic anatomy and synaptic connectivity. (B) Schematic of center-surround-context
799 receptive field diagram for 'Triple-control' model. '+' indicates facilitating effect to selection. '-'
800 indicates inhibitory effect to selection. (C) The psychometric curves of behavioral output in
801 control (black) and D1-SPNs ablation condition (blue) in 'Triple-control' model ($n = 10$, two-

802 way repeated-measures ANOVA, main effect of ablation, $F_{1,18} = 98.72$, $p < 0.0001$; interaction
803 between trial intervals and ablation, $F_{6,108} = 7.799$, $p < 0.0001$). (D) The psychometric curves
804 of behavioral output in control (black) and D2-SPNs ablation condition (red) in 'Triple-control'
805 model ($n = 10$, two-way repeated-measures ANOVA, main effect of ablation, $F_{1,18} = 99.54$, $p <$
806 0.0001; interaction between trial intervals and ablation, $F_{6,108} = 177.6$, $p < 0.0001$). (E) Change
807 of correct rate for optogenetic excitation of D1-SPNs in 2-s and 8-s trials ($n = 10$, one-sample t-
808 test, 2-s trials: $p = 0.407$; 8-s trials: $p < 0.05$). (F) Change of correct rate for optogenetic
809 excitation of D2-SPNs in 2-s and 8-s trials ($n = 10$, one-sample t-test, 2-s trials: $p < 0.05$; 8-s
810 trials: $p < 0.05$). (G) Change of correct rate for optogenetic inhibition of D1-SPNs in 2-s and 8-s
811 trials ($n = 10$, one-sample t-test, 2-s trials: $p = 0.28$; 8-s trials: $p < 0.05$). (H) Change of correct
812 rate for optogenetic inhibition of D2-SPNs in 2-s and 8-s trials ($n = 10$, one-sample t-test, 2-s
813 trials: $p < 0.05$; 8-s trials: $p < 0.05$).
814
815 **Figure 7. Computational modeling reveals direct and indirect pathways regulating action**
816 **selection in a distinct manner.** (A) Schematic for manipulation of D1-SPNs in 'Triple-control'
817 model. (B) Schematic of manipulation of D1-SPNs in the center-surround-context receptive field
818 diagram for 'Triple-control' model. '+' indicates facilitating effect to selection. '-' indicates
819 inhibitory effect to selection. (C) Correct rate change in 2s trials when manipulating D1-SPNs
820 with different manipulation strengths ($n = 10$, one-way repeated-measures ANOVA, effect of
821 manipulation strength, $F_{36,324} = 1.171$, $p = 0.238$). (D) Correct rate change in 8s trials when
822 manipulating D1-SPNs with different manipulation strengths ($n = 10$, one-way repeated-
823 measures ANOVA, effect of manipulation strength, $F_{36,324} = 13.71$, $p < 0.0001$). (E) Schematic
824 for optogenetic manipulation of D2-SPNs in 'Triple-control' model. (F) Schematic of

825 manipulation of D2-SPNs in the center-surround-context receptive field diagram for 'Triple-
826 control' model. '+' indicates facilitating effect to selection. '-' indicates inhibitory effect to
827 selection. (G) Correct rate change in 2s trials when manipulating D2-SPNs with different
828 manipulation strengths ($n = 10$, one-way repeated-measures ANOVA, effect of manipulation
829 strength, $F_{36,324} = 59.13$, $p < 0.0001$). (H) Correct rate change in 8s trials when manipulating
830 D2-SPNs with different manipulation strengths ($n = 10$, one-way repeated-measures ANOVA,
831 effect of manipulation strength, $F_{36,324} = 40.75$, $p < 0.0001$). (I) Diagram of linear modulation
832 of direct pathway. (J) Diagram of nonlinear modulation of indirect pathway.
833
834

STAR METHODS

Animals

All experiments were approved by the Salk Institute Animal Care, and done in accordance with NIH guidelines for the Care and Use of Laboratory Animals. Experiments were performed on both male and female mice, at least two months old, housed on a 12-hour light/dark cycle. C57BL/6J mice were purchased from the Jackson Laboratory at 8 weeks of age and used as wildtype mice. BAC transgenic mice expressing cre recombinase under the control of the dopamine D1 receptor (referred as D1-cre, GENSAT: EY217; minimal labeling in cortex; mostly dorsal labeling in striatum) or the A2a receptor (referred as A2a-cre, GENSAT: KG139) promoter were obtained from MMRRC, and either crossed to C57BL/6 or Ai32 (012569) mice obtained from Jackson Laboratory (Cui et al., 2013; Geddes et al., 2018; Jin et al., 2014; Madisen et al., 2012; Tecuapetla et al., 2016). Striatal neuron-type-specific NMDAR1-knockout (referred as NR1-KO) and littermate controls were generated by crossing D1-cre and A2a-cre mice with NMDAR1-loxP (also denoted as Grin1 flox/flox in the Jackson Laboratory database) mice. The behavioral experiments using NR1-KO mice were performed on 8 to 12 weeks old D1/A2a-cre + / NMDAR1-loxP homozygous mice and their littermate controls, including D1/A2a-cre +, D1/A2a-cre + / NMDAR1-loxP heterozygous and NMDAR1-loxP homozygous mice. There was no difference between the three control groups, so the data were combined.

Behavior task

Mice were trained on a temporal bisection task in the operant chamber (21.6 cm L × 17.8 cm W × 12.7 cm H), which was isolated within a sound attenuating box (Med-Associates, St. Albans, VT). The food magazine was located in the middle of one wall, and two retractable

858 levers were located to the left and right side of the magazine. A house light was (3 W, 24
859 V) mounted on the opposite wall of the magazine. Sucrose solution (10 %) was delivered
860 into a metal bowl in the magazine through a syringe pump. When a training session
861 started, the house light was turned on and two levers were extended. After a random time
862 interval (30 s on average), left and right levers were retracted and extended
863 simultaneously. Mice were able to make a choice by pressing either left or right lever.
864 Only the very first lever press after levers extension was registered as animals' choice. If
865 the interval between the levers retraction and extension was 2s, then only the left lever
866 press was active to trigger the sucrose reward; if the interval between the lever retraction
867 and extension was 8s, then only the right lever press was active to trigger the sucrose
868 reward (Howard et al., 2017). There was no punishment when mice made an unrewarded
869 choice. 2s-trial and 8s-trial were randomized and interleaved by random inter-trial
870 intervals (30 s on average). The mice were also trained in the reversed 2-8s task. In the
871 reversed 2-8s task, if the interval between the levers retraction and extension was 2s, then
872 only the right lever press was active to trigger the sucrose reward; if the interval between
873 the lever retraction and extension was 8s, then only the left lever press was active to
874 trigger the sucrose reward. Representative behavioral tracks were captured by EthoVision
875 (Noldus).
876
877 **Behavior training**
878 Mice were placed on food restriction throughout the training, and fed daily after
879 the training sessions with ~2.5 g of regular food to allow them to maintain a body weight
880 of around 85 % of their baseline weight. Training started with continuous reinforcement

881 (CRF), in which animals obtained a reinforcer after each lever press. The session began with the
882 illumination of the house light and extension of either left or right lever, and ended with the
883 retraction of the lever and the offset of the house light. On the first day of CRF, mice received 5
884 reinforcers on left and right lever. On the second day of CRF, mice received 10 reinforcers on
885 left and right lever. On the third day of CRF, mice received 15 reinforcers on left and right lever.
886 The order of left lever CRF and right lever CRF on each day was randomized across all the CRF
887 training days. After the training of CRF, animals started on the temporal bisection task (day 1).
888 Mice were trained in the temporal bisection task for 14 consecutive days. On each day, there
889 were 240 trials with 2s-trial and 8s-trial randomly intermixed at 50:50. After 14 days training,
890 mice received an interval discrimination test, in which 20% of 2s/8s trials were replaced by
891 probe trials. In probe trials, the levers retraction intervals were randomly selected from 2.3s, 3.2s,
892 4s, 5s and 6.3s. Neither choice in the probe trials was rewarded. Mice received 4 days of test,
893 interleaved by training days without probes. The animals were trained daily without interruption
894 and every day the training started approximately at same time (Howard et al., 2017). All
895 timestamps of lever presses, magazine entries and licks for each animal were recorded with 10
896 ms resolution. The training chambers and procedures for NR1-KO mice and their littermate
897 controls were exactly the same for C57BL/6J mice.

898 For the reversed task training, mice were trained in both the 2-8 s control task and
899 reversed version of 2-8s task on the same day for at least 14 days. During each day, mice were
900 trained in the 2-8s task first, and then mice were put back in the home cage for a 3-4 hours rest.
901 After the rest period, the same mice were trained in the reversed 2-8s task. The order of these
902 two tasks is fixed throughout the 14 days training.

903 **Surgery**

904 For in vivo electrophysiological data recording, each mouse was chronically
905 implanted with an electrode array which consists of an array of 2 rows × 8 columns
906 Platinum-coated tungsten microwire electrodes (35 μm diameter) with 150 μm spacing
907 between microwires in a row, and 250 μm spacing between 2 rows. The craniotomies
908 were made at the following coordinates: 0.5 mm rostral to bregma and 1.5 mm laterally
909 for dorsal striatum; 3.4 mm caudal to bregma and 1.0 mm laterally for SNr (Jin and Costa,
910 2010; Jin et al., 2014). During surgeries, the electrode arrays were gently lowered ~ 2.2
911 mm from the surface of the brain for dorsal striatum and ~ 4.3 mm for SNr, while
912 simultaneously monitoring neural activity. Final placement of the electrodes was
913 monitored online during the surgery based on the neural activity, and then confirmed
914 histologically at the end of the experiment after perfusion with 10 % formalin, brain
915 fixation in a solution of 30 % sucrose and 10 % formalin, followed by cryostat sectioning
916 (coronal slices of 40 - 60 μm).
917 For the cell type identification in striatum, the cre-inducible adeno-associated
918 virus (AAV) vector carrying the gene encoding the light-activated cation channel
919 channelrhodopsin-2 (ChR2) and a fluorescent reporter (DIO-ChR2-YFP/DIO-ChR2-
920 mCherry) was stereotactic injected into the dorsal striatum of D1-Cre or A2a-Cre mice,
921 enabling cell-type-specific expression of ChR2 in striatal D1-expressing or D2-
922 expressing projection neurons (at exactly the same coordinates of electrode array
923 implantation in striatum stated above). DIO-ChR2-YFP/DIO-ChR2-mCherry virus (1 μl,
924 one site, 10^{12} titer) was injected through a micro-injection Hamilton syringe, with the
925 whole injection taking ~10 min in total. The syringe needle was left in the position for 5–
926 10 min after the injection and then slowly moved out. Following viral injections or for

927 mice genetically expressing ChR2 under cre control (D1-Ai32, A2a-Ai32), electrode was
928 implanted as previously described (Geddes et al., 2018; Jin et al., 2014). The electrode array was
929 the same as used for dorsal striatum recording, but with a guiding cannula attached (Innovative
930 Neurophysiology) terminating ~300 μm above the electrode tips, and was implanted into the
931 same site after virus injection, allowing for simultaneous electrophysiological recording and light
932 stimulation. Following the implantation, a medal needle was inserted in the cannula and mice
933 were placed in the home cage for 2 weeks, allowing both viral expression and surgery recovery,
934 before further training and recording experiments.

935 For the optogenetic manipulation in striatum, we injected the AAV virus carrying the
936 gene for coding ChR2 (DIO-ChR2-YFP/DIO-ChR2-mCherry) or Halorhodopsin (DIO-
937 eNpHR3.0-eYFP). Virus was injected bilaterally at 0.5 mm rostral to bregma, 2 mm laterally and
938 ~ 2.2 mm from the surface of the brain with 1 μl per site. 10 min after the virus injection, we
939 bilaterally implanted optical fiber units in dorsal striatum to the same site as virus injection. An
940 optical fiber unit was made by threading a 200-μm diameter, 0.37 NA optical fiber (Thor Labs)
941 with epoxy resin into a plastic ferrule (Geddes et al., 2018; Howard et al., 2017). Optical fiber
942 units were then cut and polished before the implantation.

943 For muscimol infusion in striatum, we bilaterally implanted cannulas (Plastics One, VA)
944 in wildtype mice to the site at 0.5 mm rostral to bregma, 2 mm laterally and ~ 2.2 mm from the
945 surface of the brain. After the implantation, cannulas were covered by dummy cannulas. Mice
946 were placed in the home cage for 2 weeks, allowing surgery recovery, before further training and
947 muscimol experiments.

948 For striatal neuron-type-specific ablation experiments, D1-cre and A2a-cre mice were
949 stereotaxically injected with a cre-inducible adeno-associated virus carrying the diphtheria toxin

950 receptor (Azim et al., 2014; Geddes et al., 2018) (AAV9-FLEX-DTR-GFP; Salk GT3
951 Core, CA). Virus was injected in eight different sites. We used two sets of AP/ML
952 coordinates for each hemisphere followed by two DV depths at each AP/ML site. The
953 coordinates were +0.9 mm AP, ±1.6 mm ML, -2.2 and -3.0 mm DV and 0.0 mm AP, ±2.1
954 mm ML, -2.2 and -3.0 mm DV. A Hamilton syringe was used to inject 1 uL at the four -
955 3.0 mm DV sites and another 0.5 uL at the four -2.2 mm DV sites for a total of 3 uL
956 injected per hemisphere. Following each injection, the needle was left in place for ~5
957 minutes and then raised over ~5 minutes. This same protocol was used for each injection
958 site.
959
960 **Muscimol infusion**
961 We daily trained wildtype mice with guide cannulas (Plastics One, VA) implanted
962 until they achieved at least 80% correct rate for 3 consecutive days, we started muscimol
963 infusion experiments. Muscimol was dissolved in saline before infusion (Sigma-Aldrich;
964 0.05 ug/ul). For the infusions, mice were briefly anesthetized with isoflurane and
965 injection cannulas (Plastics One, VA) were bilaterally inserted into the guide cannulas,
966 with the injection cannulas projecting 0.1 mm beyond the implanted guide cannulas. Each
967 injection cannula was attached to an infusion pump (BASi, IN) via polyethylene tubing.
968 Animals were bilaterally infused with 200 nL of liquid (saline or muscimol) followed by
969 a five-minute waiting period before removal of the infusion cannulas. Mice were returned
970 to their home cage and started in the behavioral task 30 minutes after infusion (Geddes et
971 al., 2018). To estimate the effects of muscimol on choice, we repeated saline controls and

972 muscimol infusions at least 3 times on a single mouse to gain enough probe trials for
973 psychometric curve fitting.
974
975 **DTR-mediated cell ablation**
976 For striatal neuron-type-specific ablation experiments, D1-cre and A2a-cre were injected
977 with AAV9-FLEX-DTR-GFP in striatum using the same coordinates described above. After
978 three-week recovery, mice were food-restricted and, following completion of CRF, underwent
979 training in the 2-8s task for two weeks. Immediately after day 14 of 2-8s task training, mice were
980 randomly divided into control and treatment groups. Treatment mice were administered mice 1
981 ug of diphtheria toxin (DT) dissolved in 300 uL of phosphate buffered saline (PBS) via
982 intraperitoneal (IP) injection on two consecutive days (Azim et al., 2014; Geddes et al., 2018),
983 whereas control mice received IP injections of PBS. To allow for neuronal ablation, animals
984 were stopped in behavioral training and placed back on food. Animals resumed 2-8s task training
985 with probe trials 14 days after the first DT or PBS injection.
986
987 **Neural recordings during the task**
988 The mice with electrode array implanted were trained with exactly the same procedure as
989 described above. When mice performed the 2-8s task with 80% correct rate for 3 consecutive
990 days, we connected the array with recording cable and continued training until mice adapted to
991 the mechanics of the recording cable and were able to maintain the correct rate greater than 80%
992 (Howard et al., 2017).
993 Neural activity was recorded using the MAP system (Plexon Inc., TX). The spike
994 activities were initially online sorted using a sorting algorithm (Plexon Inc., TX). Only spikes

995 with a clearly identified waveforms and relatively high signal-to-noise ratio were used for
996 further analysis. After the recording session, the spike activities were further sorted to
997 isolate single units by offline sorting software (Plexon Inc., TX). Single units displayed a
998 clear refractory period in the inter-spike interval histogram, with no spikes during the
999 refractory period (larger than 1.3 ms) (Geddes et al., 2018; Howard et al., 2017; Jin and
1000 Costa, 2010; Jin et al., 2014). All the timestamps of animal's behavioral events were
1001 recorded as TTL pulses which were generated by a Med-Associates interface board and
1002 sent to the MAP recording system through an A/D board (Texas Instrument Inc., TX).
1003 The animal's behavioral timestamps during the training session were synchronized and
1004 recorded together with the neural activity.
1005
1006 **Neural dynamic analysis**
1007 The animal's behavior taking place during the lever retraction time period was
1008 critical to the choice to be made, so we focused on the analysis of the neural activity from
1009 levers retraction to levers extension. Neuronal firings aligned to lever retraction were
1010 averaged across trials in 20-ms bins, and smoothed by a Gaussian filter (Gaussian filter
1011 window size = 10, standard deviation = 5) to construct the peri-event histogram (PETH).
1012 The neurons showing significant firing changes during the lever retraction period were
1013 defined as task-related neurons (ANOVA); those showing no significant changes were
1014 defined as non-task-related neurons, which were not included in the further dynamic
1015 analysis.
1016 During 2s trials, mice behaved exactly the same as they did during the 0s - 2s
1017 period in the rewarded 8s trials, so we mainly analyzed firing activities in 8s trials. To

1018 avoid confounding effect by the sensory responses triggered by the lever retraction, only neural
1019 activity from 1s to 8s following lever retraction were included (Howard et al., 2017). Then we
1020 calculated firing rate index (FRI) based on the PETH from 1s to 8s for each individual neuron as
1021 follows:

$$\mathrm{FRI} = \frac{\mathrm{PETH} - \mathrm{mean}(\mathrm{PETH})}{\mathrm{std}(\mathrm{PETH})}$$

1022 We then used principal component analysis (PCA) and classification algorithm, a build-in
1023 toolbox in Matlab, to classify the task-related neurons based on types of dynamics. For striatum
1024 and SNr, we used the same algorithm to classify neurons, and we found the same types of
1025 dynamics in striatum and SNr: Type 1, monotonic decreasing; Type 2, monotonic increasing;
1026 Type 3, peak at around 4s; Type 4, trough at around 4s.
1027

1028 **Cell type classification**

1029 In dorsal striatum, we classified neurons as putative striatal projection neurons (SPNs) if
1030 they showed waveform trough half-width between 100 μs and 250 μs and the baseline firing rate
1031 less than 10 Hz. In substantia nigra pars reticulate (SNr), neurons with firing rate higher than 15
1032 Hz were classified as putative SNr GABA neurons, which are most likely the SNr projection
1033 neurons, because the percentage of GABAergic interneurons in the SNr is rather small (Deniau
1034 JM, 2007; Jin and Costa, 2010).

1035 To further identify the D1 and D2 SPNs in striatum, we utilized cre-loxp technique to
1036 exclusively express ChR2 on D1-SPNs or D2-SPNs by injecting the AAV-DIO-ChR2-YFP/
1037 AAV-DIO-ChR2-mCherry virus into dorsal striatum or genetically express ChR2 by D1-Ai32
1038 and A2a-Ai32. Optical stimulation on ChR2-expressed cells is able to directly evoke spiking
1039 activity with short latency (Geddes et al., 2018; Jin and Costa, 2010; Jin et al., 2014). Before the

1040 training session, we connected the recording cable to the electrode array for neuronal
1041 recording and inserted an optic fiber through the cannula attached to the array to conduct
1042 light into striatum for light stimulation. For better monitoring of the same cells stably
1043 during behavioral training and the later optogenetic identification, the optic fiber was
1044 well fixed to the array. After each training session, we delivered blue light stimulation
1045 through the optic fiber from a 473-nm laser (Laserglow Technologies) via a fiber-optic
1046 patch cord, and simultaneously recorded the neuronal responses, to testify the molecular
1047 identity of cells previously recorded during the behavioral training. The stimulation
1048 pattern was 100-ms pulse width with 4s interval. The stimulation pattern was repeatedly
1049 delivered for 100 trials. We very carefully regulated the laser power to a relatively low
1050 level for each individual recording session which was strong enough to evoke reliable
1051 spikes in a small population of neurons recorded from certain electrodes, since high laser
1052 powers usually induced an electrical signal much larger and very different from the spike
1053 waveforms previously recorded in the same electrode, presumably resulting from
1054 synchronized activation of a large population of cells surrounding the electrode. For
1055 neuron identification in different sessions in the same mouse, substantial effort was made
1056 to optimize the position of optic fiber to identify those units recorded from different
1057 electrodes and that were not being able to be identified in the previous session. The final
1058 laser power used for reliable identification of D1/D2-SPNs was between 1.0 and 1.5 mW
1059 measured at the tip of the optical fiber (slightly varying for different mice and different
1060 sessions). Only those units showing very short (≤6 ms) response latency to light
1061 stimulation and exhibiting exactly the same spike waveforms ($R \geq 0.95$, Pearson's
1062 correlation coefficient) during the behavioral performance and light response were

1063 considered as direct light-activated and cre recombinase positive neurons thus D1-SPNs or D2-
1064 SPNs (Geddes et al., 2018; Howard et al., 2017; Jin and Costa, 2010). Strict criteria were
1065 employed to minimize the possibility of false positives (with the risk of increasing false
1066 negatives, and hence having to perform more recordings/mice to achieve the same number of
1067 neurons).
1068

1069 **Optical stimulation during the task**

1070 For optogenetic manipulation experiments, mice were injected with AAV virus carrying
1071 were pre-trained in 2-8s task for two weeks and bilaterally implanted with optic fibers. After
1072 achieving a correct rate of 80%, stimulation trials began. D1-SPNs and D2-SPNs neurons were
1073 stimulated or inhibited bilaterally in 50% of trials using a single pulse of light (Laserglow, 473
1074 nm, 5 mW, 1 s constant for ChR2 experiments; Laserglow, 532 nm 10 mW, 1 s constant for
1075 Halorhodopsin experiments). Rewards were delivered only at correct responses during 2 and 8 s
1076 trials. Within 50% of any type of trials, mice were optogenetically stimulated (or inhibited) for 1
1077 s before lever extension (Howard et al., 2017). Mice only received stimulation (or inhibition)
1078 once per trial. Sessions with correct rate below 75% for control trials were excluded from further
1079 analysis.
1080

1081 **Computational model**

1082 We constructed a neuronal network model, including cortico-basal ganglia circuitry, to
1083 simulate the behavioral effects of ablation and optogenetic manipulation on SPNs. Specifically,
1084 cortical information corresponding to left or right choice is sent to D1- and D2-SPNs associated
1085 with these two action options (Lo and Wang, 2006; Wang, 2002). One-way collateral inhibition

is added between D2 SPNs subgroups. Signals from D1- and D2-SPNs eventually converge to two separate SNr populations through distinct pathways (Hikosaka et al., 2000; Jin et al., 2014; Mink, 2003), and exert opposing effects on SNr activity (Smith et al., 1998). Behavioral output is then determined by the dominant activity between the mutually inhibiting left and right SNr populations (Mailly et al., 2003), which could control the final motor output either through brainstem circuits or motor cortices (Aoki et al., 2019; Hikosaka, 2007; Lo and Wang, 2006; Redgrave et al., 1999). Here for simplicity, other basal ganglia nuclei such as globus pallidus and subthalamic nucleus are not included in the model.

Cortical neurons firing activities are defined as:

$$f_{left}^{cortex}(t) = k_{left}^{cortex} e^{-t_m \cdot t} + I_{noise}^{left}(t)$$

$$f_{right}^{cortex}(t) = k_{right}^{cortex} e^{-t_m \cdot t} + I_{noise}^{right}(t)$$

where $k_{left}^{cortex} = 2,\ k_{right}^{cortex} = -2$, $t_m = 0.4$ and $I_{noise}(t)$ is defined as Gaussian white noise (mean(I_{noise}^{left}) = 1, mean(I_{noise}^{right}) = 2, SD = 0.01).

Dopamine neuron firing activities is defined as:

$$f_{DA}(t) = k_{DA} e^{-t_{DA} \cdot t} + I_{noise}^{DA}(t)$$

where $k_{DA} = 3,\ t_{DA} = 0.4$ and $I_{noise}^{DA}(t)$ is defined as Gaussian white noise (mean (I_{noise}^{DA}) = 1, SD = 0.01).

Neuronal activities of D1-SPNs are defined as:

$$\tau \frac{d f_{left}^{D1}(t)}{dt} = w_0\left(E - f_{left}^{D1}(t)\right) + \widetilde{w}_{D1_left} f_{left}^{cortex}(t) + w_{D1} f_{DA}(t) + I_{noise}(t)$$

$$\tau \frac{d f_{right}^{D1}(t)}{dt} = w_0\left(E - f_{right}^{D1}(t)\right) + \widetilde{w}_{D1_right} f_{right}^{cortex}(t) + w_{D1} f_{DA}(t) + I_{noise}(t)$$

where $w_0 = 1$, $E = 20$, $\widetilde{w}_{D1_left} = 3$, $\widetilde{w}_{D1_right} = 6$, $w_{D1} = 2$, $\tau = 0.1$, $I_{noise}(t)$ is defined as Gaussian white noise (mean ($I_{noise}(t)$) = 0, SD = 0.5).

Neuronal activities of D2-SPNs in "Co-activation" module (labelled as D2-SPN 1) are defined as:

$$\tau \frac{df_{left1}^{D2}(t)}{dt} = w_0\left(E - f_{left1}^{D2}(t)\right) + \widetilde{w}_{D2_left} f_{left}^{cortex}(t) + w_{D2} f_{DA}(t) + I_{noise}(t)$$

$$\tau \frac{df_{right1}^{D2}(t)}{dt} = w_0\left(E - f_{right1}^{D2}(t)\right) + \widetilde{w}_{D2_right} f_{right}^{cortex}(t) + w_{D2} f_{DA}(t) + I_{noise}(t)$$

where $w_0 = 1$, $E = 21$, $\widetilde{w}_{D2_left} = 5$, $\widetilde{w}_{D2_right} = 5$, $w_{D2} = -0.3$, $\tau = 0.1$, $I_{noise}(t)$ is defined as Gaussian white noise (mean ($I_{noise}(t)$) = 0, SD = 0.5).

Neuronal activities of D2-SPNs in "Go/No-go" module (labelled as D2-SPN 2) are defined as:

$$\tau \frac{df_{left2}^{D2}(t)}{dt} = w_0\left(E - f_{left2}^{D2}(t)\right) + \widetilde{w}_{D2_left} f_{left}^{cortex}(t) + w_{D2_left} S_{left}(t) f_{right1}^{D2}(t) + w_{D2} f_{DA}(t) + I_{noise}(t)$$

$$\tau \frac{df_{right2}^{D2}(t)}{dt} = w_0\left(E - f_{right2}^{D2}(t)\right) + \widetilde{w}_{D2_right} f_{right}^{cortex}(t) + w_{D2_right} S_{right}(t) f_{left1}^{D2}(t) + w_{D2} f_{DA}(t) + I_{noise}(t)$$

where $w_0 = 1$, $E = 21$, $\widetilde{w}_{D2_left} = 5$, $\widetilde{w}_{D2_right} = 5$, $w_{D2_left} = -0.7$, $w_{D2_right} = -0.5$, $w_{D2} = -0.3$, $\tau = 0.1$, $I_{noise}(t)$ is defined as Gaussian white noise (mean ($I_{noise}(t)$) = 0, SD = 0.5). $S_{left}(t)$ and $S_{right}(t)$ are short-term depression functions:

$$S_{left}(t) = 3/(1 + e^{0.3(f_{right1}^{D2}(t) - 15)})$$

$$S_{right}(t) = 3/(1 + e^{0.3(f_{left1}^{D2}(t) - 15)})$$

SNr neurons receive striatal inputs as well as the local inhibitory inputs from other SNr neurons. The SNr activities are defined as:

$$\tau_{SNr}\frac{df_{left}^{SNr}(t)}{dt} = w_0\left(E - f_{left}^{SNr}(t)\right) + \widetilde{w1}_{SNr}f_{left}^{D1}(t) + \widetilde{w2}_{SNr}f_{right1}^{D2}(t) + \widetilde{w3}_{SNr}f_{left2}^{D2}(t) + w_{left}^{SNr}f_{right}^{SNr}(t) + I_{noise}^{s}(t)$$

$$\tau_{SNr}\frac{df_{right}^{SNr}(t)}{dt} = w_0\left(E - f_{right}^{SNr}(t)\right) + \widetilde{w1}_{SNr-D1}f_{right}^{D1}(t) + \widetilde{w2}_{SNr}f_{left1}^{D2}(t) + \widetilde{w3}_{SNr}f_{right2}^{D2}(t) + w_{right}^{SNr}f_{left}^{SNr}(t) + I_{noise}^{s}(t)$$

where $w_0 = 1$, $E = 40$, $\widetilde{w1}_{SNr} = -0.1$, $\widetilde{w2}_{SNr} = 0.15$, $\widetilde{w3}_{SNr} = 0.07$, $w_{left}^{SNr} = -0.027$, $w_{right}^{SNr} = -0.01$, $\tau_{SNr} = 0.2$. $I_{noise}^{s}(t)$ is defined as Gaussian white noise (mean (I_{noise}^{s})= 0, SD = 0.3).

The time-dependent choice $C(t)$ is then determined by SNr outputs $f_{left}^{SNr}(t)$ and $f_{right}^{SNr}(t)$ as follows:

$$C(t) = \begin{cases} \text{left choice (short} - \text{duration choice)}, & f_{left}^{SNr}(t) - f_{right}^{SNr}(t) < 0 \\ \text{right choice (long} - \text{duration choice)}, & f_{left}^{SNr}(t) - f_{right}^{SNr}(t) \geq 0 \end{cases}$$

For optogenetic manipulation of striatal neurons, the stimulation pattern is defined as:

$$F_{activation}(t) = \begin{cases} amp, & t_s \leq t \leq t_s + 1 \\ 0, & t < t_s \; or \; t > t_s + 1 \end{cases}$$

and for inhibition, the pattern is defined as:

$$F_{inhibition}(t) = \begin{cases} -amp, & t_s \leq t \leq t_s + 1 \\ 0, & t < t_s \; or \; t > t_s + 1 \end{cases}$$

where t_s is the onset of stimulation/inhibition, which lasts for 1 s. *amp* is defined as the strength of the optogenetic manipulation within the range of [1, 25].

To add D1-D1 collateral connections to the 'Triple-control' model, the neuronal activities of D1-SPNs are defined as:

$$\tau\frac{df_{left}^{D1}(t)}{dt} = w_0\left(E - f_{left}^{D1}(t)\right) + \widetilde{w}_{D1_{left}}f_{left}^{cortex}(t) + w_{D1_right}f_{right}^{D1}(t) + w_{D1}f_{DA}(t) + I_{noise}(t)$$

$$\tau \frac{df_{right}^{D1}(t)}{dt} = w_0\left(E - f_{right}^{D1}(t)\right) + \widetilde{w}_{D1_{right}} f_{right}^{cortex}(t) + w_{D1_left} f_{left}^{D1}(t) + w_{D1} f_{DA}(t) + I_{noise}(t)$$

where $w_{D1_left} = -0.3$, $w_{D1_right} = -0.3$.

To add D1-D2 collateral connections to the 'Triple-control' model, the neuronal activities of D2-SPNs in "Go/No-go" module (labelled as D2-SPN 2) are defined as:

$$\tau \frac{df_{left2}^{D2}(t)}{dt} = w_0\left(E - f_{left2}^{D2}(t)\right) + \widetilde{w}_{D2_left} f_{left}^{cortex}(t) + w_{D2_{left}} S_{left}(t) f_{right1}^{D2}(t) + w_{D1_{left}} f_{left}^{D1}(t) + w_{D2} f_{DA}(t) + I_{noise}(t)$$

$$\tau \frac{df_{right2}^{D2}(t)}{dt} = w_0\left(E - f_{right2}^{D2}(t)\right) + \widetilde{w}_{D2_right} f_{right}^{cortex}(t) + w_{D2_right} S_{right}(t) f_{left1}^{D2}(t) + w_{D1_right} f_{right}^{D1}(t) + w_{D2} f_{DA}(t) + I_{noise}(t)$$

where $w_{D1_left} = -0.3$, $w_{D1_right} = -0.3$.

To add D2-D1 collateral connections to the 'Triple-control' model, the neuronal activities of D1-SPNs are defined as:

$$\tau \frac{df_{left}^{D1}(t)}{dt} = w_0\left(E - f_{left}^{D1}(t)\right) + \widetilde{w}_{D1_{left}} f_{left}^{cortex}(t) + w_{D2_left} f_{left2}^{D2}(t) + w_{D1} f_{DA}(t) + I_{noise}(t)$$

$$\tau \frac{df_{right}^{D1}(t)}{dt} = w_0\left(E - f_{right}^{D1}(t)\right) + \widetilde{w}_{D1_{right}} f_{right}^{cortex}(t) + w_{D2_right} f_{right2}^{D2}(t) + w_{D1} f_{DA}(t) + I_{noise}(t)$$

where $w_{D2_left} = -0.3$, $w_{D2_right} = -0.3$.

All the modeling programs were coded in Matlab.

Psychometric curve fitting

1149 Psychometric curves for behavioral data and for theoretical curves were fit using
1150 the following equation (Brunton et al., 2013; Howard et al., 2017):

$$y = a + \frac{b}{1 + e^{\frac{c-x}{d}}}$$

1151 where a is the percentage of long-lever selection during short duration trials, b is the difference
1152 between a and the percentage of long-lever selection during long duration trials, c is the x-
1153 intercept where long-duration selection equals 0.5, and d is the rate of increase or decrease in the
1154 curve (slope). These can be interpreted as change in overall choice, long-duration choice, time,
1155 and sensitivity, respectively (Brunton et al., 2013).
1156

1157 **Statistical procedures**

1158 Statistics for the wild-type and KO mice learning data were performed on the basis of
1159 values for each mouse per day. One-way and two-way repeated measures ANOVA were used to
1160 investigate general main effects; and paired or unpaired t-test were used in all planned and post-
1161 hoc comparisons. Z-test was used for the comparison of neuron proportions (Sheskin, 2003).
1162 Statistics for the optogenetic data were performed on the basis of control and stimulated values
1163 for each mouse per stimulation condition. Statistical analyses were conducted in Matlab using
1164 the statistics toolbox (The MathWorks Inc., MA) and GraphPad Prism 7 (GraphPad Software
1165 Inc., CA). Results are presented as mean ± SEM for behavior readouts and the neuronal
1166 recording data. $p < 0.05$ was considered significant. All statistical details are located within the
1167 figure legends. The number of animals used in each experiment and the number of neurons are
1168 specified in the text and figure legend.
1169

1170

References:

Abdi, A., Mallet, N., Mohamed, F.Y., Sharott, A., Dodson, P.D., Nakamura, K.C., Suri, S., Avery, S.V., Larvin, J.T., Garas, F.N., *et al.* (2015). Prototypic and arkypallidal neurons in the dopamine-intact external globus pallidus. The Journal of neuroscience : the official journal of the Society for Neuroscience *35*, 6667-6688.

Abi-Dargham, A., Rodenhiser, J., Printz, D., Zea-Ponce, Y., Gil, R., Kegeles, L.S., Weiss, R., Cooper, T.B., Mann, J.J., Van Heertum, R.L., *et al.* (2000). Increased baseline occupancy of D2 receptors by dopamine in schizophrenia. Proceedings of the National Academy of Sciences of the United States of America *97*, 8104-8109.

Albin, R.L., Young, A.B., and Penney, J.B. (1989). The functional anatomy of basal ganglia disorders. Trends in neurosciences *12*, 366-375.

Aoki, S., Smith, J.B., Li, H., Yan, X., Igarashi, M., Coulon, P., Wickens, J.R., Ruigrok, T.J., and Jin, X. (2019). An open cortico-basal ganglia loop allows limbic control over motor output via the nigrothalamic pathway. eLife *8*.

Atherton, J.F., Menard, A., Urbain, N., and Bevan, M.D. (2013). Short-term depression of external globus pallidus-subthalamic nucleus synaptic transmission and implications for patterning subthalamic activity. The Journal of neuroscience : the official journal of the Society for Neuroscience *33*, 7130-7144.

Azim, E., Jiang, J., Alstermark, B., and Jessell, T.M. (2014). Skilled reaching relies on a V2a propriospinal internal copy circuit. Nature *508*, 357-363.

Barbera, G., Liang, B., Zhang, L., Gerfen, C.R., Culurciello, E., Chen, R., Li, Y., and Lin, D.T. (2016). Spatially Compact Neural Clusters in the Dorsal Striatum Encode Locomotion Relevant Information. Neuron *92*, 202-213.

Bastide, M.F., Meissner, W.G., Picconi, B., Fasano, S., Fernagut, P.O., Feyder, M., Francardo, V., Alcacer, C., Ding, Y., Brambilla, R., *et al.* (2015). Pathophysiology of L-dopa-induced motor and non-motor complications in Parkinson's disease. Progress in neurobiology *132*, 96-168.

Benecke, R., Rothwell, J.C., Dick, J.P., Day, B.L., and Marsden, C.D. (1987). Disturbance of sequential movements in patients with Parkinson's disease. Brain : a journal of neurology *110 (Pt 2)*, 361-379.

Brunton, B.W., Botvinick, M.M., and Brody, C.D. (2013). Rats and humans can optimally accumulate evidence for decision-making. Science *340*, 95-98.

Calabresi, P., Picconi, B., Tozzi, A., Ghiglieri, V., and Di Filippo, M. (2014). Direct and indirect pathways of basal ganglia: a critical reappraisal. Nature neuroscience *17*, 1022-1030.

Cazorla, M., de Carvalho, F.D., Chohan, M.O., Shegda, M., Chuhma, N., Rayport, S., Ahmari, S.E., Moore, H., and Kellendonk, C. (2014). Dopamine D2 receptors regulate the anatomical and functional balance of basal ganglia circuitry. Neuron *81*, 153-164.

Cools, R., and D'Esposito, M. (2011). Inverted-U-shaped dopamine actions on human working memory and cognitive control. Biological psychiatry *69*, e113-125.

Cui, G., Jun, S.B., Jin, X., Pham, M.D., Vogel, S.S., Lovinger, D.M., and Costa, R.M. (2013). Concurrent activation of striatal direct and indirect pathways during action initiation. Nature *494*, 238-242.

DeLong, M.R. (1990). Primate models of movement disorders of basal ganglia origin. Trends in neurosciences *13*, 281-285.

Deniau JM, M.P., Maurice N, Charpier S. (2007). Gaba and the basal ganglia - from molecules to systems, Vol 160 (Elsevier).

Ding, L., and Gold, J.I. (2012). Separate, causal roles of the caudate in saccadic choice and execution in a perceptual decision task. Neuron *75*, 865-874.

Durieux, P.F., Schiffmann, S.N., and de Kerchove d'Exaerde, A. (2012). Differential regulation of motor control and response to dopaminergic drugs by D1R and D2R neurons in distinct dorsal striatum subregions. The EMBO journal *31*, 640-653.

Fujiyama, F., Nakano, T., Matsuda, W., Furuta, T., Udagawa, J., and Kaneko, T. (2016). A single-neuron tracing study of arkypallidal and prototypic neurons in healthy rats. Brain structure & function *221*, 4733-4740.

Fujiyama, F., Sohn, J., Nakano, T., Furuta, T., Nakamura, K.C., Matsuda, W., and Kaneko, T. (2011). Exclusive and common targets of neostriatofugal projections of rat striosome neurons: a single neuron-tracing study using a viral vector. Eur J Neurosci *33*, 668-677.

Gallistel, C.R. (1980). The Organization of Action: A New Synthesis.

Geddes, C.E., Li, H., and Jin, X. (2018). Optogenetic Editing Reveals the Hierarchical Organization of Learned Action Sequences. Cell *174*, 32-43 e15.

Goldman-Rakic, P.S., Muly III, E.C., and Williams, G.V. (2000). D_1 receptors in prefrontal cells and circuits. Brain Research Reviews.

Gong, S., Doughty, M., Harbaugh, C.R., Cummins, A., Hatten, M.E., Heintz, N., and Gerfen, C.R. (2007). Targeting Cre recombinase to specific neuron populations with bacterial artificial chromosome constructs. The Journal of neuroscience : the official journal of the Society for Neuroscience *27*, 9817-9823.

Gradinaru, V., Zhang, F., Ramakrishnan, C., Mattis, J., Prakash, R., Diester, I., Goshen, I., Thompson, K.R., and Deisseroth, K. (2010). Molecular and cellular approaches for diversifying and extending optogenetics. Cell *141*, 154-165.

Graybiel, A.M. (1998). The basal ganglia and chunking of action repertoires. Neurobiology of learning and memory *70*, 119-136.

Graybiel, A.M., and Rauch, S.L. (2000). Toward a neurobiology of obsessive-compulsive disorder. Neuron *28*, 343-347.

Gustafson, N., Gireesh-Dharmaraj, E., Czubayko, U., Blackwell, K.T., and Plenz, D. (2006). A comparative voltage and current-clamp analysis of feedback and feedforward synaptic transmission in the striatal microcircuit in vitro. Journal of neurophysiology *95*, 737-752.

Hikosaka, O. (2007). GABAergic output of the basal ganglia. Progress in brain research *160*, 209-226.

Hikosaka, O., Miyashita, K., Miyachi, S., Sakai, K., and Lu, X. (1998). Differential roles of the frontal cortex, basal ganglia, and cerebellum in visuomotor sequence learning. Neurobiology of learning and memory *70*, 137-149.

Hikosaka, O., Takikawa, Y., and Kawagoe, R. (2000). Role of the basal ganglia in the control of purposive saccadic eye movements. Physiol Rev *80*, 953-978.

Hikosaka, O., and Wurtz, R.H. (1983). Visual and oculomotor functions of monkey substantia nigra pars reticulata. IV. Relation of substantia nigra to superior colliculus. Journal of neurophysiology *49*, 1285-1301.

Horst, N.K., Jupp, B., Roberts, A.C., and Robbins, T.W. (2019). D2 receptors and cognitive flexibility in marmosets: tri-phasic dose–response effects of intra-striatal quinpirole on serial reversal performance. Neuropsychopharmacology : official publication of the American College of Neuropsychopharmacology *44*, 564-571.

Howard, C.D., Li, H., Geddes, C.E., and Jin, X. (2017). Dynamic Nigrostriatal Dopamine Biases Action Selection. Neuron *93*, 1436-1450 e1438.

Howes, O.D., and Kapur, S. (2009). The Dopamine Hypothesis of Schizophrenia: Version III—The Final Common Pathway. Schizophrenia Bulletin *35*, 549-562.

Isomura, Y., Takekawa, T., Harukuni, R., Handa, T., Aizawa, H., Takada, M., and Fukai, T. (2013). Reward-modulated motor information in identified striatum neurons. The Journal of neuroscience : the official journal of the Society for Neuroscience *33*, 10209-10220.

Jarskog, L.F., Miyamoto, S., and Lieberman, J.A. (2007). Schizophrenia: new pathological insights and therapies. Annual review of medicine *58*, 49-61.

Jiang, H., Stein, B.E., and McHaffie, J.G. (2003). Opposing basal ganglia processes shape midbrain visuomotor activity bilaterally. Nature *423*, 982-986.

Jin, X., and Costa, R.M. (2010). Start/stop signals emerge in nigrostriatal circuits during sequence learning. Nature *466*, 457-462.

Jin, X., and Costa, R.M. (2015). Shaping action sequences in basal ganglia circuits. Current opinion in neurobiology *33*, 188-196.

Jin, X., Tecuapetla, F., and Costa, R.M. (2014). Basal ganglia subcircuits distinctively encode the parsing and concatenation of action sequences. Nature neuroscience *17*, 423-430.

Klaus, A., and Plenz, D. (2016). A Low-Correlation Resting State of the Striatum during Cortical Avalanches and Its Role in Movement Suppression. PLoS biology *14*, e1002582.

Kravitz, A.V., Freeze, B.S., Parker, P.R., Kay, K., Thwin, M.T., Deisseroth, K., and Kreitzer, A.C. (2010). Regulation of parkinsonian motor behaviours by optogenetic control of basal ganglia circuitry. Nature *466*, 622-626.

la Fougere, C., Meisenzahl, E., Schmitt, G., Stauss, J., Frodl, T., Tatsch, K., Hahn, K., Moller, H.J., and Dresel, S. (2005). D2 receptor occupancy during high- and low-dose therapy with the atypical antipsychotic amisulpride: a 123I-iodobenzamide SPECT study. Journal of nuclear medicine : official publication, Society of Nuclear Medicine *46*, 1028-1033.

Lally, J., and MacCabe, J.H. (2015). Antipsychotic medication in schizophrenia: a review. British medical bulletin *114*, 169-179.

Laruelle, M., D'Souza, C.D., Baldwin, R.M., Abi-Dargham, A., Kanes, S.J., Fingado, C.L., Seibyl, J.P., Zoghbi, S.S., Bowers, M.B., Jatlow, P., *et al.* (1997). Imaging D2 receptor occupancy by endogenous dopamine in humans. Neuropsychopharmacology : official publication of the American College of Neuropsychopharmacology *17*, 162-174.

Lauwereyns, J., Watanabe, K., Coe, B., and Hikosaka, O. (2002). A neural correlate of response bias in monkey caudate nucleus. Nature *418*, 413-417.

Lee, Y., Han, N.E., Kim, W., Kim, J.G., Lee, I.B., Choi, S.J., Chun, H., Seo, M., Lee, C.J., Koh, H.Y., *et al.* (2020). Dynamic Changes in the Bridging Collaterals of the Basal Ganglia Circuitry Control Stress-Related Behaviors in Mice. Molecules and cells *43*, 360-372.

Levine, M., and Ruha, A.M. (2012). Overdose of atypical antipsychotics: clinical presentation, mechanisms of toxicity and management. CNS drugs *26*, 601-611.

Lima, S.Q., Hromadka, T., Znamenskiy, P., and Zador, A.M. (2009). PINP: a new method of tagging neuronal populations for identification during in vivo electrophysiological recording. PloS one *4*, e6099.

Lo, C.C., and Wang, X.J. (2006). Cortico-basal ganglia circuit mechanism for a decision threshold in reaction time tasks. Nature neuroscience *9*, 956-963.

Madisen, L., Mao, T., Koch, H., Zhuo, J.-m., Berenyi, A., Fujisawa, S., Hsu, Y.-W.A., Garcia, A.J., Gu, X., and Zanella, S. (2012). A toolbox of Cre-dependent optogenetic transgenic mice for light-induced activation and silencing. Nature neuroscience *15*, 793-802.

Mailly, P., Charpier, S., Menetrey, A., and Deniau, J.-M. (2003). Three-dimensional organization of the recurrent axon collateral network of the substantia nigra pars reticulata neurons in the rat. Journal of Neuroscience *23*, 5247-5257.

Mallet, N., Schmidt, R., Leventhal, D., Chen, F., Amer, N., Boraud, T., and Berke, J.D. (2016). Arkypallidal Cells Send a Stop Signal to Striatum. Neuron *89*, 308-316.

Markowitz, J.E., Gillis, W.F., Beron, C.C., Neufeld, S.Q., Robertson, K., Bhagat, N.D., Peterson, R.E., Peterson, E., Hyun, M., Linderman, S.W., *et al.* (2018). The Striatum Organizes 3D Behavior via Moment-to-Moment Action Selection. Cell *174*, 44-58 e17.

Mattay, V.S., Goldberg, T.E., Fera, F., Hariri, A.R., Tessitore, A., Egan, M.F., Kolachana, B., Callicott, J.H., and Weinberger, D.R. (2003). Catechol O-methyltransferase val158-met genotype and individual variation in the brain response to amphetamine. Proceedings of the National Academy of Sciences of the United States of America *100*, 6186-6191.

Mink, J.W. (1996). The basal ganglia: focused selection and inhibition of competing motor programs. Progress in neurobiology *50*, 381-425.

Mink, J.W. (2003). The Basal Ganglia and involuntary movements: impaired inhibition of competing motor patterns. Archives of neurology *60*, 1365-1368.

Nonomura, S., Nishizawa, K., Sakai, Y., Kawaguchi, Y., Kato, S., Uchigashima, M., Watanabe, M., Yamanaka, K., Enomoto, K., Chiken, S., *et al.* (2018). Monitoring and Updating of Action

Selection for Goal-Directed Behavior through the Striatal Direct and Indirect Pathways. Neuron *99*, 1302-1314 e1305.

Phillips, J.G., Chiu, E., Bradshaw, J.L., and Iansek, R. (1995). Impaired movement sequencing in patients with Huntington's disease: a kinematic analysis. Neuropsychologia *33*, 365-369.

Redgrave, P., Prescott, T.J., and Gurney, K. (1999). The basal ganglia: a vertebrate solution to the selection problem? Neuroscience *89*, 1009-1023.

Schmidt, R., and Berke, J.D. (2017). A Pause-then-Cancel model of stopping: evidence from basal ganglia neurophysiology. Philosophical transactions of the Royal Society of London Series B, Biological sciences *372*.

Seeman, P. (2002). Atypical antipsychotics: mechanism of action. Canadian journal of psychiatry Revue canadienne de psychiatrie *47*, 27-38.

Sheskin, D.J. (2003). Handbook of parametric and nonparametric statistical procedures (Chapman and Hall/CRC).

Smith, Y., Bevan, M., Shink, E., and Bolam, J.P. (1998). Microcircuitry of the direct and indirect pathways of the basal ganglia. Neuroscience *86*, 353-387.

Tai, L.H., Lee, A.M., Benavidez, N., Bonci, A., and Wilbrecht, L. (2012). Transient stimulation of distinct subpopulations of striatal neurons mimics changes in action value. Nature neuroscience *15*, 1281-1289.

Taverna, S., Ilijic, E., and Surmeier, D.J. (2008). Recurrent collateral connections of striatal medium spiny neurons are disrupted in models of Parkinson's disease. The Journal of neuroscience : the official journal of the Society for Neuroscience *28*, 5504-5512.

Tecuapetla, F., Carrillo-Reid, L., Bargas, J., and Galarraga, E. (2007). Dopaminergic modulation of short-term synaptic plasticity at striatal inhibitory synapses. Proceedings of the National Academy of Sciences *104*, 10258-10263.

Tecuapetla, F., Jin, X., Lima, S.Q., and Costa, R.M. (2016). Complementary Contributions of Striatal Projection Pathways to Action Initiation and Execution. Cell *166*, 703-715.

Wang, X.-J. (2002). Probabilistic decision making by slow reverberation in cortical circuits. Neuron *36*, 955-968.

Wei, W., and Wang, X.J. (2016). Inhibitory Control in the Cortico-Basal Ganglia-Thalamocortical Loop: Complex Regulation and Interplay with Memory and Decision Processes. Neuron *92*, 1093-1105.

Wong, D.F., Wagner, H.N., Jr., Tune, L.E., Dannals, R.F., Pearlson, G.D., Links, J.M., Tamminga, C.A., Broussolle, E.P., Ravert, H.T., Wilson, A.A., *et al.* (1986). Positron emission tomography reveals elevated D2 dopamine receptors in drug-naive schizophrenics. Science *234*, 1558-1563.

Wu, Y., Richard, S., and Parent, A. (2000). The organization of the striatal output system: a single-cell juxtacellular labeling study in the rat. Neurosci Res *38*, 49-62.

Wurtz, R.H., and Hikosaka, O. (1986). Role of the basal ganglia in the initiation of saccadic eye movements. Progress in brain research *64*, 175-190.

Yokoi, F., Gründer, G., Biziere, K., Stephane, M., Dogan, A.S., Dannals, R.F., Ravert, H., Suri, A., Bramer, S., and Wong, D.F. (2002). Dopamine D 2 and D 3 receptor occupancy in normal humans treated with the antipsychotic drug aripiprazole (OPC 14597): a study using positron emission tomography and [11 C] raclopride. Neuropsychopharmacology : official publication of the American College of Neuropsychopharmacology *27*, 248-259.

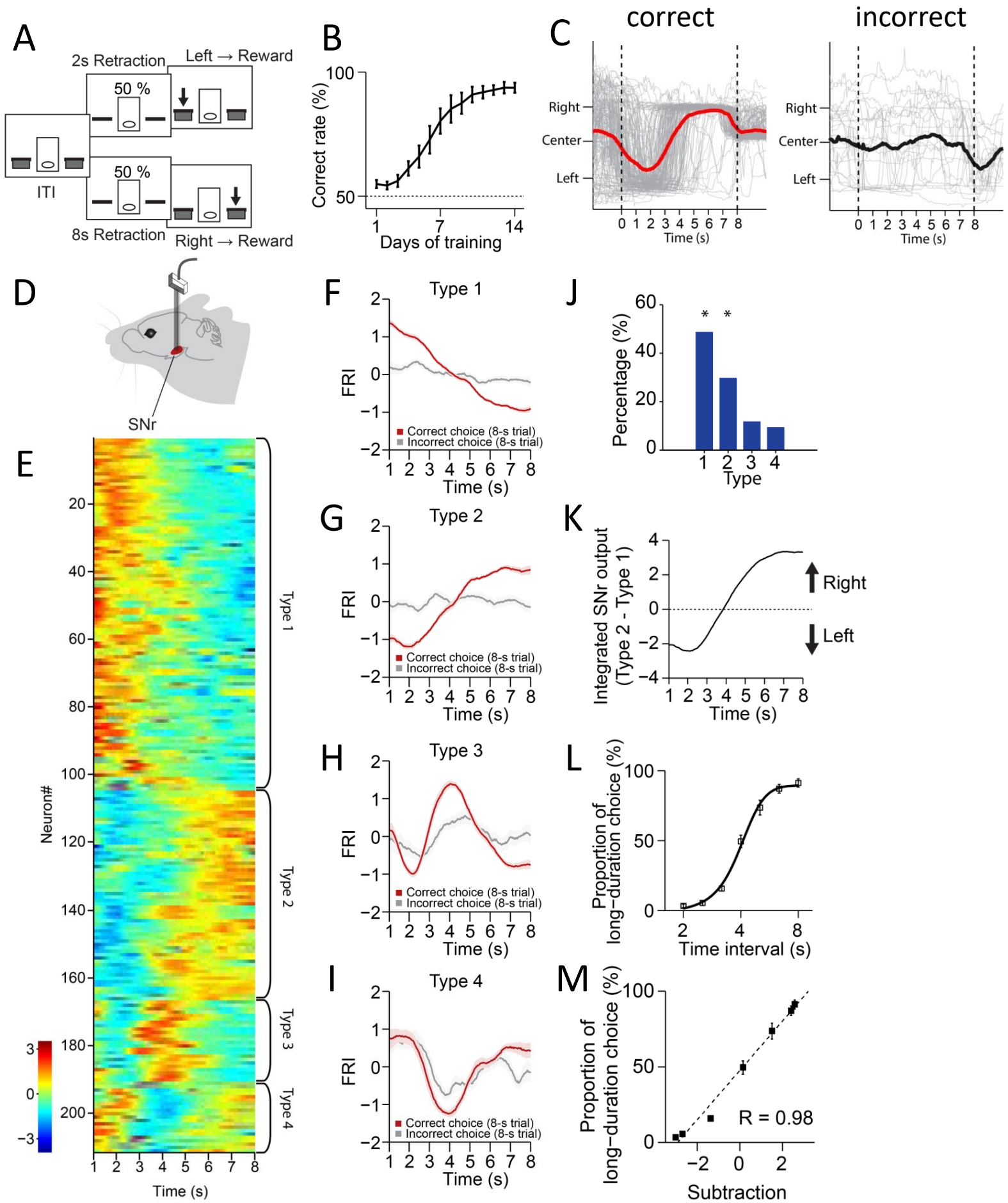

Figure 1. The neuronal dynamics in SNr during the 2-8 s action selection task. (A) Schematic diagram for the design of 2-8 s task. (B) Correct rate for wild type mice across 14 days training (n = 10 mice, one-way repeated-measures ANOVA, significant effect of training days, $F_{13,117} = 32.54$, $p < 0.0001$). (C) Movement trajectory of an example mouse in correct (left panel) and incorrect (right panel) 8-s trials (gray line: trajectory of each trials; red/black line: the average trajectory). (D) Diagram of electrode array implanted into substantia nigra pars reticulata (SNr). (E) Firing Rate Index (FRI) of neuronal activity for all task-related SNr neurons in correct 8-s trials. The magnitude of FRI is color coded and the SNr neurons are classified as four different types based on the activity dynamics. (F-I) Averaged FRI for Type 1 (F), Type 2 (G), Type 3 (H), Type 4 (I) of SNr neurons in correct (red) and incorrect 8-s trials (gray). (J) The proportion of four types of SNr neurons. Type 1 and Type 2 are major types and significantly more than Type 3 and Type 4 (Z-test, $p < 0.05$). (K) Integrated SNr output defined as the subtraction of averaged FRI between Type 1 and Type 2 SNr neurons. (L) Averaged psychometric curve (n = 10 mice) of choice behavior. (M) The correlation between the Type 1 and Type 2 FRI subtraction and the behavioral choice ($R = 0.98$, $p < 0.0005$). Error bars denote s.e.m., same for below unless stated otherwise.

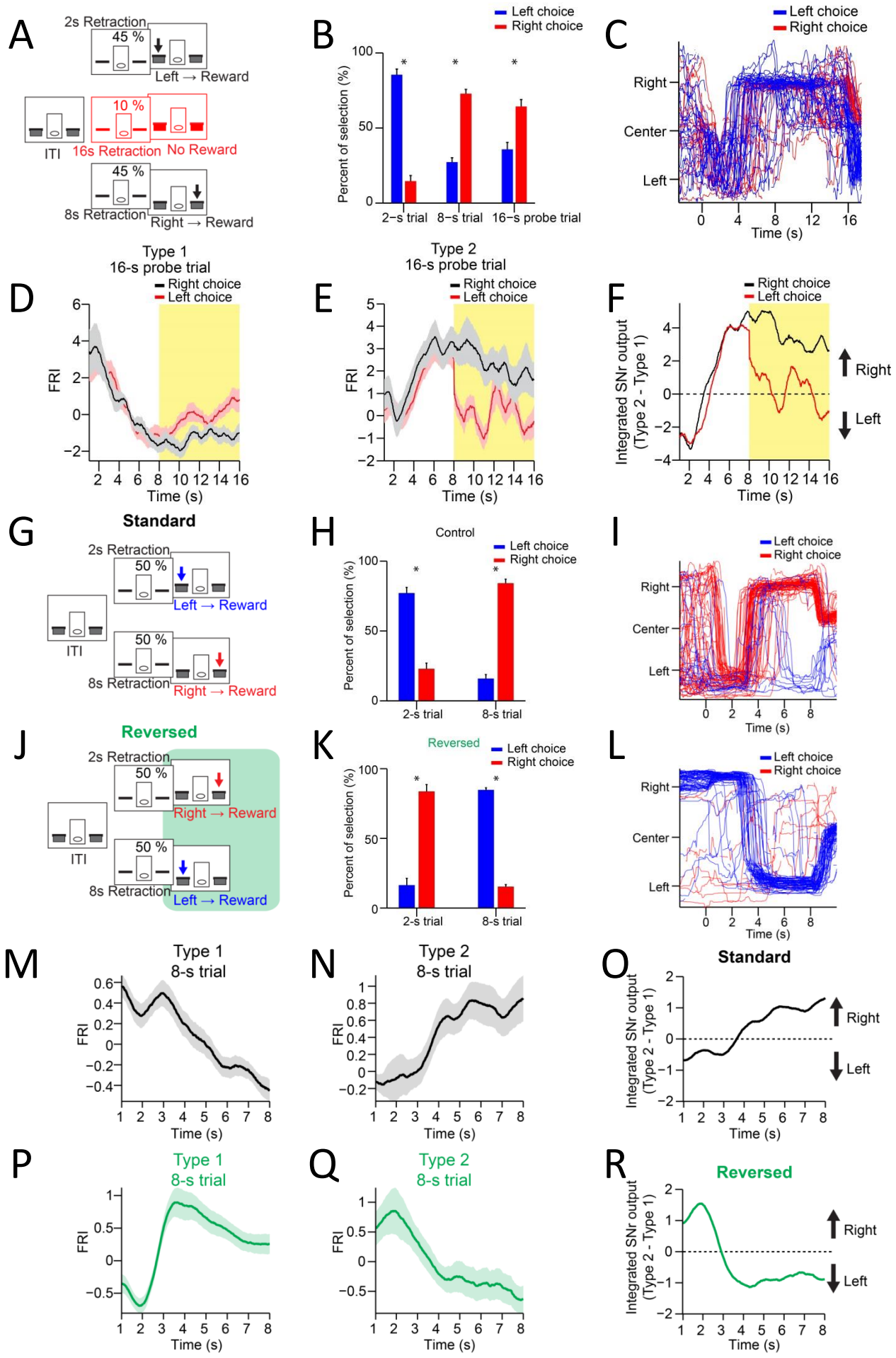

Figure 2. SNr neuronal dynamics reflect action selection but not interval time or reward value. (A) Task diagram of 2-8 s control task with 10% 16-s probe trials. (B) Percentage of behavioral choice in 2-s, 8-s and 16-s trials (blue: left choice; red: right choice) (n = 9 mice, paired t-test, $p < 0.05$). (C) Movement trajectory of an example mouse in 16-s trials (blue: left choice; red: right choice). (D) Averaged SNr Type 1 FRI in 16-s trials (red: left choice; black: right choice). Firing rates from 8s to 16s (highlighted area) are compared between left and right choice (n = 26 neurons, two-way repeated-measures ANOVA, significant difference between left and right choices, $F_{1,25} = 6.646$, $p = 0.016$). (E) Averaged SNr Type 2 FRI in 16-s trials (red: left choice; black: right choice). Firing rates from 8s to 16s are compared between left and right choice (n = 16 neurons, two-way repeated-measures ANOVA, significant difference between left and right choices, $F_{1,15} = 5.785$, $p = 0.029$). (F) Subtraction of FRI for SNr Type 1 and Type 2 neurons in 16-s probe trials (red: left choice; black: right choice). (G) Task design of 2-8 s standard task. (H) Percentage of behavioral choice in 2-s and 8-s trials (blue: left choice; red: right choice) (n = 6 mice, paired t-test, $p < 0.05$). (I) Movement trajectory of an example mouse in 8-s trials (blue: left choice; red: right choice). (J) Task design of reversed 2-8 s task. (K) Percentage of behavioral choice in 2-s and 8-s trials in the reversed 2-8 s task (blue: left choice; red: right choice) (n = 6 mice, paired t-test, $p < 0.05$). (L) Movement trajectory of the same mouse as (I) in 8-s trials in the reversed 2-8 s task (blue: left choice; red: right choice). (M) Averaged FRI of the SNr Type 1 neurons in correct 8-s trials (n = 14 neurons). (N) Averaged FRI of the SNr Type 2 neurons in correct 8-s trials (n = 11 neurons). (O) Integrated SNr output as the subtraction of FRI for SNr Type 1 (M) and Type 2 neurons (N) in the standard 2-8 s task. (P) Averaged FRI of the same neurons as (M) in correct 8-s trials of the reversed 2-8 s task. (Q) Averaged FRI of the same neurons as (N) in correct 8-s trials of the reversed 2-8 s task. (R) Integrated SNr output as the subtraction of FRI for SNr Type 1 (P) and Type 2 neurons (Q) in the reversed 2-8 s task.

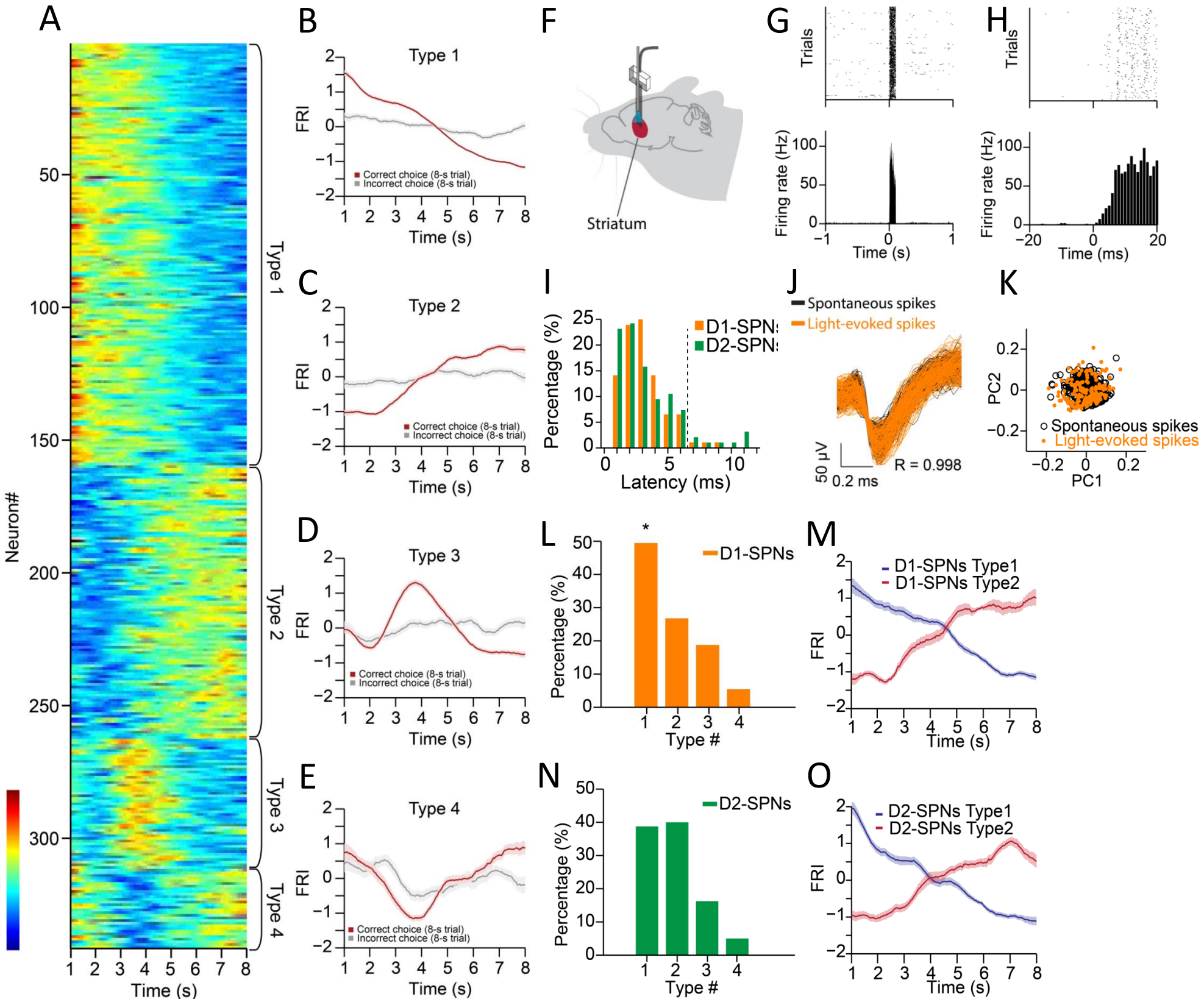

Figure 3. Neuronal activity of striatal D1- and D2-SPNs during action selection. (A) FRI of neuronal activity for all task-related SPNs in correct 8-s trials. SPNs were classified as Type 1 - 4. (B-E) Averaged FRI for Type 1 (B), Type 2 (C), Type 3 (D), Type 4 (E) of SPNs in correct (red) and incorrect 8-s trials (gray). (F) Diagram of simultaneous neuronal recording and optogenetic identification of D1- vs. D2-SPNs in dorsal striatum. (G) Top panel: Raster plot for a representative D1-SPN response to 100 ms optogenetic stimulation. Each row represents one trial and each black dot represents a spike. Bottom panel: Peristimulus time histogram (PETH) aligned to light onset at time zero. (H) PETH for the same neuron as shown in (G) with a finer time scale. (I) Distribution of light response latencies for D1- and D2-SPNs. (J) Action potential waveforms of the same neuron in (G) for spontaneous (black) and light-evoked (orange) spikes ($R = 0.998$, $P < 0.0001$, Pearson's correlation). (K) Principal component analysis (PCA) of action potential waveforms showing the overlapped clusters of spontaneous (black) and light-evoked (orange) spikes. (L) Proportion of D1-SPN subtypes. Type 1 neurons are significantly more than other three types of neurons in D1-SPNs (Z-test, $p < 0.05$). (M) Averaged FRI for Type 1 (blue) and Type 2 (red) D1-SPNs in correct 8-s trials. (N) Proportion of D2-SPN subtypes. (O) Averaged FRI for Type 1 (blue) and Type 2 (red) D2-SPNs in correct 8-s trials.

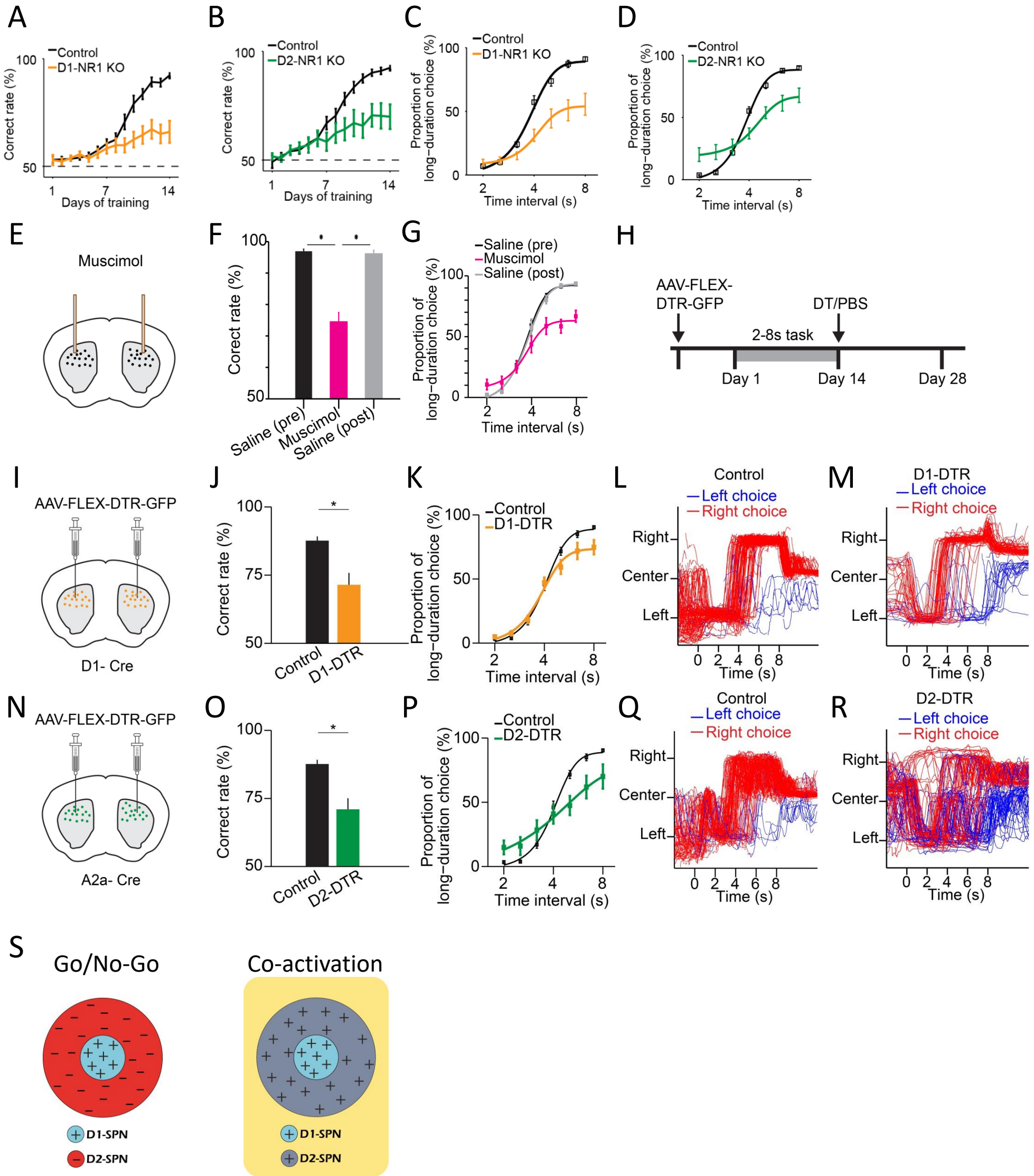
A
Control
D1-NR1 KO
Correct rate (%)
Days of training
B
Control
D2-NR1 KO
Correct rate (%)
Days of training
C
Control
D1-NR1 KO
Proportion of long−duration choice (%)
Time interval (s)
D
Control
D2-NR1 KO
Proportion of long−duration choice (%)
Time interval (s)
E
Muscimol
F
Corect rate (%)
Saline (pre)
Muscimol
Saline (post)
G
Saline (pre)
Muscimol
Saline (post)
Proportion of long−duration choice (%)
Time interval (s)
H
AAV-FLEX-DTR-GFP
DT/PBS
2-8s task
Day 1
Day 14
Day 28
I
AAV-FLEX-DTR-GFP
D1- Cre
J
Correct rate (%)
Control
D1-DTR
K
Control
D1-DTR
Proportion of long−duration choice (%)
Time interval (s)
L
Control
Left choice
Right choice
Right
Center
Left
Time (s)
M
D1-DTR
Left choice
Right choice
Right
Center
Left
Time (s)
N
AAV-FLEX-DTR-GFP
A2a- Cre
O
Correct rate (%)
Control
D2-DTR
P
Control
D2-DTR
Proportion of long−duration choice (%)
Time interval (s)
Q
Control
Left choice
Right choice
Right
Center
Left
Time (s)
R
D2-DTR
Left choice
Right choice
Right
Center
Left
Time (s)
S
Go/No-Go
D1-SPN
D2-SPN
Co-activation
D1-SPN
D2-SPN

Figure 4. Selective genetic knockout and ablation of D1- or D2-SPNs distinctly alters action selection. (A) Correct rate of control (n = 11 mice) and D1-NR1 KO mice (n = 16) in 2-8 s task during 14 days training (two-way repeated-measures ANOVA, significant difference between control and KO mice, $F_{1,25} = 10.8$, $p = 0.003$). (B) Correct rate of control (n = 17) and D2-NR1 KO mice (n = 10) in 2-8 s task during 14 days training (two-way repeated-measures ANOVA, significant difference between control and KO mice, $F_{1,25} = 8.728$, $p = 0.007$). (C) The psychometric curve for control (n = 11) and D1-NR1 KO mice (n = 16) (two-way repeated-measures ANOVA, significant difference between control and KO mice, $F_{1,25} = 12.27$, $p = 0.002$). (D) The psychometric curve for control (n = 17) and D2-NR1 KO mice (n = 10) (two-way repeated-measures ANOVA, significant difference between control and KO mice, $F_{1,25} = 9.64$, $p = 0.005$). (E) Schematic of muscimol infusion into the dorsal striatum in trained mice. (F) Correct rate for control (black: pre-muscimol, gray: post-muscimol) and mice with muscimol infusion (magenta) in dorsal striatum (n = 9 mice, paired t-test, $p < 0.01$). (G) The psychometric curve for control (n = 9 mice, black: pre-muscimol, gray: post-muscimol control) and mice with muscimol infusion (n = 9 mice, magenta) in dorsal striatum (two-way repeated-measures ANOVA, significant difference between control and muscimol infusion, $F_{2,16} = 11.74$, $p = 0.0007$). (H) Timeline for selective diphtheria toxin (DT) ablation experiments. (I) Schematic of diphtheria toxin receptor (DTR) virus (AAV-FLEX-DTR-GFP) injection in dorsal striatum of D1-Cre mice. (J) Correct rate for control (n = 9 mice) and mice with dorsal striatum D1-SPNs ablation (D1-DTR, n = 8 mice) (two-sample t-test, $p = 0.0016$). (K) The psychometric curve for control (n = 9 mice) and D1-SPNs ablation mice (n = 8 mice) (two-way repeated-measures ANOVA, main effect of ablation, $F_{1,15} = 1.84$, $p = 0.195$; interaction between trial intervals and ablation, F6,90 = 4.14, $p = 0.001$). (L) Movement trajectory of a control mouse in 8-s trials. (M) Movement trajectory of a D1-DTR mouse in 8-s trials. (N) Schematic of diphtheria toxin receptor (DTR) virus (AAV-FLEX-DTR-GFP) injection in dorsal striatum of A2a-Cre mice. (O) Correct rate for control (n = 8 mice) and mice with dorsal striatum D2-SPNs ablation (D2-DTR, n = 8 mice) (two-sample t-test, $p = 0.005$). (P) The psychometric curve for control (n = 9 mice) and D2-SPNs ablation mice (n = 8 mice) (two-way repeated-measures ANOVA, main effect of ablation, $F_{1,15} = 0.477$, $p = 0.5$; interaction between trial intervals and ablation, $F_{6,90} = 12.6$, $p < 0.001$). (Q) Movement trajectory of a control mouse in 8-s trials. (R) Movement trajectory of a D2-DTR mouse in 8-s trials. (S) Schematic of center-surround receptive field diagram for Go/No-Go (left) and Co-activation (right) models. '+' indicates facilitating effect to selection. '-' indicates inhibitory effect to selection.

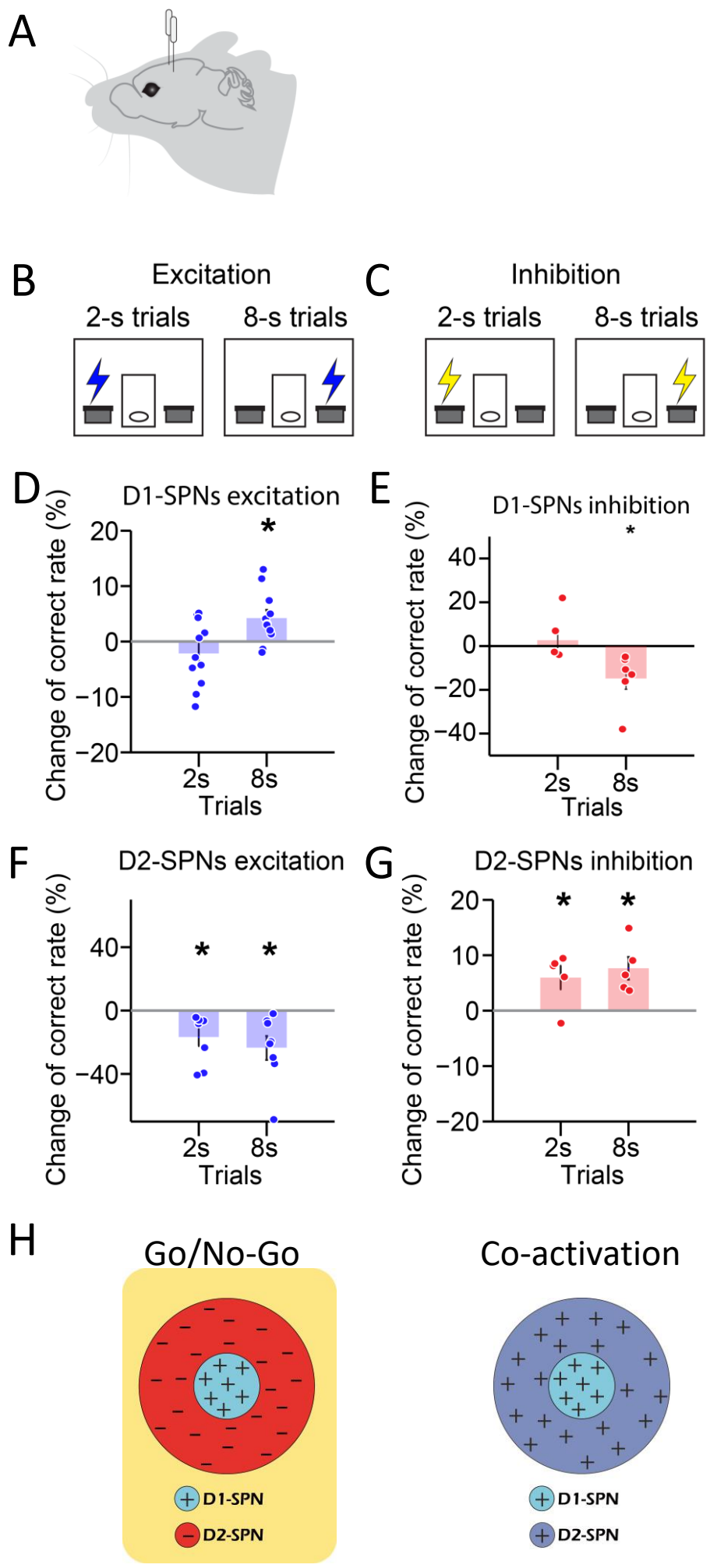

Figure 5. Optogenetic manipulation of D1- vs. D2-SPNs differently regulates action selection. (A) Schematic of optic fiber implantation for experimentally optogenetic excitation or inhibition of D1- or D2-SPNs in the dorsal striatum. (B, C) Schematic for optogenetic excitation (B) and inhibition (C) of D1-/D2-SPNs for 1 s right before lever extension in 2-8 s task. (D) Change of correct rate for optogenetic excitation of D1-SPNs in 2-s and 8-s trials (n = 11 mice, one-sample t-test, 2-s trials: $p = 0.248$; 8-s trials: $p < 0.05$). (E) Change of correct rate for optogenetic inhibition of D1-SPNs in 2-s and 8-s trials (n = 6 mice, one-sample t-test, 2-s trials: $p = 0.557$; 8-s trials: $p < 0.05$). (F) Change of correct rate for optogenetic excitation of D2-SPNs in 2-s and 8-s trials (n = 8 mice, one-sample t-test, 2-s trials: $p < 0.05$; 8-s trials: $p < 0.05$). (G) Change of correct rate for optogenetic inhibition of D2-SPNs in 2-s and 8-s trials (n = 5 mice, one-sample t-test, 2-s trials: $p < 0.05$; 8-s trials: $p < 0.05$). (H) Schematic of center-surround receptive field diagram for Go/No-Go (left) and Co-activation (right) models. '+' indicates facilitating effect to selection. '-' indicates inhibitory effect to selection.

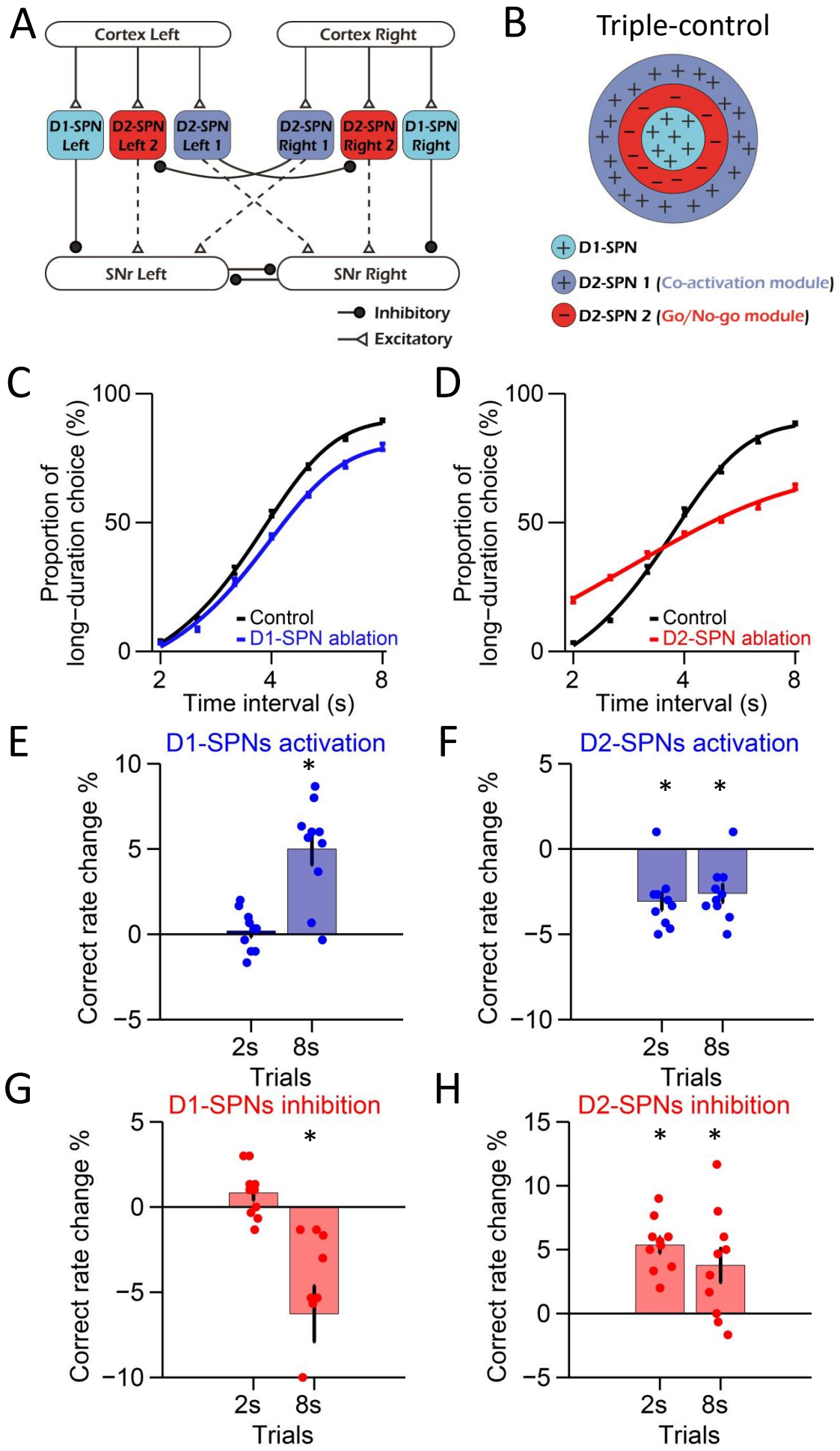

Figure 6. A triple-control computational model of basal ganglia direct and indirect pathways for action selection. (A) Network structure of the cortico-basal ganglia model based on realistic anatomy and synaptic connectivity. (B) Schematic of center-surround-context receptive field diagram for 'Triple-control' model. '+' indicates facilitating effect to selection. '-' indicates inhibitory effect to selection. (C) The psychometric curves of behavioral output in control (black) and D1-SPNs ablation condition (blue) in 'Triple-control' model (n = 10, two-way repeated-measures ANOVA, main effect of ablation, $F_{1,18} = 98.72$, $p < 0.0001$; interaction between trial intervals and ablation, $F_{6,108} = 7.799$, $p < 0.0001$). (D) The psychometric curves of behavioral output in control (black) and D2-SPNs ablation condition (red) in 'Triple-control' model (n = 10, two-way repeated-measures ANOVA, main effect of ablation, $F_{1,18} = 99.54$, $p < 0.0001$; interaction between trial intervals and ablation, $F_{6,108} = 177.6$, $p < 0.0001$). (E) Change of correct rate for optogenetic excitation of D1-SPNs in 2-s and 8-s trials (n = 10, one-sample t-test, 2-s trials: $p = 0.407$; 8-s trials: $p < 0.05$). (F) Change of correct rate for optogenetic excitation of D2-SPNs in 2-s and 8-s trials (n = 10, one-sample t-test, 2-s trials: $p < 0.05$; 8-s trials: $p < 0.05$). (G) Change of correct rate for optogenetic inhibition of D1-SPNs in 2-s and 8-s trials (n = 10, one-sample t-test, 2-s trials: $p = 0.28$; 8-s trials: $p < 0.05$). (H) Change of correct rate for optogenetic inhibition of D2-SPNs in 2-s and 8-s trials (n = 10, one-sample t-test, 2-s trials: $p < 0.05$; 8-s trials: $p < 0.05$).

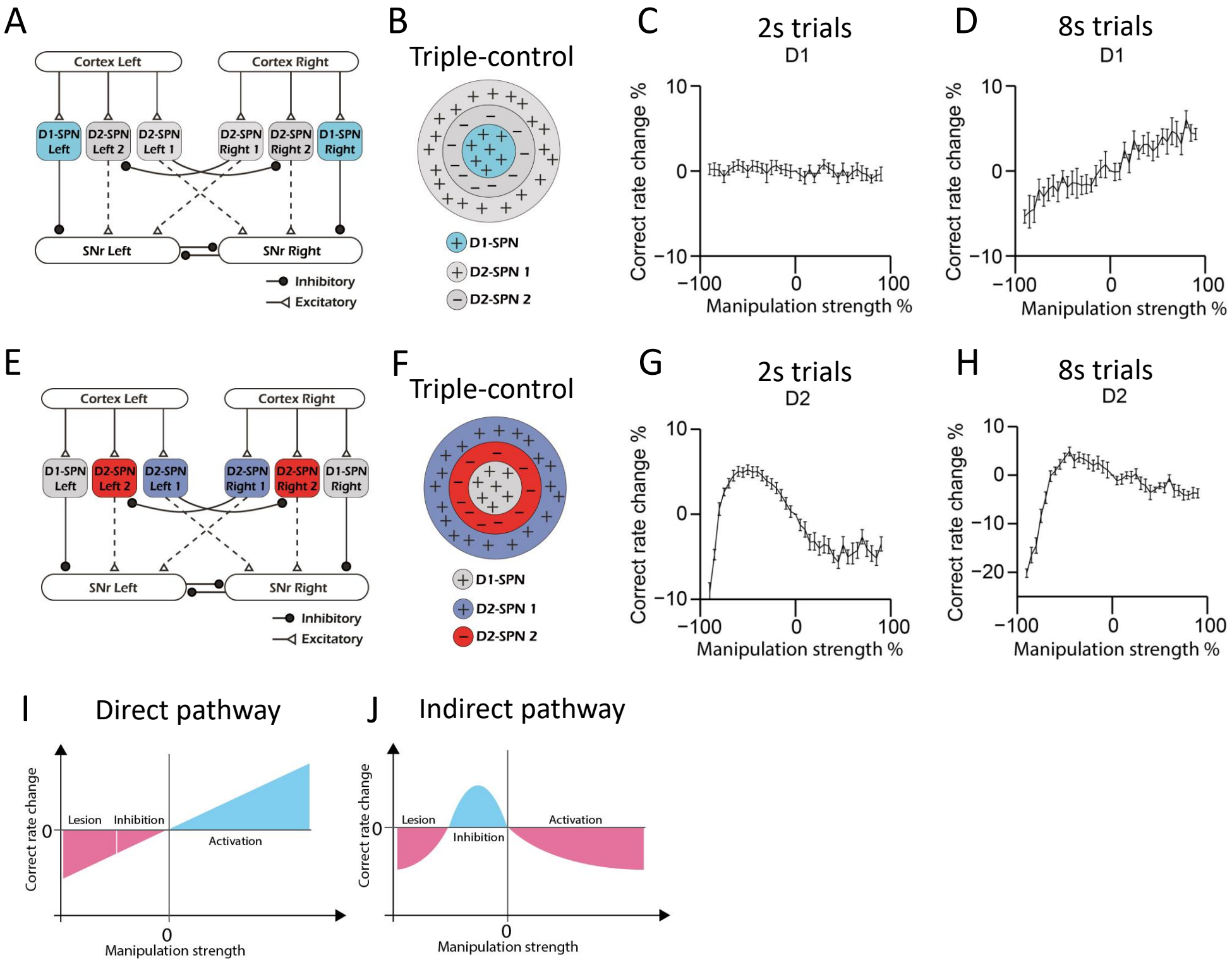

Figure 7. Computational modeling reveals direct and indirect pathways regulating action selection in a distinct manner. (A) Schematic for manipulation of D1-SPNs in 'Triple-control' model. (B) Schematic of manipulation of D1-SPNs in the center-surround-context receptive field diagram for 'Triple-control' model. '+' indicates facilitating effect to selection. '-' indicates inhibitory effect to selection. (C) Correct rate change in 2s trials when manipulating D1-SPNs with different manipulation strengths (n = 10, one-way repeated-measures ANOVA, effect of manipulation strength, $F_{36,324} = 1.171$, $p = 0.238$). (D) Correct rate change in 8s trials when manipulating D1-SPNs with different manipulation strengths (n = 10, one-way repeated-measures ANOVA, effect of manipulation strength, $F_{36,324} = 13.71$, $p < 0.0001$). (E) Schematic for optogenetic manipulation of D2-SPNs in 'Triple-control' model. (F) Schematic of manipulation of D2-SPNs in the center-surround-context receptive field diagram for 'Triple-control' model. '+' indicates facilitating effect to selection. '-' indicates inhibitory effect to selection. (G) Correct rate change in 2s trials when manipulating D2-SPNs with different manipulation strengths (n = 10, one-way repeated-measures ANOVA, effect of manipulation strength, $F_{36,324} = 59.13$, $p < 0.0001$). (H) Correct rate change in 8s trials when manipulating D2-SPNs with different manipulation strengths (n = 10, one-way repeated-measures ANOVA, effect of manipulation strength, $F_{36,324} = 40.75$, $p < 0.0001$). (I) Diagram of linear relationship between the modulation of direct pathway and correct rate of action selection. (J) Diagram of nonlinear relationship between the modulation of indirect pathway and correct rate of action selection.

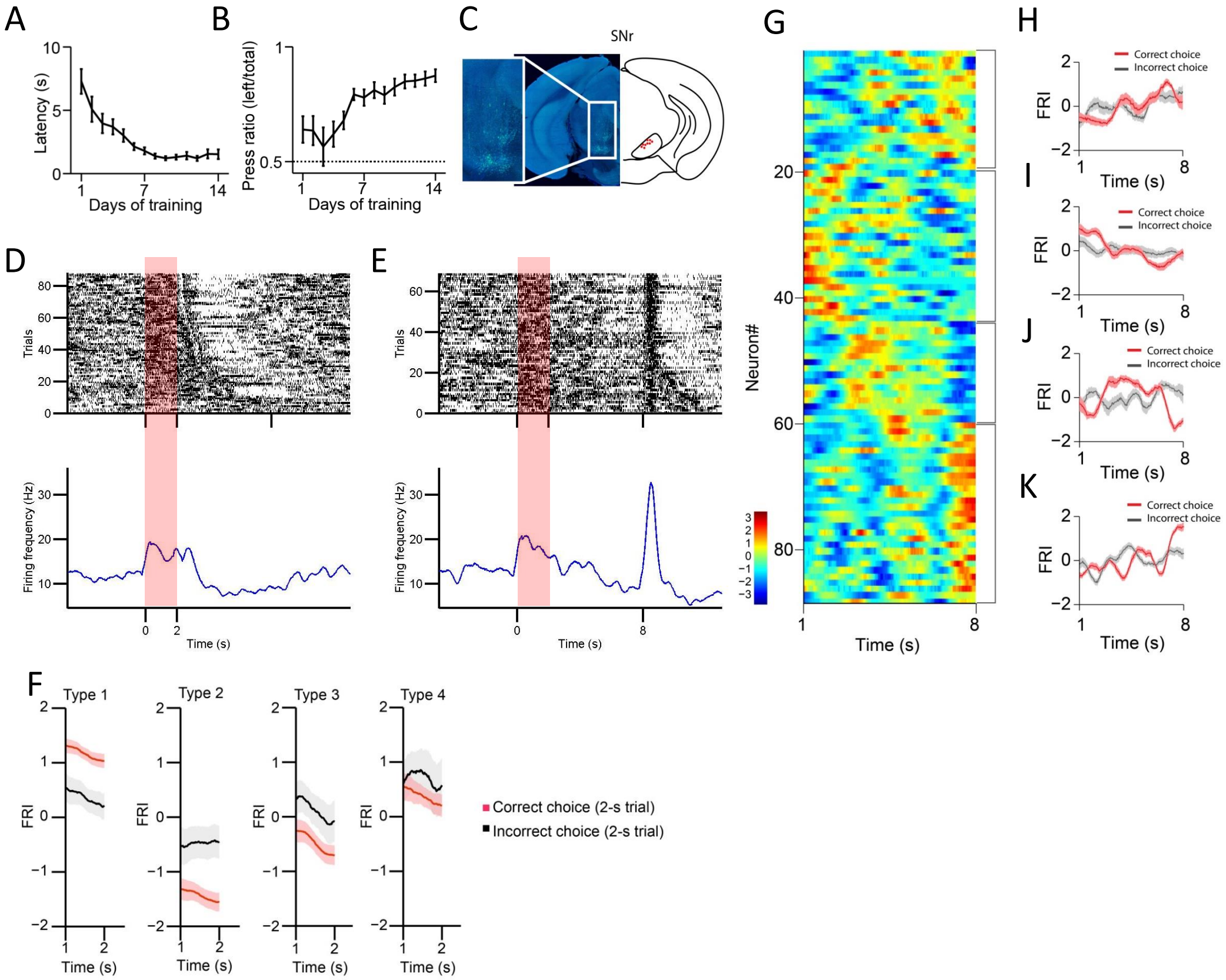

Figure S1. Behavioral performance across 14 days of training and the SNr neuronal recording on day 1. (A) Lever press latency after lever extension for wild type mice across 14 days training (n = 10 mice, one-way repeated-measures ANOVA, effect of training days, $F_{13,117} = 21.32$, $p < 0.0001$). (B) Lever press ratio for wild type mice across 14 days training (n = 10 mice, one-way repeated-measures ANOVA, effect of training days, $F_{13,117} = 6.472$, $p < 0.0001$). (C) Example of recording array placement in SNr (left) and validation of array placement in a cohort of wildtype mice (right). Inset better demonstrates small tracts formed by the array implant. (D, E) Firing activities of an example SNr neuron in correct 2-s (D) and 8-s trials (E) after 14 days training. Top panels: raster plot of spikes across trials aligned to lever retraction at time 0. Bottom panel: PETH plot. Red shaded areas highlight the initial 2-s period after the lever retraction in 2-s (D) and 8-s trials (E). (F) Averaged FRI for Type 1, Type 2, Type 3 and Type 4 of SNr neurons in correct (red) and incorrect 2-s trials (gray). (G) Firing Rate Index (FRI) of neuronal activity for all task-related SNr neurons in correct 8-s trials on day 1 of training. The magnitude of FRI is color coded and the SNr neurons are categorized as four subgroups based on the activity dynamics. (H-K) Averaged FRI of SNr neurons in correct (red) and incorrect 8-s trials (gray) on day 1 of training.

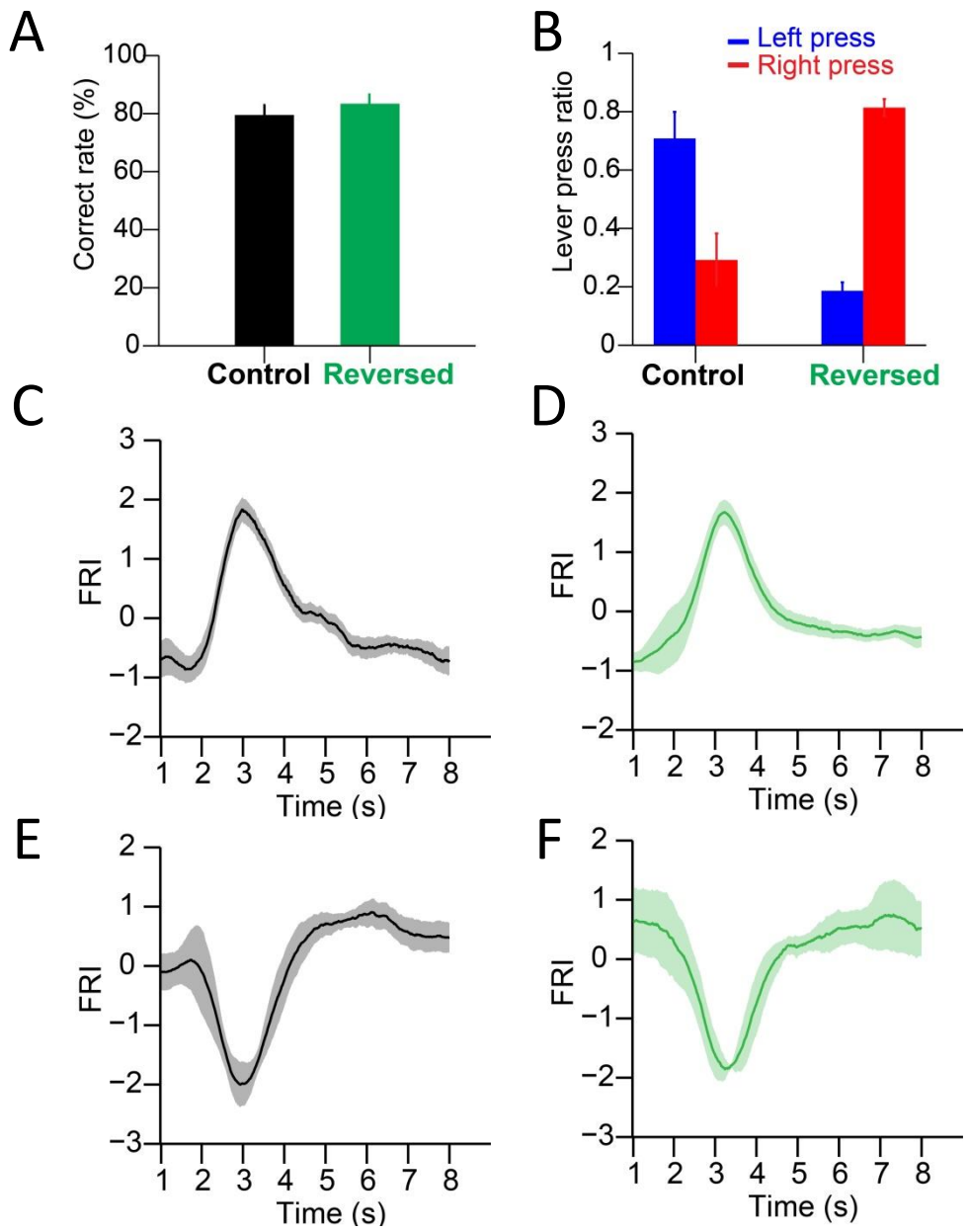

Figure S2. Behavioral statistics and neuronal dynamics of SNr neurons in the standard and reversed 2-8s tasks . (A) Correct rates of the same group of mice both in the standard and reversed 2-8s tasks (n = 6 mice, paired t-test, $p = 0.33$). (B) Lever press ratios of the same group of mice both in the standard and reversed 2-8s tasks (n = 6 mice, paired t-test, $p < 0.05$). (C) Averaged FRI of the SNr Type 3 neurons in correct 8-s trials of the standard 2-8s task. (D) Averaged FRI of the SNr Type 3 neurons in correct 8-s trials of the reversed 2-8s task. (E) Averaged FRI of the SNr Type 4 neurons in correct 8-s trials of the standard 2-8s task. (F) Averaged FRI of the SNr Type 4 neurons in correct 8-s trials of the reversed 2-8s task.

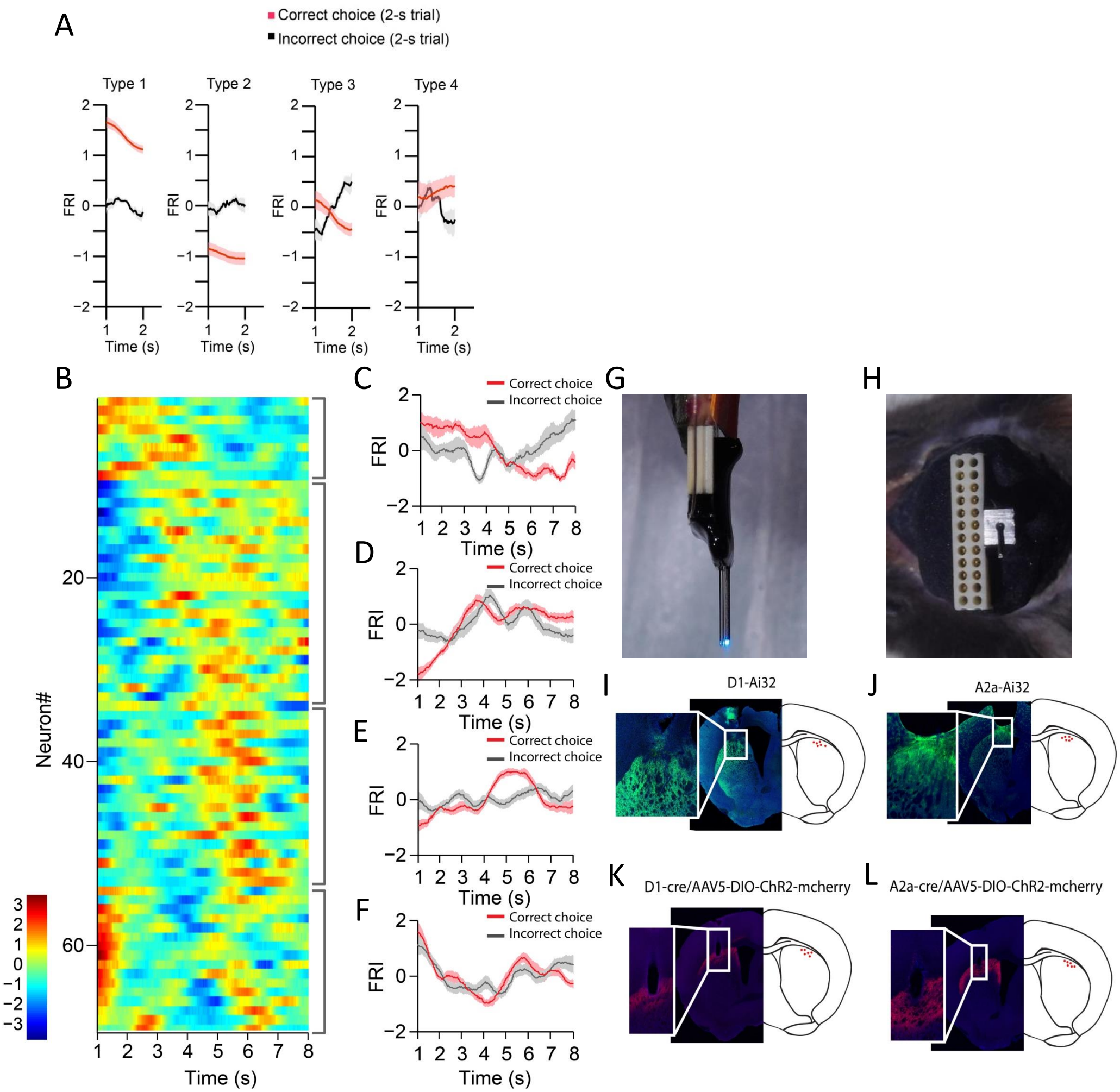

Figure S3. Striatum neuronal recording on day 1 of training, recording array and optic fiber placement validation. (A) Averaged FRI for Type 1, Type 2, Type 3 and Type 4 of SPNs in correct (red) and incorrect 2-s trials (gray). (B) Firing Rate Index (FRI) of neuronal activity for all task-related SPNs in correct 8-s trials on day 1 of training. The magnitude of FRI is color coded and the SPNs are categorized as four subgroups based on the activity dynamics. (C-F) Averaged FRI of SPNs in correct (red) and incorrect 8-s trials (gray). (G) Recording array affixed with a cannula implanted in D1-Ai32 or A2a-Ai32 mice. Light emitted by optic fiber placed through the attached cannula is in close proximity to the tips of the recording array. (H) Top-down view of the array implantation. (I) Example of array placement in dorsal striatum of a D1-Ai32 mouse (left) and validation of fiber placement in a cohort of D1-Ai32 mice (right). Inset better demonstrates the tract formed by the array implant. (J) Example of array placement in dorsal striatum of a A2a-Ai32 mouse (left) and validation of fiber placement in a cohort of A2a-Ai32 mice (right). Inset better demonstrates the tract formed by the array implant. (K) Example of fiber placement in dorsal striatum of a D1-cre mouse with AAV5-DIO-ChR2-mcherry injected (left) and validation of fiber placement in a cohort of D1-cre mice (right). Inset better demonstrates the tract formed by the fiber implant. (L) Example of fiber placement in dorsal striatum of a A2a-cre mouse with AAV5-DIO-ChR2-mcherry injected (left) and validation of fiber placement in a cohort of A2a-cre mice (right). Inset better demonstrates the tract formed by the fiber implant.

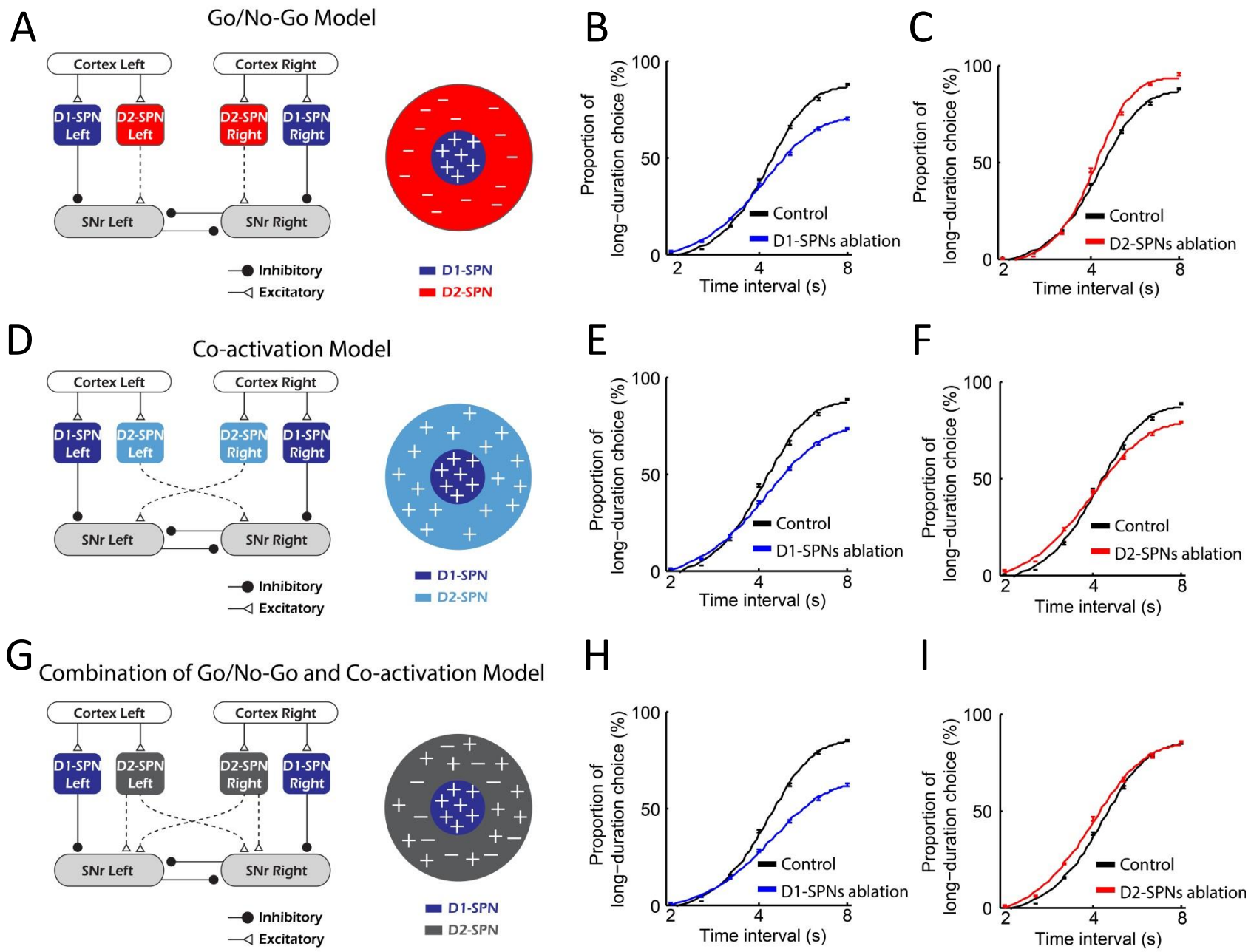

Figure S4. Simulation of lesion experiments in Go/No-Go, Co-activation and combination models. (A) Diagram of Go/No-Go model. (B) The psychometric curves of behavior outputs simulated by Go/No-Go model in control (black) and D1-SPNs ablation condition (blue). (C) The psychometric curves of behavior outputs simulated by Go/No-Go model in control (black) and D2-SPNs ablation condition (red). (D) Diagram of Co-activation model. (E) The psychometric curves of behavior outputs simulated by Co-activation model in control (black) and D1-SPNs ablation condition (blue). (F) The psychometric curves of behavior outputs simulated by Co-activation model in control (black) and D2-SPNs ablation condition (red). (G) Diagram of combination of Go/No-Go and Co-activation model. (H) The psychometric curves of behavior outputs simulated by combined model in control (black) and D1-SPNs ablation condition (blue). (I) The psychometric curves of behavior outputs simulated by combined model in control (black) and D2-SPNs ablation condition (red).

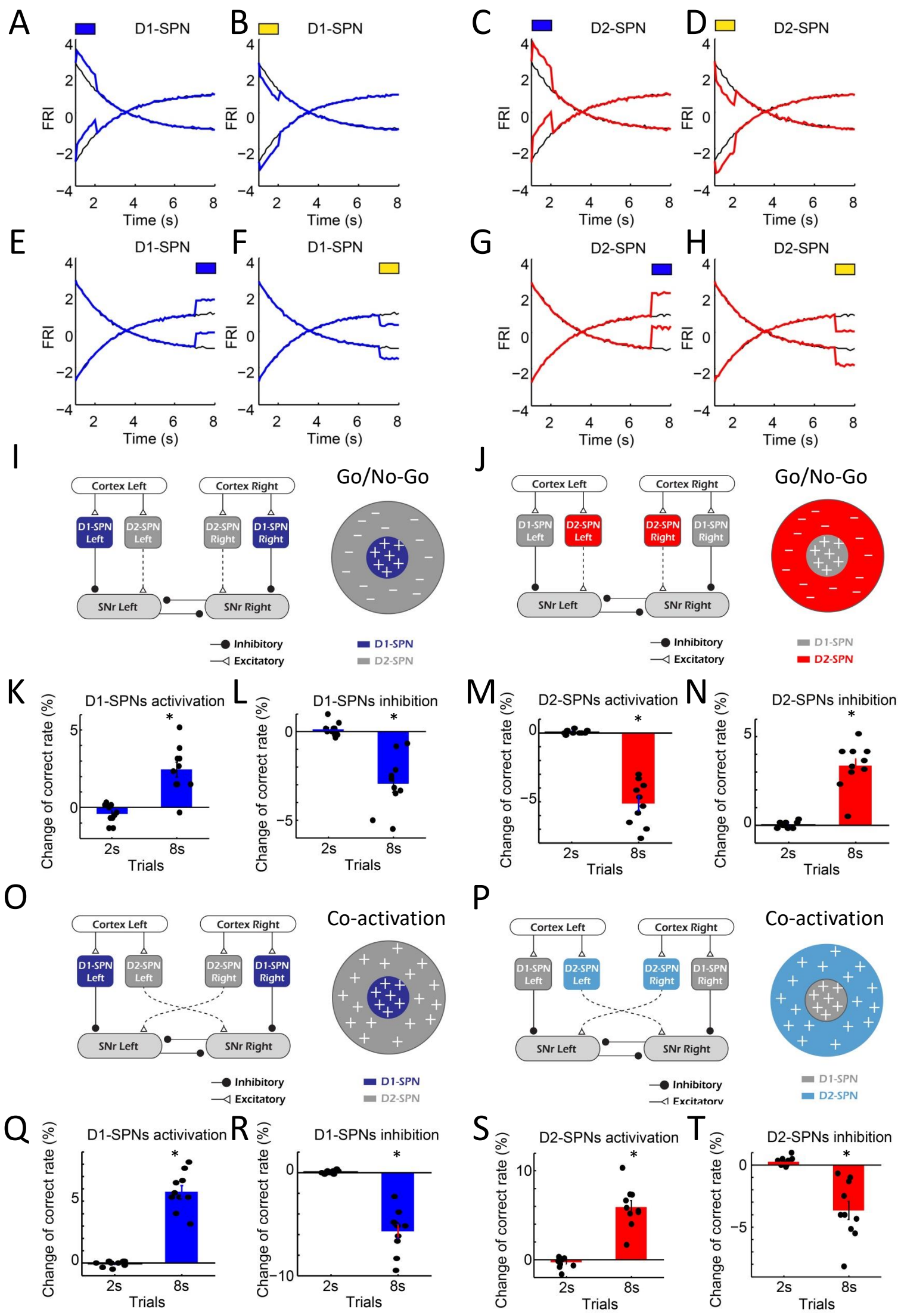

Figure S5. Simulation of optogenetic manipulation in Go/No-Go and Co-activation models. (A, B) Simulating optogenetic activation (A) and inhibition (B) of D1-SPNs at 2s. Blue bar above indicates optogenetic activation. Yellow bar above indicates optogenetic inhibition. (C, D) Simulating optogenetic activation (C) and inhibition (D) of D2-SPNs at 2s. (E, F) Simulating optogenetic activation (E) and inhibition (F) of D1-SPNs at 8s. (G, H) Simulating optogenetic activation (G) and inhibition (H) of D2-SPNs at 8s. (I, J) Diagram of D1-SPN (I) and D2-SPN (J) manipulation in Go/No-Go model. (K, L) Change of correct rate in 2-s and 8-s trials when activating (K) and inhibiting (L) D1-SPNs in Go/No-Go model. (M, N) Change of correct rate in 2-s and 8-s trials when activating (M) and inhibiting (N) D2-SPNs in Go/No-Go model. (O, P) Diagram of D1-SPN (O) and D2-SPN (P) manipulation in Co-activation model. (Q, R) Change of correct rate in 2-s and 8-s trials when activating (Q) and inhibiting (R) D1-SPNs in Co-activation model. (S, T) Change of correct rate in 2-s and 8-s trials when activating (S) and inhibiting (T) D2-SPNs in Co-activation model. One-sample test for all the change of correct rate. *$p < 0.05$.

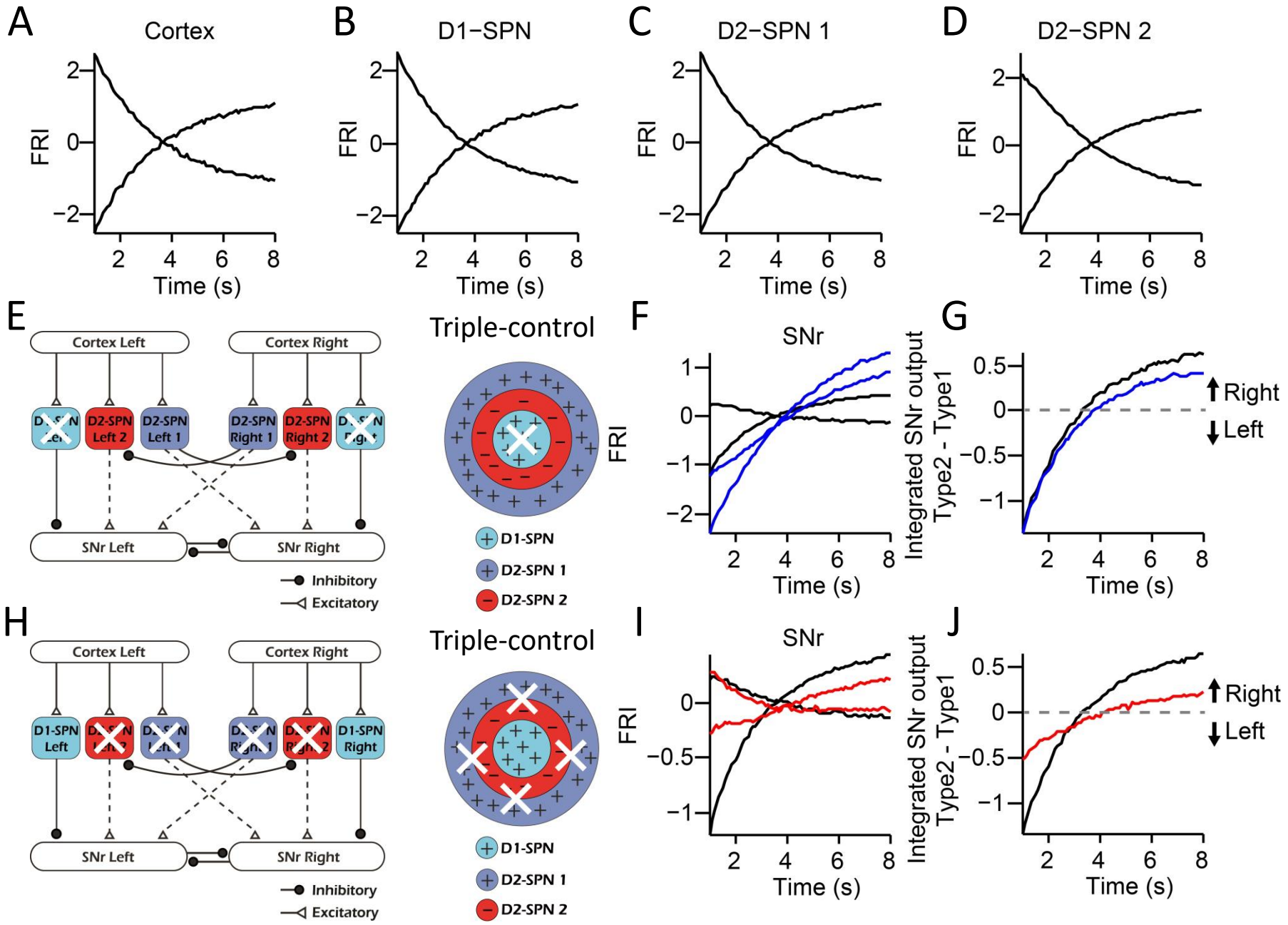

Figure S6. The neuronal activities in the "Triple-control" model and simulation of lesion experiments. (A) The simulated neuronal dynamics quantified as FRI for the cortical neurons in 8s trials. (B) The simulated neuronal dynamics quantified as FRI for the D1-SPN in 8s trials. (C) The simulated neuronal dynamics quantified as FRI for the D2-SPN 1 in 8s trials. (D) The simulated neuronal dynamics quantified as FRI for the D2-SPN 2 in 8s trials. (E) Schematic of selective ablation of D1-SPNs in the "Triple-control" model. (F) The model's Type 1 and Type 2 SNr FRI in control condition (black) and under D1-SPNs ablation (blue). (G) The subtraction of FRI between Type 1 and Type 2 SNr neurons in control (black) and D1-SPNs ablation condition (blue). (H) Schematic of selective ablation of D2-SPNs in the "Triple-control" model. (I) The model's Type 1 and Type 2 SNr FRI in control condition (black) and under D2-SPNs ablation (red). (J) The subtraction of FRI between Type 1 and Type 2 SNr neurons in control (black) and D2-SPNs ablation condition (red).

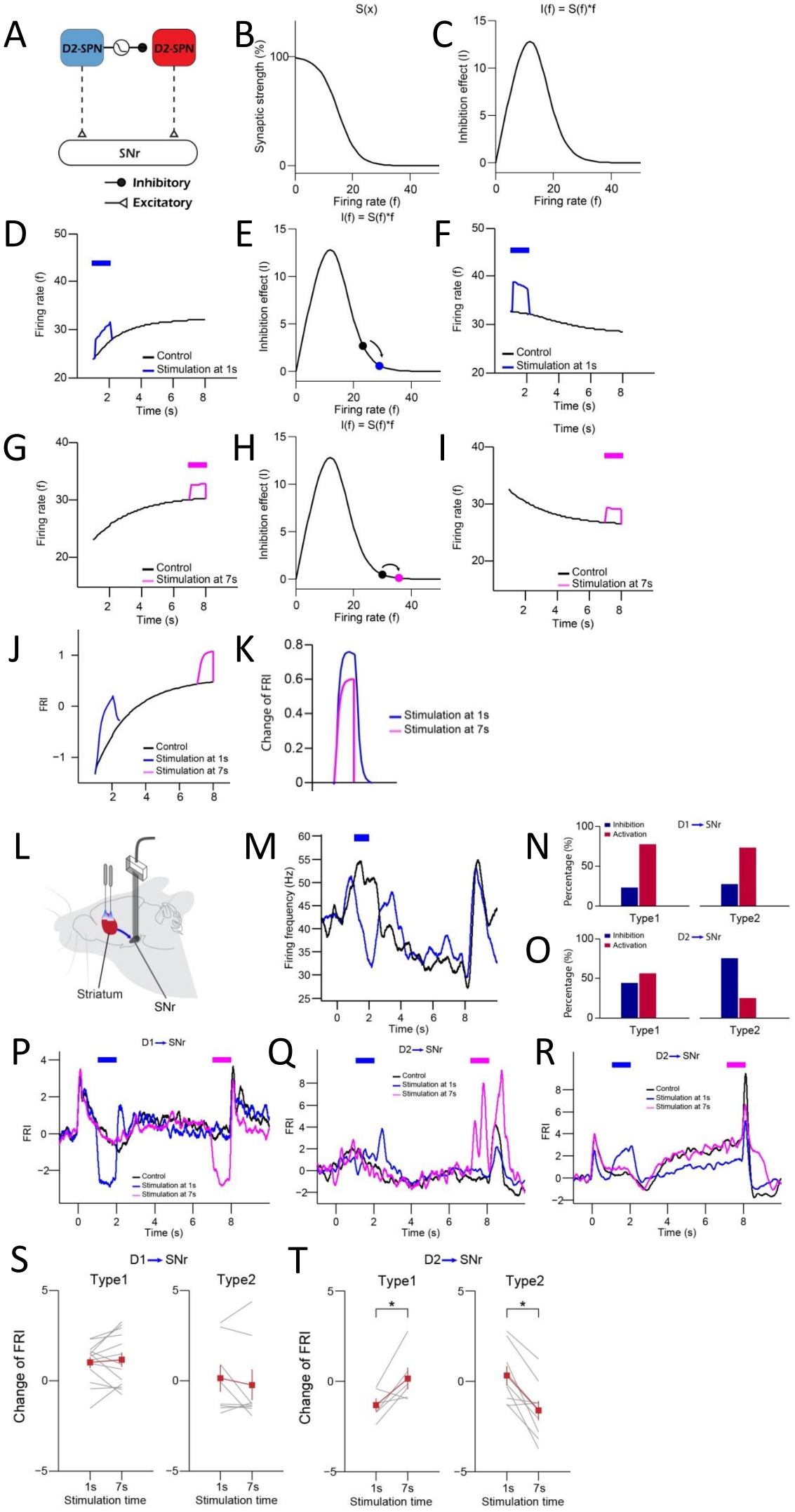

Figure S7. Optogenetic activation of D1- vs. D2-SPNs differently regulates SNr activities in model and experiments. (A) A computational motif of indirect pathway with collateral inhibitory synapse D2-SPN 1→ D2-SPN 2. The collateral synapse between D2-SPNs exhibits short-term depression. (B) Relationship between synaptic strength of D2-SPN 1→ D2-SPN 2 and the firing rate of D2-SPN 1. (C) The inhibition effect of the collateral synapse between D2-SPNs. (D) Activation of presynaptic D2-SPN 1 at 1s. (E) Synaptic inhibition effect D2-SPN 1→ D2-SPN 2 synapse when activating D2-SPN 1 at 1s. (F) Activation of D2-SPN 2 at 1s. (G) Activation of presynaptic D2-SPN 1 at 7s. (H) Synaptic inhibition effect D2-SPN 1→ D2-SPN 2 synapse when activating D2-SPN 1 at 7s. (I) Activation of D2-SPN 2 at 7s. (J) SNr neuron activities responding to activation of D2-SPNs at 1s (blue) and 7s (purple). (K) Comparison of FRI changes in SNr caused by activation of D2-SPNs at 1s and 7s. (L) Schematic of simultaneous optogenetic excitation of D1- or D2-SPNs in the dorsal striatum and recording in SNr during action selection. (M) Averaged neuronal activities of an example SNr Type 1 neuron responding to optogenetic activation of D1-SPNs at 1s during 8-s trials. (N) The percentage of SNr Type 1 (left) and Type 2 (right) neurons showing excitation (blue) and inhibition (red) when stimulating D1-SPNs. (O) The percentage of SNr Type 1 (left) and Type 2 (right) neurons showing excitation (blue) and inhibition (red) when stimulating D2-SPNs. (P) Averaged neuronal activities of an example SNr Type 2 neuron responding to optogenetic activation of D1-SPNs at 1s (blue) and 8s (purple) during 8-s trials. (Q, R) Averaged neuronal activities of SNr Type 1 (Q) and Type 2 (R) neuron responding to optogenetic activation of D2-SPNs at 1s (blue) and 7s (purple) during 8-s trials. (S) Comparison of FRI changes in SNr Type 1 (left) and Type 2 (right) neurons caused by optogenetic activation of D1-SPNs at 1s and 7s. (T) Comparison of FRI changes in SNr Type 1 (left) and Type 2 (right) neurons caused by optogenetic activation of D2-SPNs at 1s and 7s (paired t-test, $p < 0.05$).

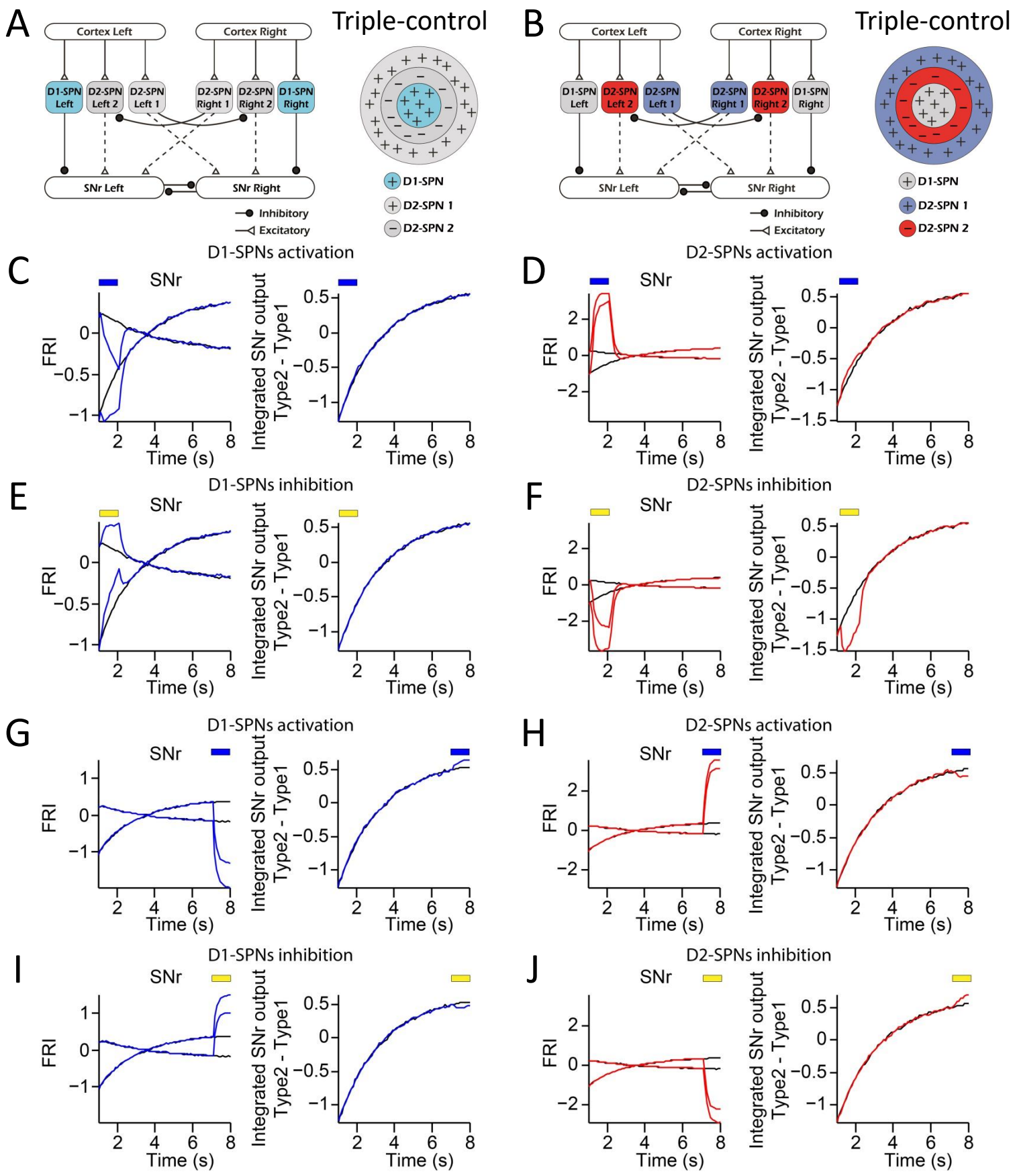

Figure S8. Computational modeling of optogenetic manipulation reveals that D1- vs. D2-SPNs differently regulates SNr outputs in the "Triple-control" model. (A, B) Schematic for optogenetic manipulation of D1-SPNs (A) and D2-SPNs (B) in the 'Triple-control' model. (C) Modeling of neuronal dynamics of SNr Type 1/Type 2 (left panel) and integrated output (right panel) under control (black) and activation (blue) of D1-SPNs at 2s. (D) Modeling of neuronal dynamics of SNr Type 1/Type 2 (left panel) and integrated output (right panel) under control (black) and activation (red) of D2-SPNs at 2s. (E) Modeling of neuronal dynamics of SNr Type 1/Type 2 (left panel) and integrated output (right panel) under control (black) and inhibition (blue) of D1-SPNs at 2s. (F) Modeling of neuronal dynamics of SNr Type 1/Type 2 (left panel) and integrated output (right panel) under control (black) and inhibition (red) of D2-SPNs at 2s. (G) Modeling of neuronal dynamics of SNr Type 1/Type 2 (left panel) and integrated output (right panel) under control (black) and activation (blue) of D1-SPNs at 8s. (H) Modeling of neuronal dynamics of SNr Type 1/Type 2 (left panel) and integrated output (right panel) under control (black) and activation (red) of D2-SPNs at 8s. (I) Modeling of neuronal dynamics of SNr Type 1/Type 2 (left panel) and integrated output (right panel) under control (black) and inhibition (blue) of D1-SPNs at 8s. (J) Modeling of neuronal dynamics of SNr Type 1/Type 2 (left panel) and integrated output (right panel) under control (black) and inhibition (red) of D2-SPNs at 8s.

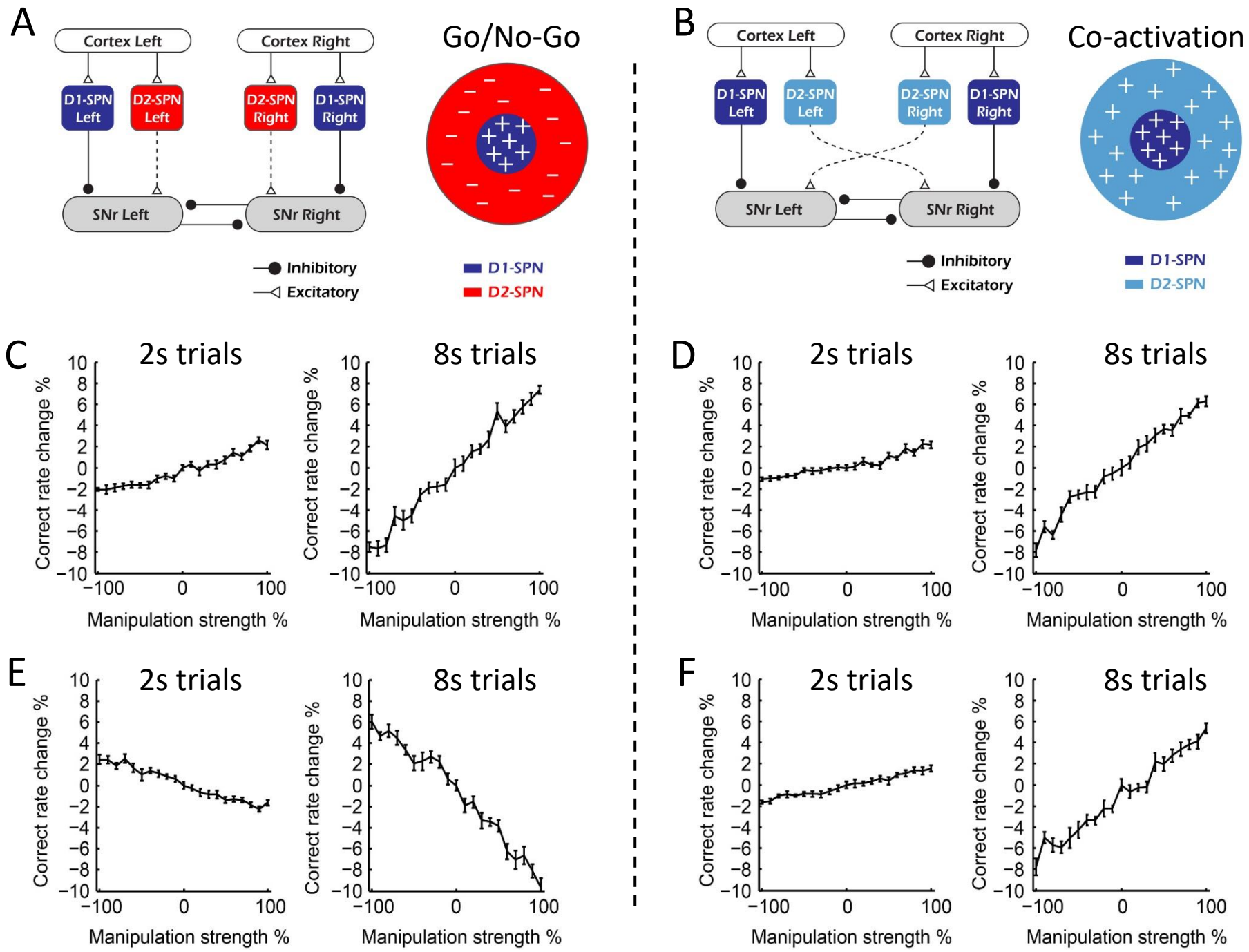

Figure S9. Computational modeling of manipulation reveals that Go/No-Go and Co-activation model differently predicts the behavioral outcomes. (A) Diagram of Go/No-Go model. (B) Diagram of Co-activation model. (C) Correct rate change in 2s (left panel) and 8s trials (right panel) when manipulating D1-SPNs in Go/No-Go model with different manipulation strengths. (D) Correct rate change in 2s (left panel) and 8s trials (right panel) trials when manipulating D1-SPNs in Co-activation model with different manipulation strengths. (E) Correct rate change in 2s (left panel) and 8s trials (right panel) when manipulating D2-SPNs in Go/No-Go model with different manipulation strengths. (F) Correct rate change in 2s (left panel) and 8s trials (right panel) trials when manipulating D2-SPNs in Co-activation model with different manipulation strengths.

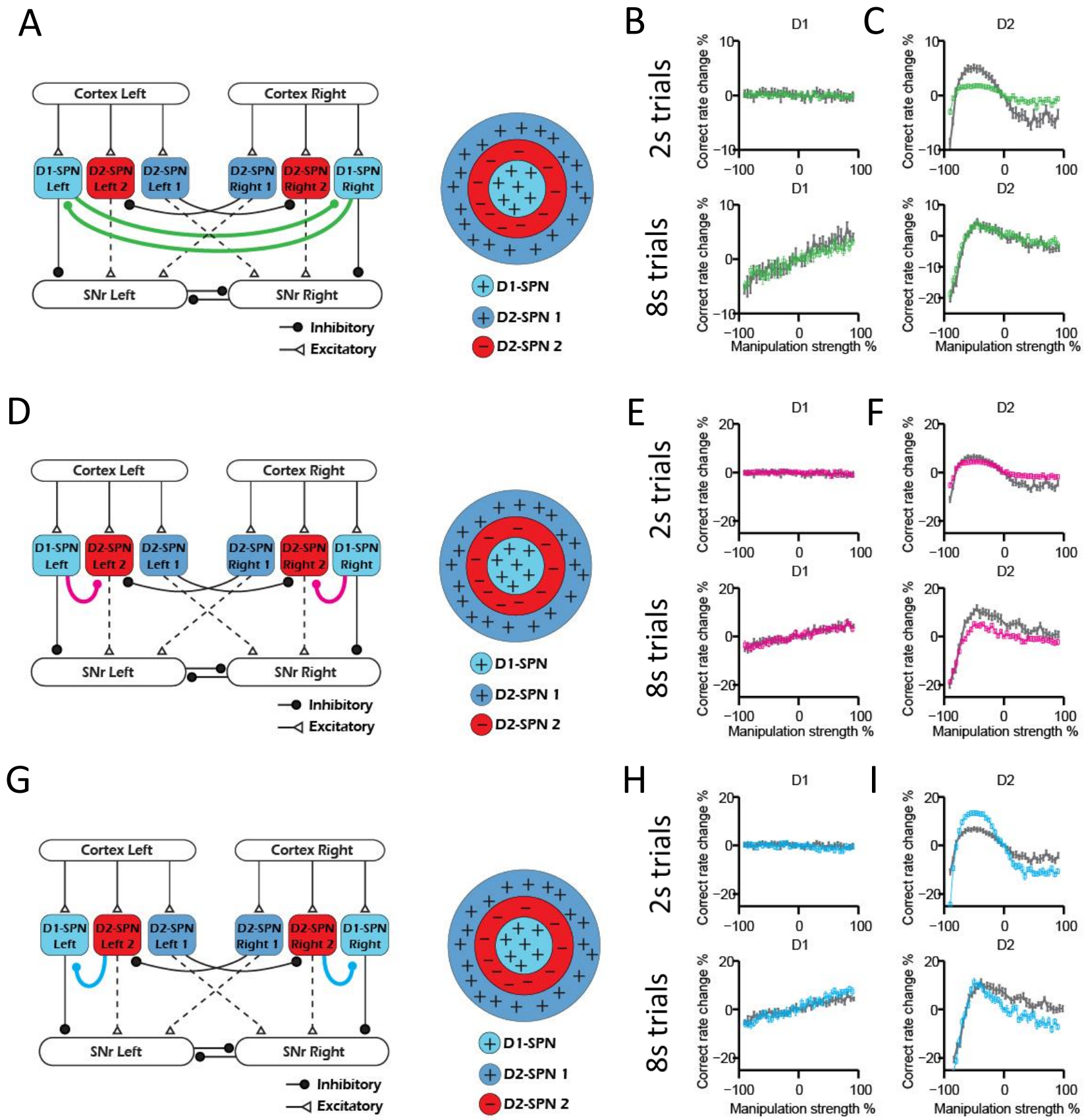

Figure S10. Computational modeling reveals that the linear and nonlinear modulation of action selection by direct versus indirect pathway qualitatively hold with additional striatal collateral connections. (A) Schematic for 'Triple-control' model with D1-D1 collateral connections. (B) Correct rate change in 2s trials (upper panel) and 8s trials (bottom panel) when manipulating D1-SPNs with different manipulation strengths (n = 10, one-way repeated-measures ANOVA, effect of manipulation strength, 2s trials: $F_{40,369} = 1.328$, $p = 0.0945$; 8s trials: $F_{40,369} = 7.595$, $p < 0.0001$). For comparison, the same simulation results as in Figure 7(C, G) are shown in gray. (C) Correct rate change in 2s trials (upper panel) and 8s trials (bottom panel) when manipulating D2-SPNs with different manipulation strengths (n = 10, one-way repeated-measures ANOVA, effect of manipulation strength, 2s trials: $F_{40,369} = 38.22$, $p < 0.0001$; 8s trials: $F_{40,369} = 34.29$, $p < 0.0001$). For comparison, the same simulation results as in Figure 7(D, H) are shown in gray. (D) Schematic for 'Triple-control' model with D1-D2 collateral connections. (E) Correct rate change in 2s trials (upper panel) and 8s trials (bottom panel) when manipulating D1-SPNs with different manipulation strengths (n = 10, one-way repeated-measures ANOVA, effect of manipulation strength, 2s trials: $F_{40,369} = 0.9335$, $p = 0.5893$; 8s trials: $F_{40,369} = 8.778$, $p < 0.0001$). For comparison, the same simulation results as in Figure 7(C, G) are shown in gray. (F) Correct rate change in 2s trials (upper panel) and 8s trials (bottom panel) when manipulating D2-SPNs with different manipulation strengths (n = 10, one-way repeated-measures ANOVA, effect of manipulation strength, 2s trials: $F_{40,369} = 40.94$, $p < 0.0001$; 8s trials: $F_{40,369} = 26.61$, $p < 0.0001$). For comparison, the same simulation results as in Figure 7(D, H) are shown in gray. (G) Schematic for 'Triple-control' model with D2-D1 collateral connections. (H) Correct rate change in 2s trials (upper panel) and 8s trials (bottom panel) when manipulating D1-SPNs with different manipulation strengths (n = 10, one-way repeated-measures ANOVA, effect of manipulation strength, 2s trials: $F_{40,369} = 0.6827$, $p = 0.9299$; 8s trials: $F_{40,369} = 10.06$, $p < 0.0001$). For comparison, the same simulation results as in Figure 7(C, G) are shown in gray. (I) Correct rate change in 2s trials (upper panel) and 8s trials (bottom panel) when manipulating D2-SPNs with different manipulation strengths (n = 10, one-way repeated-measures ANOVA, effect of manipulation strength, 2s trials: $F_{40,369} = 153.3$, $p < 0.0001$; 8s trials: $F_{40,369} = 38.38$, $p < 0.0001$). For comparison, the same simulation results as in Figure 7(D, H) are shown in gray.

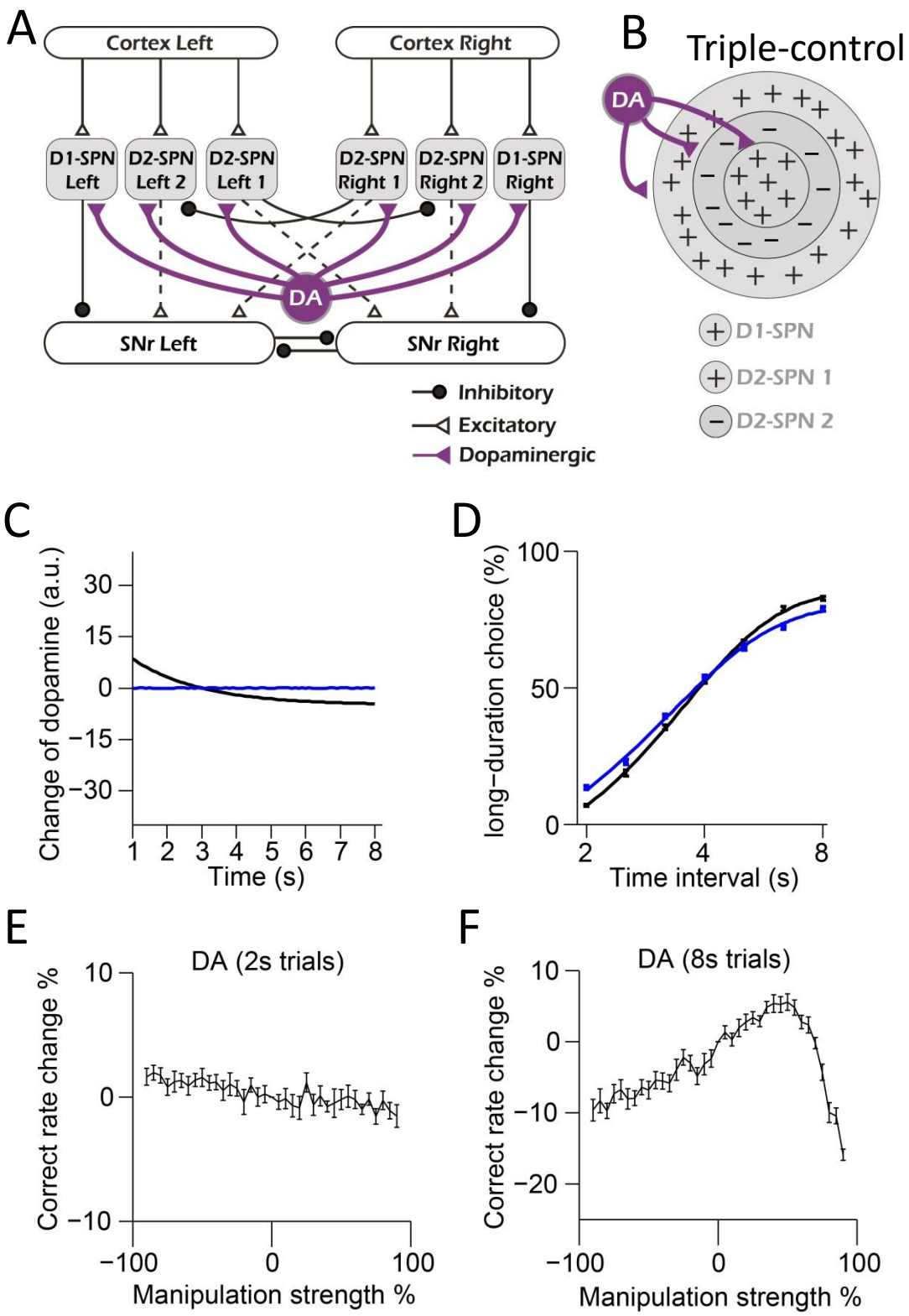

Figure S11. Computational modeling of dopaminergic modulation in the "Triple-control" model. (A) Diagram of Triple-control model with dopaminergic modulation on SPNs. (B) Schematic of center-surround-context receptive field diagram with dopaminergic modulation added for 'Triple-control' model. '+' indicates facilitating effect to selection. '-' indicates inhibitory effect to selection. (C) Simulation of two types of dopamine dynamics (black: decreasing dopamine; blue: constant dopamine with no change) in 8s trials. (D) Psychometric curves corresponding to each dopamine dynamics (n = 10, two-way repeated-measures ANOVA, main effect of ablation, $F_{1,18} = 0.8743$, $p = 0.362$; interaction between trial intervals and ablation, $F_{6,108} = 8.261$, $p < 0.0001$). (E, F) Correct rate change in 2s (E) and 8s trials (F) trials when manipulating dopamine in 'Triple-control' model with different manipulation strengths (n = 10, one-way repeated-measures ANOVA, effect of manipulation strength, 2-s trials: $F_{36,324} = 3.868$, $p < 0.0001$; 8-s trials: $F_{36,324} = 39.98$, $p < 0.0001$).